Chem Soc Rev

Structuring of metal-organic frameworks at mesoscopic/macroscopic scale

Journal:	*Chemical Society Reviews*
Manuscript ID:	CS-REV-03-2014-000106.R1
Article Type:	Review Article
Date Submitted by the Author:	18-Apr-2014
Complete List of Authors:	Furukawa, Shuhei; Kyoto University, Institute for Integrated Cell-Material Sciences Reboul, Julien; Kyoto University, Institute for Integrated Cell-Material Sciences Diring, Stéphane; Kyoto University, Institute for Integrated Cell-Material Sciences Sumida, Kenji; Kyoto University, Institute for Integrated Cell-Material Sciences Kitagawa, Susumu; Institute for Integrated Cell-Material Sciences, Department of Synthetic Chemistry and Biological Chemistry, Graduate School of Engineering, Kyoto University

Journal Name

RSCPublishing

ARTICLE

Structuring of metal-organic frameworks at mesoscopic/macroscopic scale

Cite this: DOI: 10.1039/x0xx00000x

Shuhei Furukawa,* Julien Reboul, Stéphane Diring, Kenji Sumida, and Susumu Kitagawa*

Received ooth January 2012,
Accepted ooth January 2012

DOI: 10.1039/x0xx00000x

www.rsc.org/

The assembly of metal ions with organic ligands through the formation of coordination bonds gives crystalline framework materials, known as metal-organic frameworks (MOFs), which recently emerged as a new class of porous materials. Besides the structural designability of MOFs at the molecular length scale, the researchers in this field very recently made important advances in creating more complex architectures at the mesoscopic/macroscopic scale, in which MOF nanocrystals are used as building units to construct higher-order superstructures. The structuring of MOFs in such a hierarchical order certainly opens a new opportunity to improve the material performance via design of the physical form rather than altering the chemical component. This review highlights these superstructures and their applications by categorizing them into four dimensionalities, zero-dimensional (0D), one-dimensional (1D), two-dimensional (2D), and three-dimensional (3D) superstructures. Because the key issue for structuring of MOFs is to spatially control the nucleation process in desired locations, this review conceptually categorizes the available synthetic methodologies from the viewpoint of the reaction system.

1. Introduction

The rapid expansion of research endeavors related to metal-organic frameworks (MOFs) or porous coordination polymers (PCPs) in recent years is ascribed in part to the designability of the pores at the molecular length scale.[1,2] These materials are constructed through the formation of coordination bonds between metal ions as nodes and organic ligands as spokes, and possess open framework structures with inherently high microporosities. The judicious choice of molecular components allows the design of pore size, pore shape, and pore surface functionality. This modularity in MOF synthesis allows for tuning of the interactions between the framework scaffold and targeted molecular adsorbates, and presents MOFs as an intriguing class of porous materials with a high potential for applications in storage, separation and catalysis.[3,4]

While most efforts are still devoted to the synthesis of new MOF structures and the exploration of new properties, the macroscopic structure or physical form of MOF systems, namely the crystal size, morphology and the shape of crystal aggregates, is also beginning to receive an increasing focus from researchers in the field.[5-7] In particular, the size control of MOF crystals into the nanoscale or mesoscale regime certainly presents new opportunities for applications in microenvironments.[8] For instance, MOFs acting as carriers of drugs or bioactive compounds were developed to target cellular or biological environments,[9] and nanosized MOFs were integrated into electronic sensor devices to improve their performance.[10,11] In addition to these new applications, thorough studies related to the crystal size control of MOFs has led to the discovery of new intrinsic phenomena only observed in this scale. In one interesting example, nanosized MOF crystals of the flexible $Cu_2(bdc)_2(bpy)$ (bdc = 1,4-benzenedicarboxylate and bpy = 4,4'-bipyridine) framework were demonstrated to exhibit new structural transformation behavior (a so-called shape-memory effect) and an additional structural state not observed within micrometer-sized powder crystals of the same compound.[12] Such observations highlight a new way to tune the property of MOFs by designing their physical form rather than changing their composition. This is orthogonal to a conventional molecular chemistry approach because the control of crystal size and morphology do not require chemical modifications of the framework.

From the viewpoint of controlling the physical form of MOFs, researchers have recently made significant advances in constructing more complex MOF architectures, or in other words, creating higher-order mesoscopic superstructures composed of nanocrystals as building blocks. Such hierarchically structured MOF architectures can be categorized into four dimensionalities (Fig. 1): (a) zero-dimensional (0D) architectures including hollow capsules or microspheres, (b) one-dimensional (1D) architectures such as nanorods or

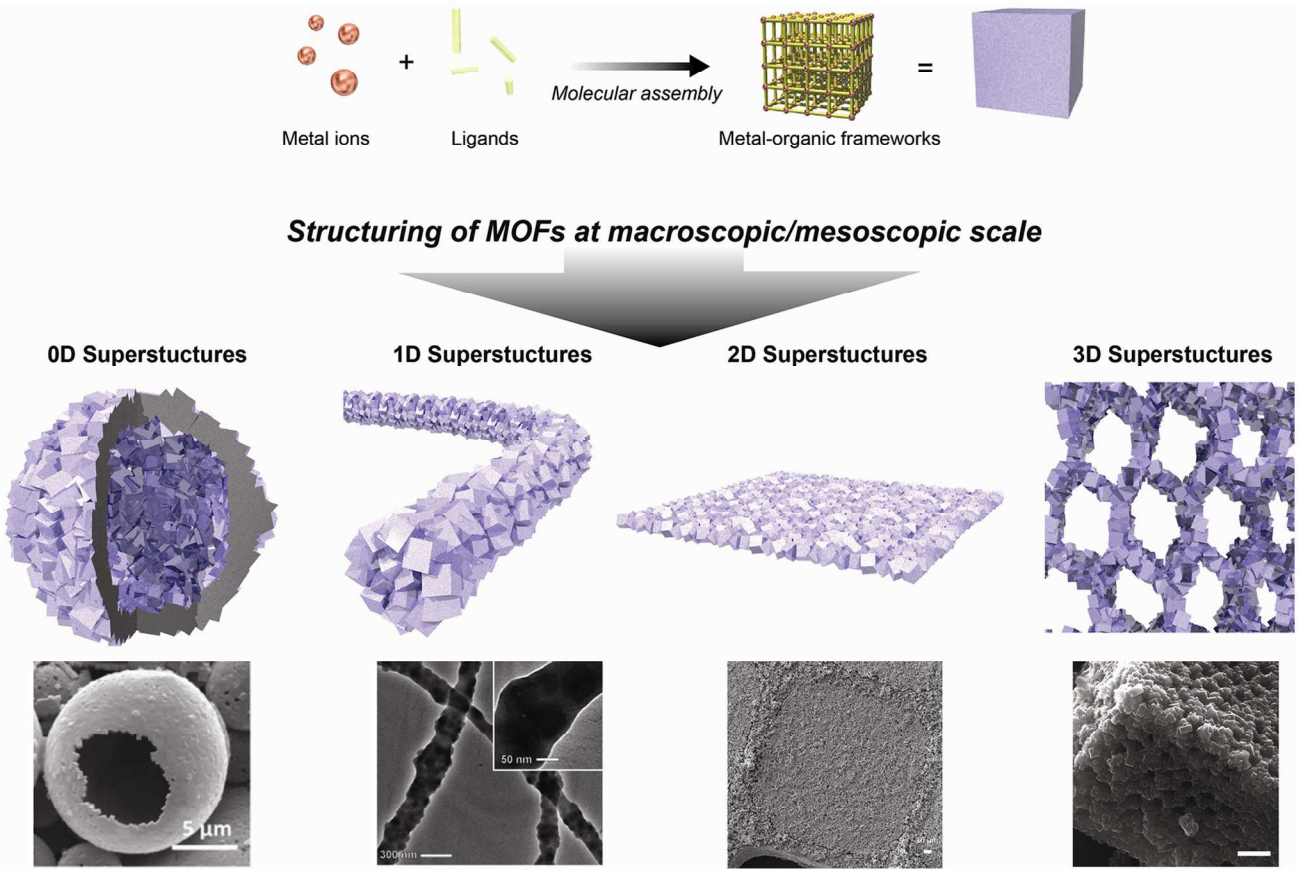

Figure 1. Conceptual illustration of structuring of MOFs at the microscopic/mesoscopic scales. The assembly of metal ions with organic ligands constructs molecular framework structures. By further assembling these nanosized crystals of MOFs, superstructures can be shaped into four different dimensionalities, zero-dimensional (0D) superstructures presented as hollow spheres, one-dimensional (1D) superstructures as fibrous morphology, two-dimensional (2D) superstructures as membranes or patterns on substrates, and three-dimensional (3D) superstructures with continuous and extended systems. Electron microscopy images representing each dimensionality are used with permission from ref. 35 for 0D, ref. 62 for 1D, ref. 153 for 2D, ref. 57 for 3D.

nanofibers, (c) two-dimensional (2D) architectures characterized as thin films, membranes or patterns, and (d) three-dimensional (3D) architectures that consist of continuous and extended systems. All of these types of superstructures are designed to enrich the tremendous material performance derived from the inherent microporosity of MOFs, and may enhance their performance in a variety of applications via selection of superstructures of the appropriate dimensionality.

In this review, we focus on the synthetic strategies developed for the structuring of mesoscopic or macroscopic MOF superstructures, and the new applications that have originated from the synergy between the different length scales within the hierarchical structure, in which the framework dominates the microporous properties and the higher-order architecture improves its overall performance. In order to structure MOF crystals in a desired dimension and therefore towards structures possessing the target functions, the key for success is both to spatially control the crystallization process of MOFs and to manipulate the single-crystal characteristics (shape, size and crystallographic orientation). At first glance, such overall control may appear as an arduous challenge. Indeed, as for any crystalline material, the driving force for MOF crystallization can be very strong, and making alterations to this process can be hard to achieve. However, owing to the highly reactive surfaces of MOFs (composed of partially coordinated organic ligands or uncoordinatively unsaturated metal centers),[13] modulation of the coordination equilibrium, and the large number of MOF frameworks available (which implies a large range of possible synthesis conditions), many of the chemical and microfabrication methods established for the structuring of conventional organic and inorganic compounds (including the use of crystal growth modifiers, hard or soft templates, spin- or dip-coating, spray-drying, microcontact printing, lithography approaches) could be employed for both controlling the crystal aspects and gaining spatial control of MOF crystal deposition so far. Interestingly, in addition to these common methods, strategies that take advantage of the intrinsic multicomponent character of this class of material have also been implemented (separated biphasic reaction system). The main advantage of these approaches lies in the possibility to produce either freestanding structures (in the case of both liquid-liquid and liquid-solid biphasic systems) or structured composites (exclusively in the case of liquid-solid biphasic systems).

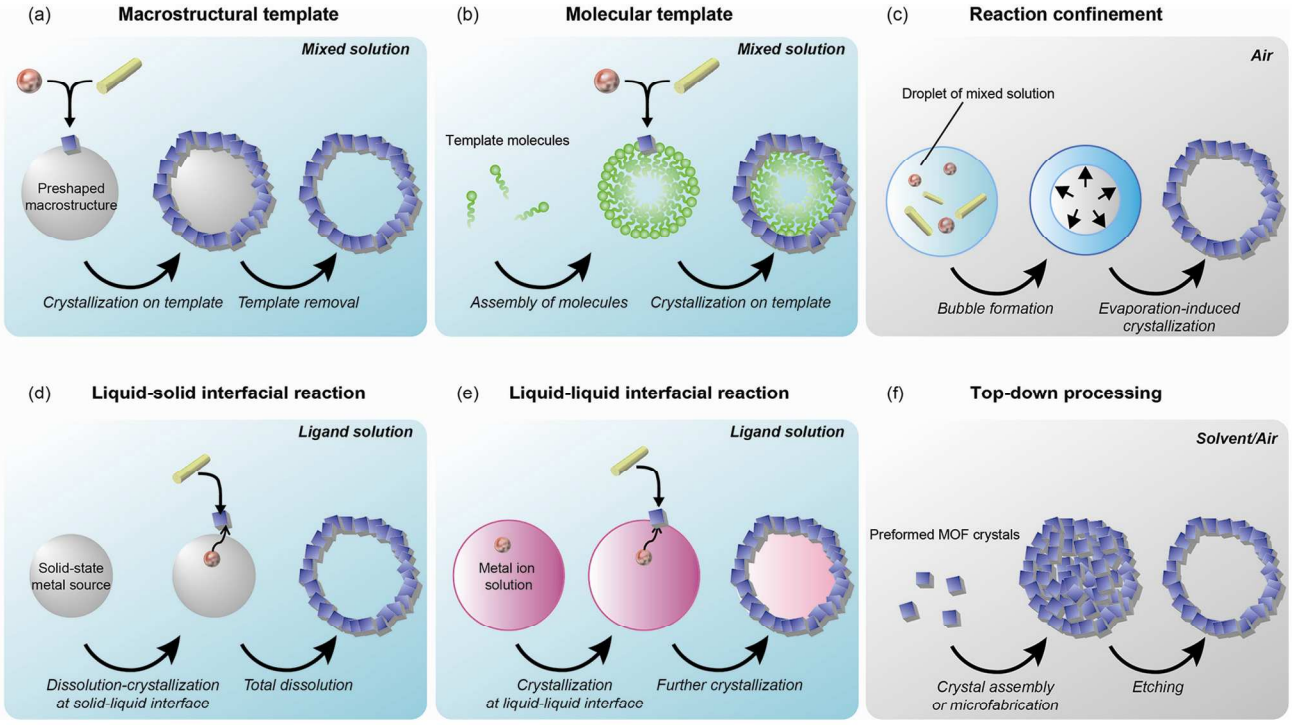

Figure 2. Conceptual illustration of synthetic strategies for structuring of MOFs. The case of 0D structuring is only represented for clarity. (a) The macrostructural template strategy consists of a preshaped macrostructured template in a mixed reaction solution of metal ions and organic ligands. Crystallization of MOFs occurs at the template surface and subsequent removal of template provides MOF superstructures. (b) The molecular template method gives a similar crystallization process but a self-assembling molecular template is used instead of a macrostructural hard template. (c) The reaction confinement strategy also uses a mixed reaction solution, but without a template. The evaporation of the mixed solution spatially localizes the MOF crystallization. (d) Liquid-solid interfacial reaction systems separate the chemical components into two different phases; a metal, metal oxide or metal hydroxide is used as a solid metal source, and the ligands are dissolved in solution. The dissolution of solid-state metal sources provides metal ions at its surface and the crystallization is localized at the liquid-solid interface. (e) The liquid-liquid interfacial reaction protocol has a similar biphasic reaction system but the metal ions are also dissolved in solution. The key to localize the reaction at the interface is to create a shaped liquid-liquid interface by using immiscible liquid components. (f) Top-down processing represents the assembly of preformed MOF crystals into desired shapes by microfabrication techniques or spontaneous colloidal assembly. Subsequent etching processes provide further control of the macroscopic structures.

The following discussion is intended to give the reader a detailed coverage of the synthetic strategies available for the creation of MOF superstructures. The main strategies that have been reported to date are first conceptually categorized in Section 2. Each of these strategies is discussed in the context of the different dimensionalities in turn (from 0D to 3D). The syntheses and properties of 0D and 1D architectures are described in Sections 3 and 4, respectively. Then, following a discussion of the synthetic strategies of 2D architectures in Section 5, an account of the various applications available for 2D architectures is given in Section 6. Lastly, the syntheses and properties of 3D architectures in presented Section 7.

2. Synthetic strategies

The synthesis of MOFs is essentially dominated by coordination-driven molecular scale assembly. Here, the reaction between metal ions and organic ligands leads to the initial formation of MOF nuclei, followed by crystal growth processes arising from additional coordination bond formation at the surface of nuclei.[7] The main difficulty in structuring MOF superstructures with a desired dimensionality has been in developing suitable methods that localize such coordination reactions within a desired space. Recent investigations of MOF crystallization processes, coupled with the application of synthetic protocols of solid-state materials into MOF synthesis as well as the implementation of modern microfabrication technology, the shaping of MOFs in the micrometer or submicrometer scales has been realized via the high precision of spatial localization of the reactions. Here we categorize the reported procedures into the following six general strategies from the viewpoint of the reaction system (Fig. 2).

(1) *Macrostructural template* (hard template) methods certainly represent one of the simplest strategies for the structuring of MOF superstructures. The preshaped solid-state macrostucture is introduced into the reaction solution at the time of MOF synthesis. The MOF nuclei in solution become attached to the active surface of the template and subsequently undergo crystal growth while being immobilized by the template. In this method, all the precursors are already mixed in the reaction solution such that not all crystallization is confined to the surface of the template system. However, the bulk MOF

crystals that are precipitated are safely removed from the system by simple washing processes since the macrostructural template allows for easy handling the resulting materials. The materials are obtained as MOF composites containing the template material; or an etching process that removes the template can afford pure MOF superstructures.

(2) *Molecular template* (soft template) methods assist MOF structuring through specific interactions with MOF precursors (metal ions or organic ligands). In most cases, the template molecules simultaneously introduced into the reaction system, such as surfactants (e.g. amphiphiles or block copolymers), are assembled in-situ to form superstructures that induce the nucleation of the MOF on their surface in a similar manner to the above-mentioned macrostructural template method. The other main example of molecular templates are those that inhibit or enhance the crystal growth in a desired direction through the use of molecules that specifically interact with MOF precursors, leading to the anisotropic growth of the MOF crystals. This method is particularly implemented for the fabrication of one-dimensional superstructures. In these cases, the template molecules are inherently incorporated into resulting architectures.

(3) *Reaction confinement* (evaporation and gelation) serves to direct the MOF structuring process without a templating additive. This method simply relies on a biphasic system, in which one liquid phase contacting all MOF precursors is forced by the other phase to be concentrated, leading to nucleation. One predominant example in this area is evaporation-induced crystallization. By controlling the evaporation location and speed, crystallization starts at the air-liquid interface and the superstructures form adopting the shape of interfaces. This method is well suited to microfabrication technologies, which are good at handling very small amounts of liquids, such as microdroplets. Such an air-liquid interface is also deliberately generated by the introduction of supercritical CO_2 gas into the reaction medium. Another way to confine the reaction is achieved by gelation. Instead of the air phase, the use of a poor solvent as a liquid counterphase induces the confinement of the reaction in a similar manner.

In contrast to these three methods (1~3), in which the MOF nucleation is induced by a monophasic or mixed reaction solution containing both the metal source and the linker, the following two strategies (4~5) employ biphasic reaction systems. Namely, the MOF precursors are separated into two different phases (liquid or solid phases). The reaction system allows the coordination reaction to occur only at the interface between the two phases where the precursors encounter each other, and thus provides localization of nucleation at the interface. As such, the following two categories can be introduced.

(4) *Liquid-solid interfacial reaction* (sacrificial reaction) methods represent those that take advantage of the metal ion precursors being in the solid state. Instead of using conventional metal salts that are solubilized prior to the reaction, solid metal sources such as metals, metal oxides, or metal hydroxides that produce ions by a sacrificial dissolution process that occurs only under certain conditions are used. As a result of the dissolution of the organic counterparts in the reaction solvent beforehand, the dissolved metal ions react with ligands at the solid-liquid interface, leading to the localization of the MOF crystals at the interface. Since a wide variety of approaches are available for shaping of such solid metal ion sources (e.g. sol-gel process), this provides the opportunity for structuring MOFs in any dimensionality.

(5) *Liquid-liquid interfacial reaction* methods allow the localization of the reaction to an interface between one solution that contains the metal ions and second solution that containing the organic ligands. In this case, the key for success is to generate a sharp interface between the two liquids. One possible pathway is to use immiscible liquids such as oil-in-water, and another method is the use of a microfluidic environment that creates a laminar flow.

(6) *Top-down processing* is the last strategy, which is unique from the other five above-mentioned strategies that attempt to spatially control the bottom-up assembling process between the metal ions and organic ligands. Owing to recent developments related to the synthesis of nanocrystals of MOFs, microfabrication technologies allow the direct assembly of superstructures using preformed nanocrystals as the building blocks. Chemical etching and delamination processes are also categorized into this category as an alternative strategy that constructs the structure without implementing fabrication instruments.

In this review, we classify the synthetic procedures of MOF superstructures into these six strategies and the following sections describe key fabrication concepts based on these methods for structuring of MOF architectures in each of the dimensionalities.

3. Zero-dimensional superstructures

The assembly of chemical components into zero-dimensional architectures is rather characteristic compared to the other higher order architectures with extended architectures. This is because the 0D assemblage simply compartmentalizes a space; either an interior space or an external environment. When the interior is filled with the one type of material and the 0D architecture work as a shell, materials with this configuration would be recognized as composites. The composites materials are basically fabricated by macrostructural template method, in which one particle-type material is used as a support for the crystallization of MOFs with a core-shell configuration. Several examples are illustrated in the section 3.1.

On the other hand, the 0D architectures give more characteristic feature when the interior space becomes void. The formation of such hollow superstructures is one of the important approaches in the field of materials science to take a benefit from the structuralization in mesoscopic/macroscopic scale. This is because the formation of an internal cavity produces a lot of opportunities in potential applications[14] in energy storage,[15] chemical catalysis,[16] photonics,[17] protocell,[18] and biomedical carriers.[19]

When the structure is permeable to specific ions or molecules, the internal cavity becomes accessible from an external environment and gives a new application of hollow structures.[20] Therefore, the construction of hollow architectures with nanoporous system as a shell is indeed a prerequisite for exhibiting a high performance of 0D structures.

MOFs are certainly one of the best candidates as nanoporous materials. Thanks to the recent progress of synthetic methodologies and the understanding of crystallization processes, recently several examples of 0D architectures of MOFs started to be reported. We categorize the following subsections by the synthetic schemes introduced in Section 2. There are several examples of hollow structures of cyano-bridging coordination polymers such as Prussian blue.[21] However, we do not involve them in this review article because the synthetic method is basically far different from those for typical MOFs.

3.1. Macrostructural template–composites.

One of the straightforward methods to construct 0D structures is to use a sphere-like macrostructural template as a hard template, similar to the fabrication of zeolite composites.[22] Aguado and coworkers demonstrated the fabrication of spherical MOF composites with millimeter-sized alumina beads.[23] The α- or γ- alumina beads with the size of 1.5 mm was simply soaked into the reaction solution of SIM-1, $Zn(mcIm)_2$ (HmcIm = 4-methyl-5-imidazolecarboxyaldehyde), and were heated at 85 °C for 48 h. Using such a large size of beads, unnecessary pure crystals of SIM-1 was easily removed by simple ethanol washing process. Interestingly, the γ-alumina bead contained SIM-1 crystals in the inner part of spherical beads due to the intrinsic mesopores of the beads. On the other hand, α-alumina supported the homogeneous coating over its outer surface with SIM-1 crystals with the thickness of 15 μm and formed the core-shell type composites, α-alumina@SIM-1. The same authors expanded the research to the other type of framework, SIM-2(C_{12}), which was fabricated by post-synthetic method to SIM-1.[24] The reaction of dodecylamine with the carboxyaldehyde moiety of α-alumina@SIM-1 composites directly led to the imine formation and to the successful post-synthetic introduction of long alkyl chains into the SIM shell. These alkyl chains totally changed the property of composites to hydrophobic, even evidenced by the floating behavior on the water surface.

Instead of the use of the millimeter sized alumina sphere, Téllez and co-workers used mesoporous silica spheres (MSSs) with the size of a few μm and coated then with ZIF-8 ($Zn(Me\text{-}Im)_2$, Me-Im = 2-methylimidazolate) crystals as shell.[25] The synthesis was carried out through the multi-step reaction processes, so-called, *in-situ* seeding and secondary crystal growth. The initial seeding process gave a uniform ZIF-8 seed layer with the size around 180 nm. The subsequent secondary growth was essential to obtain a homogeneous well-intergrown crystal shell with the 410 nm thickness. By repeating the growth process, the shell became thicker to the size of 550 nm. The resulting core-shell MSS@ZIF-8 composite with hierarchical mesopores/micropores have a totally different sorption property from the naked MSSs. Covering the hydrophilic MSSs with the ZIF-8 shell certainly changed the water absorption property of MSSs to be hydrophobic because the hydrophobic nature of ZIF-8 exposed to the external environment only dominates the adsorption property of whole composite.

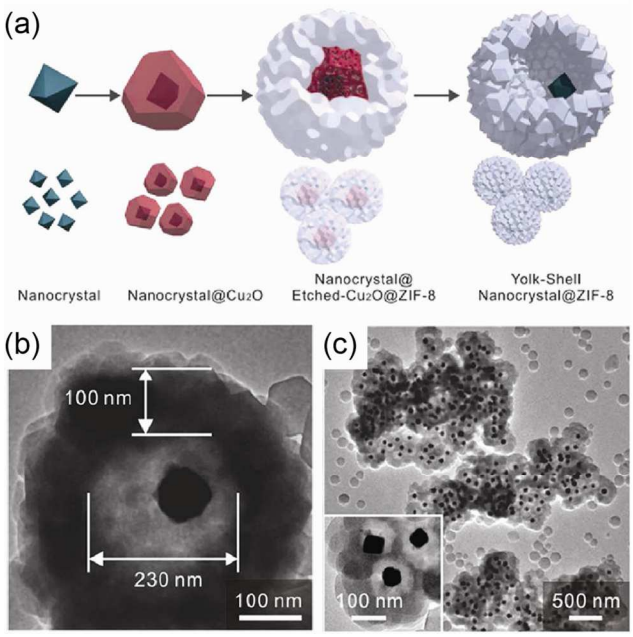

Figure 3. (a) Schematic illustration of growth procedure for yolk-shell Pd@ZIF-8. (b, c) TEM images of yolk-shell Pd@ZIF-8. The Pd octahedral core with edge sized of 60 nm is embedded in the hollow structure of ZIF-8 as a shell with thickness of ca. 100 nm. Adapted from ref. 26 with permission Copyright© 2012 American Chemical Society.

Compared to the above examples with large spheres with the sizes in millimeter or micrometer scales, the fabrication of 0D yolk-shell type composites in the mesoscopic scale was elegantly demonstrated.[26] Tsung and co-workers first covered a palladium octahedral nanocrystal with the size of 60 nm in copper(I) oxide, followed by the crystallization of ZIF-8 on the surface of Cu_2O template. During this crystallization process, the Cu_2O layer was simultaneously and spontaneously etched off, which leads to the formation yolk-shell architecture, in which the Pd nanocrystals was incorporated in the hollow cavity of ZIF-8 polycrystalline shell, namely the yolk-shell Pd@ZIF-8 (Fig. 3). The average size of this composite is less than 500 nm (the thickness of ZIF-8 shell is ca. 100 nm and the internal cavity size is ca. 230 nm). In this procedure, the Cu_2O layer worked as a sacrificial template; however, the dissolved copper ions were not used to form the framework but were simply etched away from the material. The effect of the ZIF-8 shell on the molecular discrimination based on its microporosity was clearly confirmed by the catalytic activity of the embedded Pd nanocrystal. Gas-phase hydrogenation of ethylene that is smaller than the pore aperture (3.4 Å) of ZIF-8 was successfully demonstrated. On the other hand, the yolk-

shell Pd@ZIF-8 composite showed no detectable activity for the larger size of substrate, cyclooctane.

Indeed, the first example of such 0D MOF composites was reported by Furukawa, Kitagawa and co-workers as a MOF crystal itself was used as the macrostructural template and a second MOF polycrystals were grown on the top of the template surface.[27] In this case the 200 μm single crystal of $Zn_2(1,4\text{-ndc})_2(dabco)$ was used as the template and the copper analogous framework, $Cu_2(1,4\text{-ndc})_2(dabco)$, was grown as a shell (ndc = 1,4-naphthalene dicarboxylate, dabco = 1,4-diazabicyclo[2,2,2]octane). Due to the similar lattice parameters to each other, the epitaxial relationship between the core and shell frameworks was observed by surface X-ray diffraction experiments. The same authors and other research groups subsequently reported the MOF@MOF concept for another type of frameworks, such as a IRMOF system.[28,29] The group of Furukawa and Kitagawa also demonstrated the integration of two porous properties into the zero-dimensional architecture.[30,31] Namely, the combination between the template crystal of $Zn_2(bdc)_2(dabco)$ with a large porosity and the second framework of $Zn_2(adc)_2(dabco)$ with a small porosity allows the resulting material to give the size selectivity to the shell crystal and the high molecular storage to the core crystal (bdc = 1,4-benzenedicarboxylate, adc = 1,9-anthracene dicarboxylate). The core-shell crystal successfully demonstrated the extraction of cetane (n-hexadecane) from its branched isomer, isocetane.[30]

3.2. Macrostructural template–hollow architectures.

By contrast to the synthesis of composite materials described above, the macrostructural template approach to form hollow architectures is to require an important step as the removal of template itself. Similar to the synthesis of yolk-shell MOF composite,[26] the sacrificial template is essential to produce the interior void in 0D superstructures. Oh and coworkers nicely demonstrated two-step synthesis.[32] Calboxylate-terminated polystyrene spheres (PSs) with the size of 870 nm were used as the mascrostructural template to grow the ZIF-8 on the surface, leading to the core-shell PS@ZIF-8 material. The subsequent etching process by DMF efficiently etched off the PS sphere from the composite and formed the hollow ZIF-8 material. In order to maintain the perfect spherical shape after the etching process, the 100 nm thickness of the ZIF-8 shell was required, which was achieved by three cycles of ZIF-8 crystallization process; otherwise, products akin to flat balloons were obtained. This approach was expanded to the fabrication of other type of MOF hollow superstructures of MIL-100(Fe) ($\{Fe_3O(H_2O)_2F\}(btc)_2$) or $Cu_3(btc)_2$ (or known to be HKUST-1) through the formation of PS@MIL-100(Fe) or PS@$Cu_3(btc)_2$, respectively (btc = 1,3,5-bezene tricarboxylate).[33]

3.3. Molecular template.

Another method to produce hollow architectures is to compartmentalize a spherical space by molecular assemblages from the other continuous phase containing MOF precursors. In most cases surfactants assembling into spherical micelles are used as molecular templates and the crystallization or the aggregation of MOFs occur at the surface of surfactants.

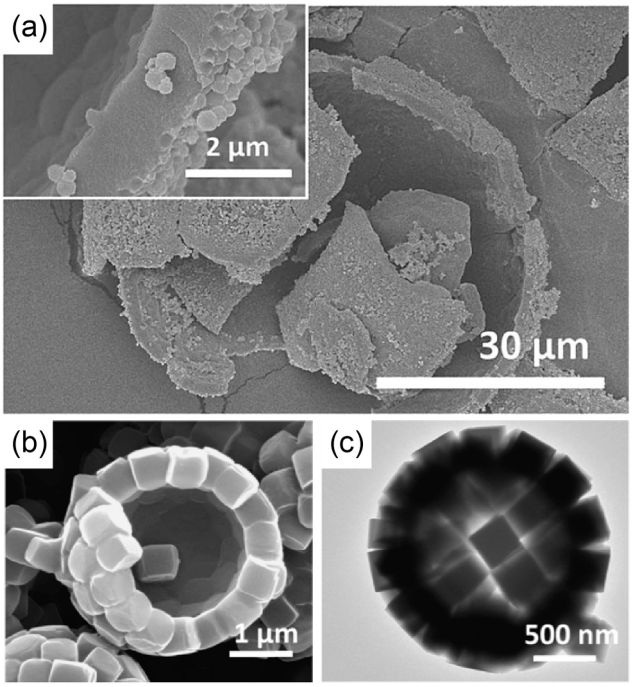

Figure 4. (a) SEM image of a single broken capsule of ZIF-8@PS derived from Pickering emulsion. Adapted from ref. 34 with permission Copyright© 2013 WILEY-VCH Verlag GmbH & Co. KGaA, Weinheim. (b) SEM and (c) TEM images of hollow superstructures of Fe-soc-MOF. Adapted from ref. 35 with permission Copyright© 2013 American Chemical Society.

Huo, Bradshaw and co-workers took an advantage of the oil-in-water Pickering emulsion.[34] The Pickering emulsion is known to be an emulsion that is stabilized by solid particles at the biphasic interface. Here the preformed nanocrystals of ZIF-8 with the size around 350 nm was used as a stabilizer. The Pickering emulsion was reliably produced by adding 0.4 g of dodecane to a dispersion of 0.2 g of ZIF-8 nanoparticles in 10 mL of water and by agitation using the shear force instrument at 16,500 rpm for 2 min. In order to isolate hollow superstructures, the styrene and divinylbenzene components (2:3) and initiator, azobisisobutyronitrile (AIBN), were incorporated in the oil phase, and the subsequent polymerization reaction at 65 °C was carried out the maintain the Pickering emulsion structure. Hollow composite microcapsules were formed, as the dodecane is a poor solvent for the cross-linked PS network leading to phase separation and precipitation at the interface. The resulting capsule consist of PS membrane embedding the ZIF-8 nanoparticles wherein, namely ZIF-8@PS hollow structures (Fig. 4a). Interestingly, this hollow structure was formed when the ZIF-8:monomers mass ratio in the system is 1:1.75. When increasing the amount of monomers to the mass ratio (ZIF-8:monomers) of 1:2.25, the core-shell materials of PS@ZIF-8 were formed, in which macroporous PS core were decorated by a shell of ZIF-8 nanoparticles. The resulting size of ZIF-8@PS hollow microcapsule was 41 ± 13 μm with the shell thickness of 1.8 μm. When decreasing the amount of monomers to the mass

ratio (ZIF-8:monomers) of 1:1.25, the thickness of the ZIF-8@PS shell was reduced to 1.0 μm. The generality of this synthetic protocol was demonstrated by the incorporation of MIL-101(Cr) ($Cr_3(\mu_3\text{-}O)OH(bdc)_3(H_2O)_2$) or UiO-66 ($Zr_4O_4(OH)_4(bdc)_6$) nanocrystals, instead of ZIF-8 particles, into the PS membrane with maintaining the hollow superstructures. The characteristics of this strategy defined by the usage of preformed MOF nanocrystals would give a large benefit for the usage of various MOF system, compared to the in-situ formation of MOF crystals, which is highly disturbed by the reaction system. The ability to keep molecules in hollow cavity was demonstrated by the incorporation of large dye molecules of oil red O (ORO). Compared to the PS shell itself that released 80% of ORO from the cavity after 12 h, the ZIF-8@PS composite shell only released 9.7% of dye. This observation indicates that the ZIF-8-polymer interface is largely free of major defects.

By contrast to the two-step procedure, Zeng, Eddaoudi and co-workers demonstrated a one-step synthesis of hollow superstructures based on Fe-soc-MOF, $[Fe_3O(abtc)_{1.5}(H_2O)_3](NO_3)(H_2O)_3$ (abtc = 3,3',5,5'-azobenzenetetracarboxylate).[35] The key for success is to add the emulsifier of tween-85 (polyethylene (20) sorbitan trioleate) into the reaction solution for the synthesis of the Fe-soc-MOF nanocrystals. This synthesis is namely divided into the following processes. First, the emulsion was formed by vigorously stirring the mixture at the room temperature with the assistance of tween-85. Monodispersed Fe-soc-MOF cubes were generated after heating the mixture at 120 °C for 40 min in the presence of *tert*-buthylamine, followed by the spontaneous assembly of the pre-synthesized cubes at the interface of the spherical droplets to form monolayer MOF shells. Indeed, when using PVP (polyvinylpyrrolidone) instead of tween-85, monodispersed MOF cubes were obtained as the same authors described the synthesis of size-controlled nanocrystals of indium or gallium analogous frameworks.[36] By controlling the amount of tween-85, the size of resulting hollow superstructures changed; large hollow spheres (10-20 mm) was obtained by adding 0.01-0.03 mL of tween-85 and small spheres (3-5 mm) for 0.05 mL of tween-85. In both cases, the uniqueness of this synthesis is to produce beautiful monolayer shell structures.

The similar molecular template approach but at the gas-liquid interface was demonstrated by Zhang and co-workers.[37] The successful synthesis of hollow superstructures of $Zn_3(btc)_2$ framework was reported at a CO_2-ionic liquid interface of CO_2 bubble. When applying a high pressure of CO_2 (more than 4.1 MPa) into the reaction mixture of $Zn_3(btc)_2$ in 1,1,3,3-tetramethylguanidine trifuluoroacetate with a surfactant of N-ethyl perfluorooctylsulfonamide (N-EtFOSA), the hollow MOF tetrahedra were obtained. Interestingly, without the surfactant of N-EtFOSA, the morphology of superstructures changed to the spherical shape. This method has an advantage to easily remove the CO_2 bubbles by simply reducing the pressure to ambient pressure.

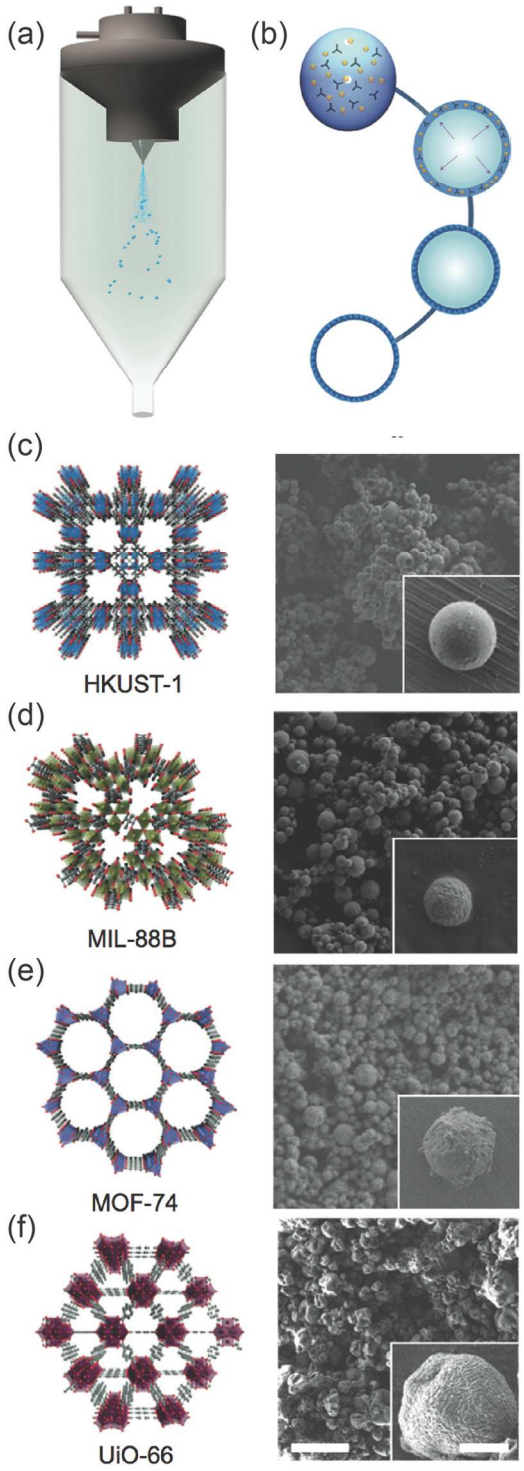

Figure 5. (a) Schematic showing the spray-drying process used to synthesize HKUST-1 superstructures. Blue dots, sprayed solution; blue spheres, formed spherical superstructures. (b) Proposed spherical superstructure formation process (emphasized by purple arrows), which implies the crystallization of nanoMOF crystals. Within a droplet, the MOF precursors (metal ions, orange; spheres and ligands, tri-rods) concentrate and crystallize at the surface into spherical superstructures. Some of synthesized MOFs, (c) HKUST-1, (d) MIL-88B, (e) MOF-74, and (f) UiO-66. Scale bars: 10 μm, 2 μm (inset). Adapted from ref. 38 with permission © 2013 Nature Publishing Group.

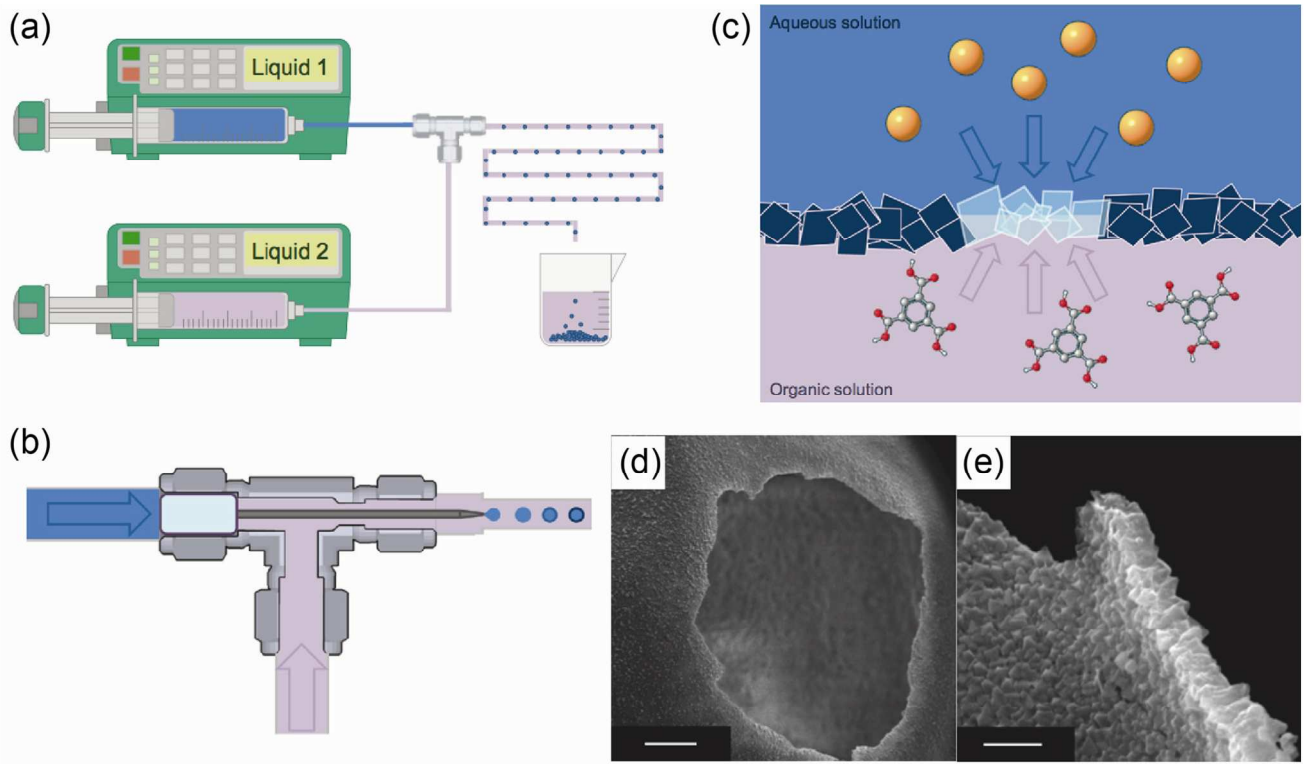

Figure 6. (a) Overview of the process of liquid-liquid interfacial reaction. Both immiscible liquids are supplied by syringe pumps to a T-junction, where the formation of aqueous solution droplets in the continuous organic phase takes place. The capsule shell (dark blue) is formed at the liquid–liquid interface while these droplets travel through hydrophobic tubing, before collection in ethanol takes place. (b) Cut-away view of the T-junction showing details of the emulsification step. The metal-ion-containing aqueous solution (blue) flows through a tapered capillary centred in the tubing, and the ligand-containing organic solution (purple) flows around it. (c) Interfacial preparation of a MOF layer using a biphasic synthesis mixture consisting of an aqueous metal-ion-containing solution (blue) and an organic ligand solution (purple). Crystallite formation takes place primarily at defects remaining in the layer, resulting in self-completing growth. (d) SEM image of capsule crushed with a needle tip showing its hollow interior. Scale bar, 25 μm. (e) Cross-sectional view of the capsule wall, showing its thin and uniform thickness. Scale bar, 2 μm. Adapted from ref. 39 with permission © 2011 Nature Publishing Group.

3.4. Reaction confinement by evaporation.

The elegant example of the shaping of MOF into the hollow superstructures was demonstrated by confining the crystallization of MOFs using evaporation process. Maspoch and co-workers demonstrated a spray-drying method to produce hollow superstructures of a variety of MOFs (Fig.5).[38] This method allows for the confinement of the MOF reaction in microdroplets, in which all precursors are embedded. By inducing the solvent evaporation in the microdroplet, the precursors are radially diffused to the droplet surface and are concentrated at the surface region. Once the concentration reaches the critical value, the MOF crystallization occurs at the droplet surface and the resulted crystals are accumulated to form a hollow superstructure. This method is quite general as evidenced by the fabrication of a variety of MOF hollow structures, including $Cu_3(btc)_2$ (or HKUST-1), Cu(bdc), NOTT-100 (Cu_2(bptc), bptc = 3,3',5,5'-biphenyltetracarboxylate), MIL-88A (Fe_3O(fumarate)$_3$), MIL-88B-NH_2 ($Fe_3O(NH_2$-bdc$)_3$, NH_2-bdc = 2-amino-1,4-benzenedicarboxylate), MOF-14 ($Cu_3(btb)_2$, btb = 4,4',4"-benzene-1,3,5-triyl-tribenzoate), MOF-74 (or also known to be CPO-27; M_2(dhbdc), M = Zn(II), Mg(II), and Ni(II), dhbdc = 2,5-dihydroxy-1,4-benzenedicarboxylate), UiO-66, ZIF-8, MOF-5 ($Zn_4O(bdc)_3$), IRMOF-3 ($Zn_4O(NH_2$-bdc$)_3$). The sizes of these hollow structures are in the range of a few μm. Note that the size could be miniaturized down to the submicrometer scale by the implementation of advanced instrumentation.

Such a technology-based system allows for the modification of mixing condition by the improvement of instrumentation. The usage of a three-fluid nozzle system at the inlet indeed provides an opportunity to incorporate another material into the hollow superstructures simply by addressing another liquid containing functional species into the reaction solution of MOFs. The synthesis of composites of iron oxide@$Cu_3(btc)_2$ was successfully demonstrated and the composite was used for the extraction of molecule by a magnet.

3.5. Liquid-liquid interfacial reaction.

As described above, the confinement of reaction at the interface of droplet is one of the elegant strategies to form hollow superstructures.[38] Indeed, biphasic system is a promising method to easily form such interfaces. However, all the cases described above, the mixture of precursors is introduced into one phase and the other phase works rather as a template. Since all MOFs are basically constructed by two main components, metal ions and organic ligands, one way to fully take this

advantage is to separately dissolve components into each phase; for instance, metal ions in water and organic ligands in organic solvent. Hence, the coordination reaction only occurs at the interface between two phases.

De Vos and co-workers demonstrated a very beautiful method to form hollow spheres using this strategy.[39] Note that this was a first example of MOF hollow superstructures. A water phase containing copper(II) ions were introduced into an organic phase of 1-octane containing H_3btc. Since these phases are immiscible, the injection of water by a syringe produces the water droplet in organic phase under the continuous flow. The components encounter and react with each other only at the interface of two immiscible phases, leading to the formation of hollow structures of $Cu_3(btc)_2$ with maintaining the droplet spherical shape. The size of hollow capsules would be controlled by adjusting the ratio of the inner and outer flows, thus the injection speed of each phase. The lower limit of the size of hollow spheres in the current system was 375 ± 15 μm in diameter and the thickness of the MOF layer was 1.5-2 μm. The delineation of the interfacial layer strongly influenced on the thickness of the resulting material. By adding ethanol to the aqueous droplets, the liquid-liquid interface becomes les well-defined as the ethanol diffuses out. As a consequence, the reaction between the precursors is less strictly confined to a thin layer, leading to the formation of thicker MOF layer (4 μm).

3.6. Top-down processing.

Compared to the above-mentioned assembling strategies, this section focuses on top-down etching processes, in which the pre-synthesized MOF crystals are partially dissolved and are transform into zero-dimensional architectures. Eswaramoorthy, Maji and co-workers demonstrated the transformation from the cubic crystal morphology of M(squarate)(H_2O) (M = Co(II), Zn(II) and Cd(II)) to a unique cubic cage-like architecture by selective etching of the {100} facets.[40] The reaction of metal hydroxide, M(OH)2, with squaric acid and PVP as a capping agent at 180 °C yielded the M(squarate)(H_2O) framework. After 24 h reaction, the cubic crystal with the size of a few μm was observed. Extension of the reaction time to 48 h showed the sign of holes sprouting out from the faces of the cubes. When elongating the reaction to 96 h, perfectly symmetric shape assisted cubes to cages were obtained. However, the cage was broken down upon further continuing the reaction to 120 h. Because the other metal precursors, such as nitrates, chlorides, or acetates, did not give such a cage-like architecture, hydroxyl ions present in the reaction medium play a crucial role in etching the faces.

4. One-dimensional superstructures

The structuring of nanoparticles into one-dimensional (1D) assemblies is an emerging area of research, not only providing a bridge between the nanoscale world and meso- or macroscale objects, but also holding great potential in photonics, optoelectronics, magnetic devices, sensing and biotechnology applications. A variety of strategies towards the assembly of inorganic nanoparticles have been successfully investigated, either by bottom-up, templated approaches or via top-down template-free structuring.[41] However, although tremendous progress has been achieved over the past few years in controlling the crystal size of metal-organic frameworks in the nanoscale, except for a very limited number of reports, their one-dimensional assemblies remain largely unexplored.

Here we introduce the synthetic approaches of 1D MOF assemblages or composites according to the categories described in Section 2.

4.1. Macrostructural templates.

A straightforward bottom up approach to achieve 1D structuring of metal-organic frameworks in the meso-macroscale involves the use of structured templates that can favour a heterogeneous nucleation process and direct the MOF crystal growth in a desired direction. Cui and co-workers used preformed macrostructural templates to create 1D heterostructures consisting in silica nanowires (SiNWs) coated with a porous MOF shell.[42] As depicted in Fig. 7a-c, the 1D core-shell composites were achieved by a step-by-step procedure using successive deposition of metal ions and organic ligands on the surface of the silica nanowires. Inspired from the layer-by-layer growth of MOFs onto two-dimensional substrates, (see Section 5, 2-D superstructures) this approach usually requires a suitable surface-functionalization of the template to induce chemical interaction with the framework components and thus to favour the heterogeneous nucleation process. In this work, SiNWs were first functionalized with carboxyl groups, then alternatively soaked in an ethanol solution of copper acetate and ethanol solution of 1,3,5-benzenetricarboxylic acid (H_3btc), at room temperature. After 40 cycles, X-ray photoelectron spectroscopy (XPS) and X-ray diffraction (XRD) analysis confirmed the formation of a crystalline shell of $Cu_3(btc)_2$ around the SiNWs. Transmission electron microscopy (TEM) observations support a layer-by-layer growth mechanism of the polycrystalline shell, since the thickness increases of 2-3 nm every cycle, which is in the order of the unit cell dimension. Importantly, when the step-by-step procedure was performed on SiNWs without surface modification, only non-uniform coatings could be achieved, even after a larger number of growth cycles. As observed for planar substrates, the surface functionality of the nanostructured template is crucial for an optimal growth of the framework. It is worth mentioning that in this example, the choice of the metal precursor is not trivial since copper acetate has been known to promote a much faster nucleation compared to the more commonly used copper nitrate.[43,44]

Preformed carbon nanofibers (CNF) were also used as a one-dimensional structuring template. Kurungot, Banerjee and co-workers have recently achieved the one-dimensional confinement of MOF nanocrystals in the cavity and on the outer walls of CNF (Fig. 7d-f).[45] In a typical procedure, zinc salt and H_2bdc were first sonicated in the presence of CNF and then reacted under classical MOF-5 synthetic conditions. As revealed by XRD, the CNF have a structure-directing effect and

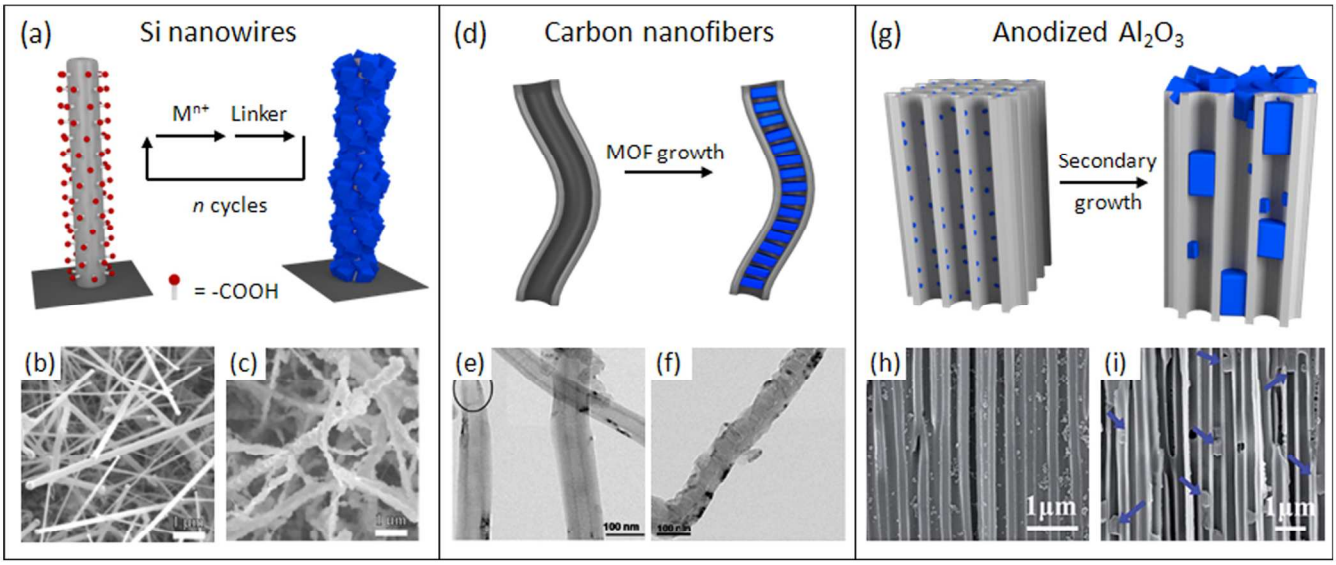

Figure 7. (a) Schematic of the synthesis of HKUST-1 on SiNWs by using step-by-step (SBS) growth. (b) SEM images of as-grown SiNWs and (c) HKUST-1-coated SiNWs after 40 cycles of step-by-step growth. Adapted with permission from Ref. 42. Copyright© 2011 Springer Verlag. (d) Scheme of the preparation of hybrid MOF@CNF using pristine CNFs. (e) TEM images of pristine CNFs and (f) MOF@CNF with one-dimensionally stacked MOF-2 nanocrystals in the inner cavity of the fibers. Adapted from Ref. 45 with permission from The Royal Society of Chemistry. (g) Illustration of the confined secondary growth of ZIF-8 crystal in the macroporous AAO. (h) SEM images of AAO after in situ seeding of ZIF-8 and (i) after a secondary growth process. Adapted from Ref. 50 with permission from The Royal Society of Chemistry.

induced the formation of the thermodynamically less stable MOF-2 (Zn(bdc)) phase, instead of the expected MOF-5 ($Zn_4O(bdc)_3$). Though this structure-directing effect is not fully clarified, it occurs with a fraction of CNF as low as 1 %. HR-TEM images of the MOF-2@CNF composite unambiguously revealed the one-dimensional stacking of MOF-2 nanocrystals in the entire length of the inner cavity of the fibers, while the outer walls remained unaltered. Interestingly, when CNF were treated with hydrogen peroxide to introduce functional groups on their walls prior the reaction with MOF precursors, the resulting hybrid material showed additional MOF-2 nanocrystals immobilized on the outer surface of the fibers. XPS analysis of the composite suggests a direct linkage between the functionalized CNF and zinc ions from the MOF-2 framework, highlighting the importance of the surface functionalization process. Finally, in addition to improved thermal stability, the MOF-2@CNF composite also presented significant increase in the H_2 and CO_2 gas uptake, compared to the pristine MOF-2.

In contrast to the 1D preformed macrostructural template, 1D macrostructural voids also worked as a template to fabricate the 1D MOF architectures wherein. This has been demonstrated by Sutter and coworkers who immobilized $Cu_3(btc)_2$ crystals into the 1D macroporous channels of anodized aluminium oxide (AAO).[46] Although several groups had already used AAO as a substrate for the fabrication of MOF-based membranes,[47-49] intended for separation applications, this is the first report where particular attention has been paid to optimize the crystal growth within the 1D macropores of AAO. Indeed, reactions under typical solvothermal conditions usually lead to the formation of dense layers of MOFs on the surface of AAO, but almost no crystals grow within the macropores, due to their rapid occlusion during the early stage of MOF formation. To tackle this issue, Sutter and coworkers developed a dynamic step-by-step procedure, in order to force the solutions of precursors to flow through the AAO channels. Under optimized reaction conditions and cycles, submicrometer crystal of $Cu_3(btc)_2$ were grown all over the length of the channel of an AAO membrane. Alternatively, Wang and co-workers proposed an *in situ* seeding method to prepare ZIF-8/AAO composite membranes.[50] Following the soaking of the AAO support in a ZIF-8 precursor solution, ammonium hydroxide was added to accelerate the deprotonation of the imidazole ligand. This induced the rapid formation of ZIF-8 nanocrystals (20 nm), which were homogeneously distributed along the macroporous walls of AAO. Those nanoparticles then acted at seeds during a secondary growth procedure, which afforded defect-free ZIF-8 layers plugged on both side of AAO. Interestingly, cross-sectional SEM images reveal the presence of elongated microcrystals of ZIF-8, with unusual morphologies, unambiguously directed by the 1D macropore structure (Fig 7g-i). Inducing the nucleation of ZIF-8 within the macroporous structure is crucial. Indeed, when the AAO was soaked in a precursor solution that already contained ammonium hydroxide, no seed nanoparticles could be observed in the channels. Moreover the secondary growth process afforded ZIF-8 membranes of poor quality presenting intercrystal gaps, which was reflected by lower performances in gas separation experiments compared to the membranes obtained via the fast *in situ* seeding method.

4.2. Molecular templates.

The induction of anisotropy in the crystal growth of MOFs constitutes another method to fabricate 1D MOF

superstructures. The key to success is the usage of additives that enhance or inhibit the growth in a specific direction. For instance, graphene oxide (GO) nanosheets can be considered as "free standing surfaces", suggesting that they might be used for the templated growth of metal-organic frameworks, if suitably functionalized. Indeed, the intercalation of GO into MOF crystals has been reported,[51] however, its structure directing effect was not clearly evidenced until recently, presumably because the chelating carboxylic groups, while present on the edges of GO nanosheets, are mainly absent from their basal planes. Loh and co-workers modified reduced graphene oxide with benzoic acid in order to introduce carboxylic functions on both sides of the graphene sheets, as confirmed by FTIR spectroscopy.[52] The benzoic acid functionalized graphene (so-called BFG) was then used as structure-directing agent for the heterogeneous nucleation of MOF-5, as depicted in Fig. 8. As confirmed by electron microscopy and X-ray diffraction, the amount of BFG strongly influences the morphology of the resulting BFG@MOF hybrid. At low concentration, sheets of GO intercalate and act as dividers in the MOF crystals, resulting in plate-like structures. However, increasing the BFG content to 5% induces a morphological transition into nanowire, together with changes in the crystallographic phase. SAED pattern suggest an anisotropic growth along the [220] direction of the MOF crystal. Interestingly, these (220) exposed facets also present the highest concentration of Zn_4O clusters, which is consistent with strong interaction with the carboxylic functionalized basal planes of GO. Micro-Raman investigation highlighted the integration of BFG into the nanowires core as well as on their tips. Importantly, the average diameter of the hybrid nanowires, roughly 300 nm, coincides well with the dimension of the graphene nanosheets. The results suggest the potential of free-standing nanosheets for the formation of other anisotropic hybrid MOF structures with adjustable metrics and properties.

Coordination modulation has proven to be a valuable tool to modulate both the size and morphology of MOF crystals, especially in the nano-scale.[44,53] Kitagawa and co-workers reported the first example modulated growth of MOF nanorods by anisotropic oriented attachment.[54] In the pillared-layer type framework $Cu_2(1,4\text{-ndc})_2(dabco)_n$, copper paddlewheels connect 1,4-ndc linkers to form 2D-grid layers. Dabco pillars further coordinate to the axial position of copper along the <001> direction and segregate the 2D layers to form the 3D porous framework. During the synthesis, the addition of a monocarboxylic modulator induces a competition with 1,4-ndc for the coordination to the copper ions, thus inhibiting the crystal growth in the <100> direction. However, the dabco-copper interactions remain unaffected, which results in a dominant crystal growth along the <001> direction and the formation of square-rod shaped nanocrystals. Interestingly, time-course TEM observations clearly suggest that the nanorods with high aspect ratio are formed by oriented attachment of cubic nanocrystals (80 nm). Notably, when pyridine is used in combination with acetic acid, the crystal growth is also altered in the [001] direction (copper-dabco interaction) and cubic nanocrystals are isolated.[55]

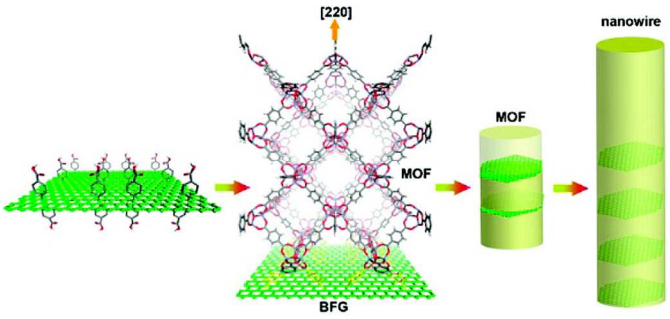

Figure 8. Scheme of proposed bonding between functionalized graphene and MOF via COOH groups along [220] direction and the assembly into nanowire structure with incorporated benzoic acid functionalized graphene. Reprinted with permission from ref. 52 Copyright© 2013 American Chemical Society.

4.3. Liquid-solid interfacial reaction.

Similar to the macrostructural template approach described in the section 4.1, 1D metal oxide material was utilized simultaneously as a macrostructural template and as a reservoir of metal ions to be consumed for the MOF construction. In this method, one of the components for the MOF synthesis, the metal ions, is separately stocked in the metal oxide scaffold and the other counterpart of organic ligand is simply dissolved in the liquid phase. Zheng and co-workers fabricated freestanding as well as vertically standing arrays of metal oxide semiconductor@MOF core-shell 1D heterostructures (Fig. 9).[56] Inspired by the so-called coordination replication approach (the detail discussed in Section 7.4),[57] zinc oxide (ZnO) nanorods not only served as 1D growth templates but also provided the Zn(II) ions during the formation of the well-studied ZIF-8 structure. XRD and TEM analysis unambiguously confirm the formation of ZnO@ZIF-8 nanorods with a core-shell structure. As can be expected from the proposed growth mechanism, the compact MOF shell layer grows at the expense of the ZnO nanorod thickness, which becomes thinner with increasing the reaction time. Fine tuning of the reaction conditions, i.e. solvent composition and reaction temperature, is essential since the formation of the well-defined ZnO@MOF nanorods depends on an appropriate balance between the dissolution rate of Zn(II) ions and their coordination rate with 2-methylimidazole.

The advantageous formation of a microporous shell was demonstrated by applying ZnO@ZIF-8 nanorod arrays as photoelectrochemical (PEC) sensors. Briefly, under UV-excitation the semi-conducting ZnO nanorods generate photoinduced charge-carriers (electrons and holes), which can recombine with each other, or migrate to surface trapping sites and react with redox species, thus generating a photocurrent in a PEC setup. Owing to a well-defined pore structure, the ZIF-8 shell selectively restricted access to the charge-separated states localized on the ZnO semi-conducting core, to molecules with suitable size. As such, the ZnO@ZIF-8 nanorod arrays displayed distinct photoelectrochemical response to hole scavengers with different molecular size (H_2O_2 versus ascorbic

acid). Detection of hydrogen peroxide in serous buffer solution was demonstrated by using this set up.

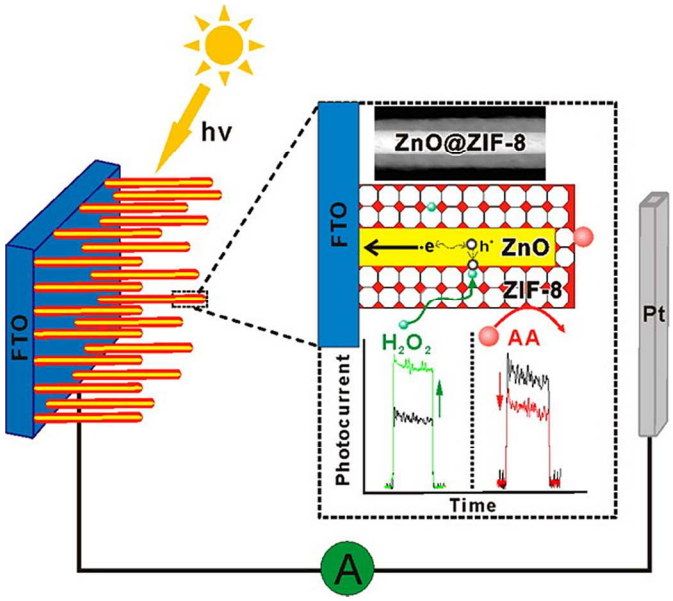

Figure 9. Schematic representation of the H_2O_2 selective PEC sensor obtain from ZnO@ZIF-8 nanorod arrays. Reprinted with permission from ref. 56 Copyright© 2010 American Chemical Society.

4.4. Liquid-liquid interfacial reaction.

"Lab-on-a-Chip" approaches have recently opened up new avenues for the fabrication of 1D-nanostructures.[58,59] In this context, Dittrich and co-workers proposed a microfluidic approach for controlling the assembly between metal ions and organic building blocks to form metal-organic 1D-nanostructures at the liquid-liquid interface.[60] The reactants solutions, injected simultaneously in a microfluidic environment, create a laminar flow which can direct the formation of coordination polymer structures at the interfacial region. Specifically, aqueous solutions of copper nitrate and L-aspartate (Asp) under basic conditions were separately injected in two input channels of a microfluidic device. Diffusion-controlled mixing of the reactant at the liquid-liquid interface induced the rapid formation (within microseconds) of 1D chains of Cu(Asp) as confirmed by X-ray diffraction. Scanning electron microscopy (SEM) observation revealed the presence of bundles of well-aligned nanowires. Varying the flow rate of the reactants solutions did not significantly alter the morphology of the resulting fibers, however increasing the reactants concentration lead to the formation of a Cu(II)-Asp xerogels, which also comprised oriented fibers. This interfacial synthesis was further extended to nanofibers of Ag(I)-cysteine (Cys) and Zn(II)-4,4'-bipyridine (bpy) coordination polymers, again affording bundles of nanosized wires. This elegant andsimple approach has not yet been applied to the preparation porous MOF assemblies, perhaps one limitation being the need for framework systems with very rapid nucleation and crystal growth at room temperature. However, the recent implementation of solvo- and hydrothermal conditions in the microfluidic synthesis of MOFs[61] is promising for the development of a wide range of 1D porous MOF assemblies.

4.5. Top-down processing-electrospinning.

Electrospinning is a straightforward method that allows for an easy generation of nanofibers from a wide variety of compounds. This simple top down approach can be used to create composite materials by confining nanostructured objects along the one-dimensional fibers. Smarsly and co-workers first reported electrospun hybrid PVP (polyvinylpyrrolidone) nanofibers with entrapped ZIF-8 nanoparticles.[62] Homogenous distribution of the filler MOF particles within the organic polymer matrix was achieved by using ZIF-8 nanocrystals with narrow size distribution dispersed in a methanol solution of PVP. As confirmed by SEM observations, the nanofiber diameter could be tuned between 150-300 nm, according to the polymer concentration. MOF loading as high as 50% with respect to the organic polymer matrix could be achieved. As can be expected, the crystal size is an important factor to obtain homogeneous MOF dispersions. Indeed, micrometer-sized MOF particles afford heterogeneous composite morphologies (pearl necklace or spider web morphologies) and are more likely stuck on/in the nanofibers, however their loading can be up to 80%.[63,64] Interestingly, gas adsorption isotherms revealed that the MOF porosity remains fully accessible in the composite fibers, although the adsorption kinetics were somehow decreased compared to pure MOFs, as a result of the polymer coating. By taking advantage of this accessible microporosity, those electrospun MOF composites can be used for adsorption and separation application.

Li and co-workers prepared a nanofibrous mat with embedded MOF nanocrystals and used it as skeleton for the secondary growth of $Cu_3(btc)_2$ or ZIF-8, resulting in free-standing membranes which were applied for N_2/CO_2 separation.[64] Similar to the previous report, ZIF-8@PVP nanofibers were electrospun on a macroporous SiO_2 support which allowed the preparation of a densely packed ZIF-8 membrane after the secondary growth process.[65] Considering the simplicity of the electrospinning technique and the large variety of MOFs obtainable in the nanoscale, numerous applications can be expected for those new composites, as for example the development of functional textiles.[63,66]

Júnior and co-workers have reported the incorporation of lanthanide-based MOFs into polyvinyl alcohol (PVA) nanofibers.[67] The morphologies of the resulting hybrids are rather heterogeneous due to the micrometer size of the Ln/Tb MOF crystals, however the composite materials are highly luminescent, owing the emissive properties of Eu(III) or Tb(III) centers. By modulating the Eu/Tb ratio in the MOF framework, a variety of nanofibers with strong emission ranging from green to red could be obtained.

Kitagawa, Furukawa and co-workers have recently reported a new nanofiber hybrid consisting of core/shell gold nanorod (GNR)@MOF nanoparticles embedded in a polymethylglutarimide (PMGI) matrix.[68] The core-shell structure of this new platform is composed of an individual

GNR core surrounded by an aluminium-based MOF shell Al(OH)(1,4-ndc). This unique structure was obtained via selective deposition of an aluminium oxide precursor onto the surface of GNR, followed by its replication into Al(OH)(1,4-ndc). Interestingly, the combination of the microporous shell and the photothermal properties of GNR core allowed implementing a motion-induced molecular release, owing to the conversion of visible light into thermal energy when GNRs are excited into their plasmon band. The controlled light-induced release was demonstrated with anthracene as a guest molecule. Finally, the core-shell nanoparticles where homogeneously incorporated into PMGI nanofibers as confirmed by TEM and confocal microscopy observations. Considering the biocompatibility of PMGI nanofibers, this work paves the way towards the use of MOF@nanofibers composites as extracellular matrixes for the spatiotemporally controlled release of drug molecules.[69]

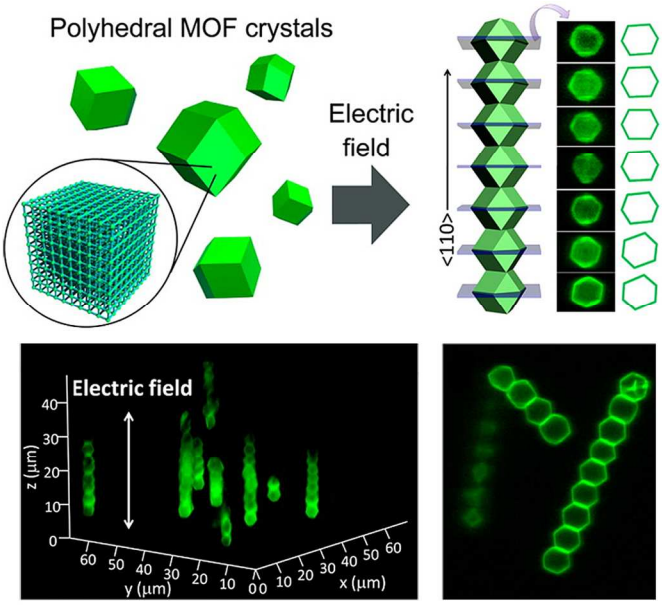

Figure 10. Illustration of the electric field assembly of ZIF-8 microcrystals and typical *in situ* observations of 1-D chains of rhombic dodecahedra along the direction of electric field by confocal microscopy. Reprinted with permission from ref. 70. Copyright© 2013 American Chemical Society.

4.6. Top-down processing-external electrical field.

A unique template-free approach to direct the assembly of polyhedral MOF crystals under electrical field was recently report by Granick and co-workers.[70] First, micrometer-sized crystals of ZIF-8 with narrow size distribution and well-defined polyhedral morphologies were obtain using a combination of coordination modulators (1-methylimidazole and PVP). To allow confocal microscopic visualization, the surface of the crystals was further functionalized with a fluorescent dye.[13,71] As illustrated in Figure 10, applying an electrical field to a ZIF-8 suspension, sandwiched between ITO electrodes, resulted in the formation of one-dimensional MOF arrays. Indeed, the polyhedral particles rapidly attached to one another to form linear chains along the direction of the electrical field. Interestingly, the well-defined rhombic dodecahedra particles reoriented to form almost perfect intercrystal {110} facet-to-facet contacts, which remained locked into place even after external field is removed. If extendable to other type of MOFs, this unprecedented face-to-face linear arrangement might be promising to achieve anisotropic molecular flow along the superstructures.

5. Two-dimensional superstructures: synthesis

Fabrication of two-dimensional MOF assemblies composed of well-intergrown crystals facilitates the integration of MOFs into efficient detection, separation or conduction systems (see Section 6). The impressive number of articles dedicated to the synthesis of MOF thin films, membranes or patterned surfaces published these last few years clearly emphasizes the importance of this research field. As in the case of any other class of functional materials, the fast development of two-dimensional structuration compared to zero- (see section 3), one- (see section 4) and three-dimension (see section 7) structuration can be explained by the easiness with which plane interfaces are created, characterized and implemented into devices. Such structuration dimension is hence more likely to be applied in a variety of different application fields and on a larger scale. The latest developments regarding the synthesis of PCP thin films published since the pioneering work by Fisher and collaborators[72] were recently addressed in comprehensive reviews.[73-75] Here again, synthesis routes to two-dimensional PCP structures can be classified into the six strategies mentioned in Section 2.

5.1. Macrostructural template.

So far, structuration of MOF crystals supported on a hard template was achieved through three main procedures: (i) direct nucleation-growth process, (ii) layer-by-layer (or liquid-phase epitaxy) and (iii) seeding and secondary growth.

5.1.1. Direct nucleation-growth process. This strategy relies on the promotion of the heterogeneous nucleation of MOF at a substrate surface by lowering the interface energy between the crystal being formed and the substrate. The nucleation and growth process is commonly achieved by immersing a substrate bearing the suitable nucleating agents on its surface within reaction solutions containing both metal and ligand precursors.

The simplest case is the use of flat substrates that bear preexistent reactive groups exposed on the surface.[76-78] The basic surface of Al_2O_3 substrates was shown to be suitable for promoting the nucleation of MOF such as $Cu_3(btc)_2$ containing acidic ligands. On the other hand, the acidic surface of SiO_2 substrates was suitable to facilitate the nucleation of MOFs possessing both acidic and basic organic ligands such as $Zn_2(bdc)_2(dabco)$. In this process, the substrate is immersed within the reaction mixture containing the metal cations and the organic ligands and is further submitted to a solvothermal treatment. Although it is easily implemented, this strategy

suffers from the low density of MOF nuclei formed on the solid surface that often leads to the formation of discontinuous membranes composed of poorly intergrown crystals. In order to increase the number of nucleation sites on the solid surface and to improve the strength of MOF attachment onto the support, strategies based on the modification of the solid surface with chemical species capable of trigger MOF nucleation were developed. So far, various nucleating agents were investigated.

Bein and co-workers introduced a strategy based on the deposition of self-assembled monolayers (SAMs) possessing terminal functions capable of mimicking chemical functions involved in the construction of the MOF.[79] SAMs are convenient surface nucleation agents because they can cover a wide variety of substrates (e.g. metals or oxides), they are easy to prepare and they possess various terminal functionalities. SAMs can easily be patterned using microcontact-printing methods, making possible the synthesis of patterned MOF films.[72,80] Furthermore, the organization of SAMs into ordered assemblies resembling a two-dimensional crystalline interface allows for the growth of films with a preferential crystallographic orientation through an epitaxial growth process.[81] Importantly, the orientation of the crystals can be tuned by using different functional groups for surface functionalization. Wöll and co-workers demonstrated the effect of COOH- and OH-terminated SAMs on the orientation of $Cu_3(btc)_2$. Out-of-plane XRD measurements showed that COOH-terminated SAMs lead to (001) oriented $Cu_3(btc)_2$ films, while the OH-terminated SAMs induce a (111) orientation.[43]

The epitaxial nature of the MOF growth process from SAMs was also shown to induce a polymorph selection. Fe(OH)(bdc) possesses two polymorphs, the monoclinic Fe-MIL-53(Fe) and the hexagonal Fe-MIL-88B. The monoclinic Fe-MIL-53 compound is obtained under homogeneous nucleation conditions, while the hexagonal Fe-MIL-88B phase is formed on COOH-terminated SAMs immersed in the same precursor solution. The match between the hexagonal symmetry of SAMs and the hexagonal symmetry of Fe-MIL-88B crystals is assumed to allow such polymorph selection.[82]

Beside the traditional thiol-based SAMs, different other types of SAMs were used. For instance, thick films of $Zn(5abIm)_2$ (ZIF-22; 5abIm = 5-azabenzimidazole)[83] and $Zn(Ica)_2$ (ZIF-90; Ica = imidazole-2-carboxaldehyde)[84-86] were synthesized on metal oxide surfaces modified with 3-aminopropyltriethoxysilane (APTES). The use of glycine assemblies was also recently employed to attach $Cu_3(btc)_2$ films on a palladium surface.[87]

The coverage of the substrate surface with nucleating agents other than SAMs was investigated with success. Falcaro et al. precisely localized MOF-5 crystals by using mineral microparticles both as nucleating seeds and carriers for embedding controlled functionality into MOF crystals.[88] The authors showed that nanostructured α-hopeite microparticles possess exceptional ability to nucleate MOF crystals. In a one-pot synthesis procedure, where a solution contains both the precursors of the α-hopeite microparticles and of the MOF-5, the α-hopeite microparticles formed in the first few minutes of reaction act as nucleating agent on which the heterogeneous nucleation of the crystals occurs. Interestingly, this procedure reduces the MOF-5 synthesis time by 70% when compared with conventional method. The α-hopeite microparticles can be isolated before MOF-5 nucleate and subsequently deposited on a substrate, promoting the formation of dense films or patterns

Qiu and collaborators elaborated a strategy where a poly(methyl methacrylate) (PMMA) membrane is first spin-coated on a solid substrate and then converted into poly(methacrylic acid) (PMAA) *via* a hydrolysis step with sulfuric acid.[89] Carboxylic acid functions accessible on the surface of the PMMA-PMAA layer act as nucleation and anchorage sites for the MOF crystals when the PMMA-PMAA-coated substrate is immersed into MOF precursors.

Jeong et al. selected anodized alumina discs coated with conductive thin films of amorphous carbon or graphite as substrates. Deposition of well-packed MOF-5 crystals on these substrates was performed through a domestic microwave irradiation in 5-30 seconds.[47] In contrast, only few MOF crystals were observed on bare anodized alumina under the same treatment. The authors explained the effect of the surface upon the MOF coverage by considering the difference in the electric and/or dielectric properties between the different substrates used. The authors assumed that the rapid temperature rise at the conductive surfaces (amorphous carbon and graphite) via Joule heating (i.e., electron–phonon interaction) upon the absorption of microwave energy on the surfaces causes a significant increase in the rate of the heterogeneous nucleation. The crystallographic orientation, together with a strong adherence of the MOF crystals observed during sonication tests was explained by the probable generation of carboxylic group on the surface of the graphite sheets under the intense microwave irradiation.

Localization of the nucleation on the substrate was also achieved by the immobilization of one of the MOF precursors on its surface. Jeong and co-workers reported a general method to prepare ZIF membranes based on the modification of α-Al_2O_3 substrates with the imidazolate ligand prior to the growth of the ZIF crystals.[90] An organic ligand solution was dropped on the hot support resulting in strong covalent bonds between the support and the ligand. Both $[Zn(bIm)_2]_n$ (ZIF-7; bIm = benzimidazole) and ZIF-8 films were synthesized under hydrothermal treatment after immersion of the modified substrates in the precursor solution. A gel-layer procedure was developed by Bein and co-workers, where metal salt-containing poly(ethylene glycol) gel layer is deposited on a SAM-functionalized surface.[81] An appropriate solution of either organic ligand was then carefully poured on top of the gel layer and the crystal films were obtained at room temperature through a slow diffusion process.

5.1.2. Layer-by-layer (or liquid-phase epitaxy). The liquid-epitaxial layer-by-layer method (LbL) consists in the sequential combination of the reaction components. The surface of the growing MOF film is repeatedly immersed into separate solutions of the metal precursor and organic ligands with a

washing step between each immersion in order to remove unreacted reactants. The stepwise growth allowed by the LbL method makes possible to achieve well-defined layer thickness or crystallite sizes, together with precisely controlled crystallographic orientation.[91] For a MOF film grown by a LbL with a linear growth mode, the domain size in the growth direction corresponds to the number of applied cycles multiplied by the cell dimension.[92] Interestingly, it has been shown that this linear increase of the layer thickness as a function of the number of immersion cycle takes place only after few initial deposition cycles.[93,94] This delay presumably corresponds to rather disordered nucleation events. The LbL method also offers the possibility of the *in situ* monitoring of the MOF growth with sub-monolayer resolution *via* quartz crystal microbalance technique (QCM) or by surface plasmon resonance spectroscopy (SPR).[43, 95-97] Informations about the LbL process can be found in recent reviews. [98,99]

LbL process was used to grow films of MOFs made of one type of ligand, such as $Cu_3(btc)_2$,[91] and also two different ligands, such as the pillared layer systems of general formula $M_2(L)_2(P)$, where L is a dicarboxylate species and P is a dinitrogen-based pillaring ligand.[100-101] The carboxylate ligands (L) of this isoreticular family are linked into (4,4)-connected 2-D grid-like layers via paddlewheel secondary building units (SBUs), which are further connected with each other by the dinitrogen pillars (P) into 3-D open framework structures of high porosity. Accounting for the generalizability of this method, the LbL approach was also recently employed to grow functional films composed of MOF containing bulky porphyrin or other light-harvesting and catalytic linkers on 3-aminopropyl-trimethoxysilane (3-APTMS)-modified substrates.[102] Kitagawa and collaborators also prepared highly oriented thin films made of the Hofmann-type clathrate MOF, $Fe(pz)[Pt(CN)_4]$ (pz = pyrazine and CN = cyanide).[103]

The efficiency of LbL processes for the synthesis of films with a high degree of crystalline order and orientation as well as smooth surfaces was exploited for the synthesis of heterostructured films composed of one MOF layer grown epitaxially from the surface of a MOF sublayer. Notably, this approach provides a powerful mean to tune the porous properties of MOF membranes and makes possible the integration of two spatially separated functions into one membrane. As shown on Fig. 11, Furukawa, Shekhah, and co-workers synthesized perfectly oriented $Zn_2(1,4\text{-ndc})_2(dabco)$ on $Cu_2(1,4\text{-ndc})_2(dabco)$ thin films by following the LbL procedure.[104] The groups of Furukawa,[105] and Fischer,[106] further developed this strategy and added a post-synthetic modification step of the organic linkers after the heteroepitaxial growth.

Makiura, Kitagawa and co-workers combined the LbL procedure with the Langmuir-Blodgett approach (LB) for the growth of oriented MOFs composed of two-dimensional monolayers.[107-109] In this approach, $Cu_2(CoTCCP)(Py)_2$ nanosheets composed of cobalt-containing porphyrin units (CoTCCP = 5,10,15,20-tetrakis(4-carboxyphenyl)-porphyrinatocobalt(II)) linked together by binuclear copper paddle-wheel units containing pyridine (Py) as coordination-saturating ligands were formed by means of LB and subsequently transferred from the liquid subphase to a solid substrate. The successive repetition of this procedure (LbL growth) resulted in the formation of an oriented film named "nanofilm of metal-organic frameworks on surface" (NASF-1). Notably, this procedure allows for the fine-tuning of the overall thickness of the film by adjusting the number of deposited layers.

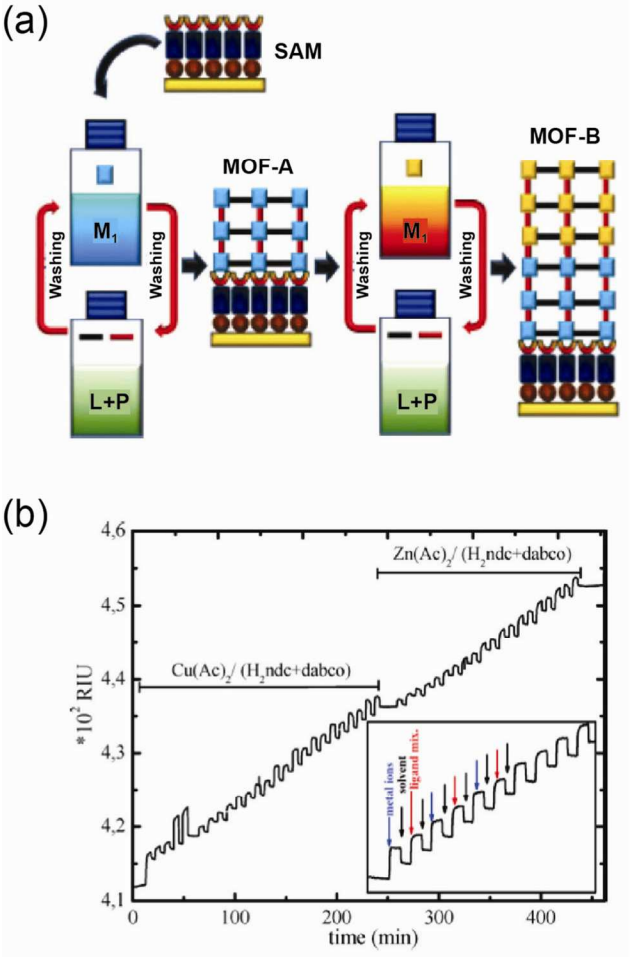

Figure 11. (a) The layer-by-layer method for the heteroepitaxial growth of MOF thin films. The sample is repeatedly immersed in solutions of the metal precursor (M1) and the organic linker mixture (L + P) to fabricate thin films of MOF-A. After several cycles, the fabricated thin film is repeatedly immersed in solutions of the metal precursor (M2) and the organic linker mixture (L + P) to fabricate thin films of MOF-B). (b) Surface plasmon resonance (SPR) signal as a function of time recorded in situ during the step-wise treatment of a SAM with $Cu(OAc)_2$ and a mixture of H_2ndc and dabco, and $Zn(OAc)_2$ and mixture of H_2ndc and dabco. Adapted from Ref. 104 with permission from The Royal Society of Chemistry.

5.1.3. SEEDING AND SECONDARY GROWTH. This strategy is based on the decoupling of the MOF nucleation and growth steps. First, a MOF seed layer is deposited on the surface of a substrate, which is subsequently immersed into a dilute solution containing the MOF precursors. The decoupling facilitates the control of the nucleation site location and of their density. It also decreases the importance of the nature of the substrate, making the strategy applicable to wide range of supports. This strategy relies on the impregnation of the substrate surface with

an aged precursor solution containing the MOF seeds.[110-118] Deposition of the seeds is commonly achieved by spin-coating, rubbing, dip-coating or by the infiltration of the seed suspension within the pores of the substrate. Gascon et al. spin-coated on α-alumina porous supports a slurry composed of cross-linked one-dimensional Cu(II)-btc coordination polymers, priory obtained by the modification of the original $Cu_3(btc)_2$ recipe.[119] A dense coating of $Cu_3(btc)_2$ crystals with no preferred orientation was obtained after a second step under hydrothermal conditions in the presence of the MOF precursors. Li et al. recently reported an original method for the deposition of seeds based on an electrospinning process as described in the section 4.5.[64] In this method, spinnable solutions containing $Cu_3(btc)_2$, ZIF-8, $Fe_3(\mu_3\text{-}O)OH(bdc)_3(H_2O)_2$ (MIL-101(Fe)) or the luminescent $Zn_2(bpdc)_2(bpee)$ (bpdc = 4,40-biphenyldicarboxylate and bpee = 1,2-bipyridylethene) crystal seeds dispersed into a polystyrene (PS) or polyvinylpyrrolidone (PVP) solution were randomly deposited on a substrate as nanofibers via electrospining process. A film made of well-intergrown crystal is obtained after few secondary growth cycles (Fig. 12). $Eu(btc)(H_2O)$ thin films were also recently prepared by a similar method.[120]

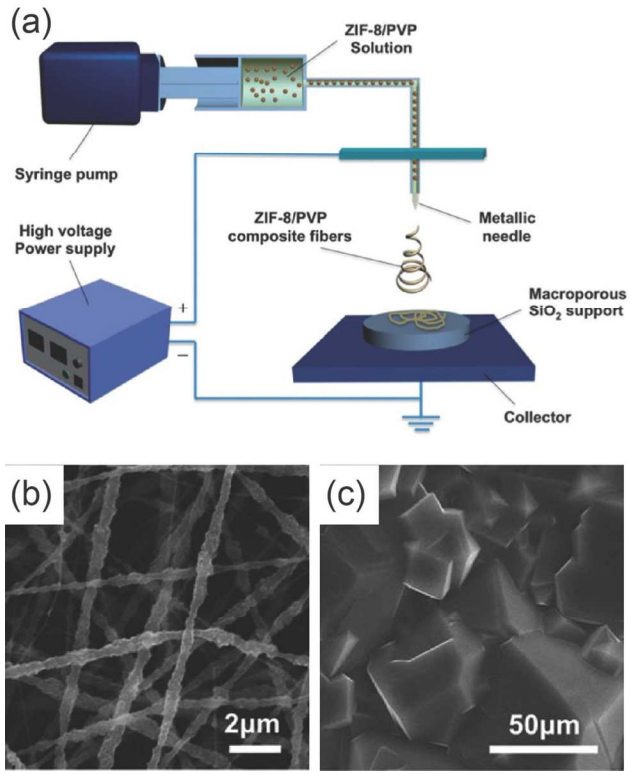

Figure 12. (a) Schematic diagram of the electrospinning process for the support (macroporous SiO_2 wafer) seeding. SEM images of (b) the PVP nanofibers containing ZIF-8 crystals and (c) the ZIF-8 membrane obtained after the secondary growth. Adapted from Ref. 64 with permission from The Royal Society of Chemistry.

5.2. Reaction confinement.

In this strategy, the solution of MOF precursors is used as ink. After its deposition on a substrate in a spatially controlled fashion, the evaporation of the solvent under controlled temperature lead to the heterogeneous crystallization of the MOFs. The success of this procedure relies on two critical parameters: (i) the nature of the solvent, which must stabilize the MOF precursors and imposes a crystallization process exclusively driven by the evaporation of the solvent and (ii) the wettability of the substrate. The latter parameter is critical since it determines the structural characteristics of the final MOF-based materials. Surfaces with low wettability are suitable to confine the crystallization within small droplets and hence to synthesize MOF single crystal with a patterned disposition. In contrast, surfaces with high wettability are suitable to homogeneously disseminate the precursors over the substrate in view of synthesizing continuous MOF films.

De Vos and co-workers spatially organized $Cu_3(btc)_2$ small single crystals on a microscope cover glass by using a process called "lithographically controlled wetting".[121] This process consists in placing a stamp inked with the precursor solution in contact with a surface. Because of the capillary force, the precursor solution remains in between the PDMS stamp protrusion and the glass surface. Importantly, the authors replaced water and ethanol as solvent by the dimethyl sulfoxide (DMSO) in order to prevent the crystallization of $Cu_3(btc)_2$ at room temperature and to impose the evaporation of the solvent as the main driving force for nucleation. Crystallization of single crystals of the same size occurs in the confined space of each droplet. A common preferred orientation, most likely imposed by the confinement between the stamp and the substrate, was demonstrated.

Following a similar concept, Maspoch and co-workers synthesized single-crystal $Cu_3(btc)_2$ arrays by using a pen-type lithography technique, namely the fluidic-enhanced molecular transfer operation (FEMTO).[122,123] One advantage of this method compared to the "lithographically controlled wetting" described previously is that it enables the creation of any desired pattern in a given experiment without the need for prefabricated stamps. Microdroplets of $Cu_3(btc)_2$ precursor solubilized in DMSO were brought into contact with gold surfaces functionalized with SAMs terminated with various functionalities (Fig. 13). Contact angle between the DMSO precursor solution and the surface were systematically studied to determine the affinity and wettability of the surface with the solution. CH_3- and CF_3-terminated SAMs proved to be ideal for the fabrication of well-defined droplet arrays, whereas these arrays could not be fabricated on the OH- and COOH-terminated SAMs. The DMSO precursor solution partially spread out on the NH_2-terminated SAM. Interestingly, the authors found that the terminal group on the top of the SAMs, were critical in determining the number and dimensions of the $Cu_3(btc)_2$ crystals grown within each droplet. Surfaces with lower wettability such as CF_3-terminated SAM made possible the creation of well-defined single-crystal $Cu_3(btc)_2$ arrays. A crystal growth preference along the [111] direction was

determined using XRD for both the NH_2- and CF_3-terminated SAMs.

Tertfort and co-workers used inkjet printing to controllably spread a stable MOF precursor solution on various substrates.[124] Here again, the authors focused on the deposition of $Cu_3(btc)_2$. Due to the crucial role of the viscosity and surface tension of the ink for the inkjet printing process, the authors added ethylene glycol (EG) within the previously reported DMSO precursor solution. Both continuous films and patterned surfaces were prepared. The generality of the approach was demonstrated by synthesizing other types of MOFs such as $Zn_2(adc)_2(dabco)_2$.

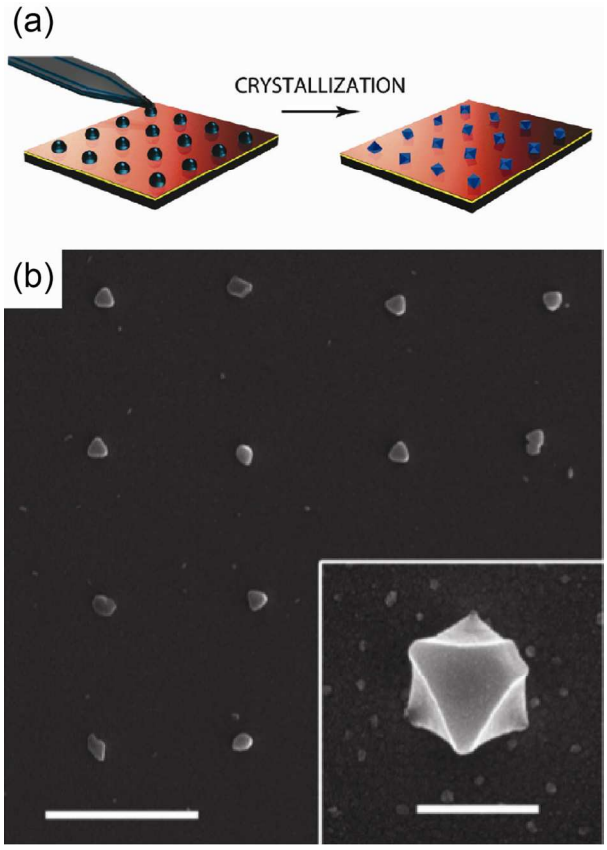

Figure 13. (a) Illustration of the direct-write pen-type lithographic approach. (b) Field-emission scanning electron microscopy (FE-SEM) image of a single-crystal HKUST-1 array composed of crystals with edge dimensions of 550 (scale bare = 5 μm, and (inset) 500 nm). Reprinted with permission from ref. 122 Copyright© 2011 American Chemical Society.

Jeong and collaborators synthesized continuous membranes made of $Cu_3(btc)_2$ and ZIF-8.[125] Porous supports were soaked with a MOF precursor solution and subjected to elevated temperature. In this method, rapid solvent evaporation from the supports drives the flow of the precursor solution from inside the supports to outside and crystallization occurs simultaneously inside and outside the supports.

Atomic layer deposition was also employed to localize both metal source and organic ligands at the surface of a support and hence confine the MOF crystallization.[126] In this strategy, zinc acetate and bdc ligands were evaporated at 190°C and 220°C and pulsed with inert gas valving. The precursor films were then crystallized for 12 h in a humidity-controlled chamber at a relative humidity of 60% followed by recrystallization with DMF in an autoclave at 150°C for 120 min. A continuous film was obtained by repeating the ALD process on a same sample after the DMF recrystallization step. The thickness of the films could be controlled by the number of deposition cycles.

5.3. Sacrificial template.

In this method, the surface of the substrate provides the metal cations required for the formation of the MOF crystals through its partial or total dissolution.

The partial dissolution of the substrate surface was first used to induce the formation of a dense layer of seeds in order to grow uniform MOF films through a two-step process. The seed formation is first achieved by bringing the substrate in contact with a solution of organic ligands under solvothermal conditions. This step is then followed by a step of secondary growth where the reactive substrate is immersed within a reaction solution containing both the ligands and a second metal source. This "reactive seeding" procedure was pioneered by the group of Qiu who synthesized a $Cu_3(btc)_2$ film by utilizing a copper net both as support and copper ion source for the formation of the MOF seeds.[127] After a first step of oxidation, the partially oxidized copper net was introduced into a water/ethanol solution of copper nitrate and H_3btc and then placed under solvothermal conditions for three days resulting in a defect free $Cu_3(btc)_2$ membrane. The "reactive seeding" procedure was also applied with hydroxides and oxides as substrates. Peng et al. synthesized $Cu_3(btc)_2$ films by employing copper hydroxide nanostrands (CHN) deposited on a porous anodic alumina oxide membrane.[128] $Cu_3(btc)_2$ seeds were grown on the CHN immersed in a H_3btc solution at room temperature. The seeded substrate was then placed in an ethanol/water mixture of both the metal and the organic linker. A film composed of well-packed $Cu_3(btc)_2$ crystals supported of the alumina substrate was obtained after one day of secondary growth at 120°C. The group of Jin used porous alumina substrates to synthesized Al(OH)(bdc) (MIL-53)[129] and $Al_{12}O(OH)_{18}(H_2O)_3(Al_2(OH)_4)(btc)_6$ (MIL-96).[113] ZnO supports were also recently utilized for the preparation of homochiral $Zn_2(bdc)(L\text{-}lac)(DMF)$[130] (L-lac = L-lactate) and Zn(nbIm)(nIm)[131] (ZIF-78; nbIm = 5-nitrobenzimidazolate and nIm = 2-nitroimidazolate) membrane.

Recently, substrates were also used as the only source of metal ions through their partial or total dissolution. In this up-to-date version of the "reactive seeding" strategy, formation of the crystalline MOF film is achieved in one step without the requirement of any metal salts as a second source of metal ions. This strategy is considered as cost-efficient and environmentally friendly since, in contrast to the "reactive seeding", it does not require the use of any salts as secondary metal source.

Qiu and collaborators first synthesized a film of $Zn_3(btc)_2$ onto a zinc wafer.[132] Surface of the zinc slices were first oxidized in hydrogen peroxide solution in ordered to form a soluble zinc hydroxide coating. The activated zinc wafer was

then placed in the presence of H_3btc and treated under hydrothermal conditions for 24h at 140°C. The recovered MOF film was composed of a uniform array of rod-like crystals firmly anchored on the substrate and was used as volatile organic compounds (VOCs) sensor. The same group applied a similar procedure for the formation of $Ni_2(L\text{-asp})_2(bpy)$ (L-asp = L-aspartate and bpy = 4,4'-bipyridine) films through the partial dissolution of nickel nets (Fig. 14).[133]

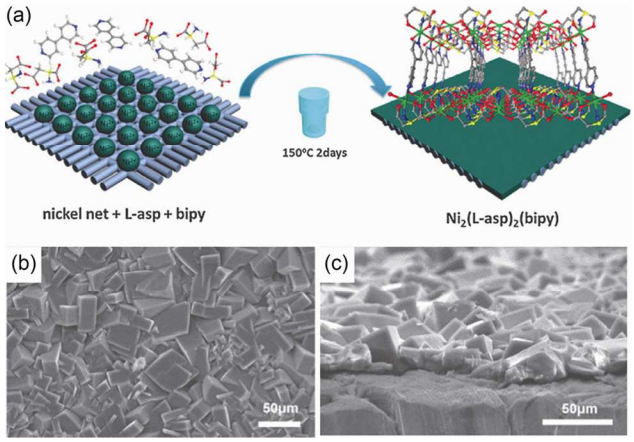

Figure 14. (a) Illustration of the synthesis procedure followed to produce $Ni_2(L\text{-asp})_2(bpy)$ films using a nickel net as only metal source. (b) SEM image of the $Ni_2(L\text{-asp})_2(bpy)$ films. (c) A cross-section SEM picture of the $Ni_2(L\text{-asp})_2(bpy)$ membrane. Adapted from Ref. 133 with permission from The Royal Society of Chemistry.

De Vos et al. partially converted copper anodes into supported $Cu_3(btc)_2$ films *via* an electrochemical synthesis procedure.[134,135] The electrochemical dissolution of the copper anode released the copper ions into the solution containing H_3btc. Varying the water content of the solution as well as the voltage and frequency of the applied tension allowed the modulation of the thicknesses and the degree of intergrowth of the films. The same authors also developed an original approach to grow $Cu_3(btc)_2$ films based on galvanic displacement.[136] A solution of H_3btc ligands and silver nitrate in DMSO was first deposited onto a copper-coated substrate. Solvent was then evaporated during a heating treatment at 80°C. Copper ions necessary for the construction of the $Cu_3(btc)_2$ were produced through a replacement process during which metallic silver were reduced to metallic silver.

Falcaro et al. converted copper plates and nets into $Cu_3(btc)_2$ films by applying a two steps procedure, where copper hydroxide nanotubes first prepared from a copper metal surface, were rapidly converted into $Cu_3(btc)_2$ crystals through a dissolution-recrystallization process.[137] Peng et al. synthesized HKUST-1 free-standing membranes on centimeter scale at room temperature by using free standing copper hydroxide nanostrand (CHN) films as sacrificial substrates.[138]

Furukawa, Kitagawa and co-workers combined sol-gel processes and pseudomorphic replacement process[139] to replicate pre-shaped alumina phase into MOF-based mesostructures.[57] Following a similar approach, the group of Ameloot recently synthesized films and patterns made of ZIF-8 crystals in the absence of any solvent.[140] The authors covered pre-shaped zinc oxide sacrificial films or patterns with a finely ground 2-methylimidazole (HmIm) powder and then placed it in an oven at the HmIm melting temperature. During the melting process the excess liquid HmIm quickly wetted the complete surface, leading to a homogeneous reaction with the precursor film. Notably, the combination of sol-gel technology and replication processes makes possible the design of MOF patterns by adjusting both the localization and the amount of metal centers deposited on the substrate during the sol-gel procedure.

5.4. Liquid-Liquid interface.

This approach relies on the utilization of a liquid-liquid biphasic synthesis mixture, each phase containing one of the two MOF precursors. In this approach, MOF crystallization takes place only at the liquid-liquid interface, where the different precursors or reagents come into contact through a diffusion phenomenon. The interface between the two solutions acts as a template for the formation of a continuous and well-defined MOF membrane.

De Vos and collaborators synthesized thin films of $Cu_3(btc)_2$ and ZIF-8 by layering a 1-octanol solution of the organic linker on top of an aqueous solution of metal precursor.[39] Crystallization occurred at the interface of the two immiscible solvents at room temperature and continuous films were recovered.

The group of Wang developed a method based on biphasic systems to promote the crystallization of ZIF-8 on porous nylon membrane.[141,142] In this strategy, two methanol or water solutions, each containing one of the two ZIF-8 precursors, are placed on both side of a nylon membrane. Porous nylon membrane acts as the substrate for ZIF-8 film growth. It also separates the linker (HmIm) solution and zinc nitrate solution, leading to a concentration gradient of HmIm and Zn(II) near the surface of the nylon membrane. This concentration gradient gave the high local molar ratios of HmIm/Zn(II) beneficial for ZIF-8 crystallization.

Hara and co-workers covered the surface of porous α-alumina supports with a $Cu_3(btc)_2$ membrane by a similar procedure, where a copper(II) nitrate trihydrate aqueous solution and an ethanol H_3btc solution were placed at each side of the porous support.[143] Zhu et al. synthesized free-standing membranes composed of the zinc-bdc-based MOF frameworks MOF-5, Zn(bdc)(DMF) (MOF-2), $Zn_3(OH)_2(bdc)_2$ (MOF-69c) and $Zn_5(OH)_4(bdc)_3$ at a DMF-hexane interface.[144] In this works, the MOF precursors, $Zn(NO_3)_2$ and H_2bdc were dissolved in DMF, whereas triethylamine (TEA), used as deprotonating agent, was dissolved in a hexane phase. Formation of well-defined membranes was determined by both precursor and TEA concentration. High precursor and low catalyst concentrations yielded well-defined and asymmetric membranes. One side of the membrane is composed of particulate MOF-5 crystals, while the other side is mainly made of MOF-2 crystals. Two transitional phase, MOF-69c and $Zn_5(OH)_4(bdc)_3$ were identified in between these two layers. This distribution of different MOFs was explained by the

existence of a pH gradient across the membrane inferred by the diffusion of TEA from the DMF phase to the hexane phase.

5.5. Top-down approaches.

Two general top-down procedures were developed for the structuration of MOF crystals so far: (i) the assembly of preformed MOF crystals and (ii) the delamination of single crystals composed of two-dimensional sheets.

5.5.1. Assembly of preformed MOF crystals. Recent progresses in size and shape control of MOF crystals, such as the development of the coordination modulation process,[54] the use of microwave irradiations[145] or microemulsion processes,[146] makes possible the utilization of MOF crystals as mesoscopic building blocks for the construction of 2-dimensional polycrystalline superstructures. Sequential procedures, where the preparation of stable suspensions of crystals is followed by the application of physical microfabrication processes, were recently reported. As it is illustrated in the section 6.1.3 of this review, the assembly of preformed MOF crystals in two-dimension opens a land of opportunities for the development of new hybrid materials for optical devices.[147]

MOF films were obtained by casting nanocrystals on solid platforms via simple chemical solution deposition processes. The group of Gérard Férey prepared smooth films with a high optical quality by the deposition of nanocrystals of, $Fe_3OCl(muc)_3$ (MIL-89; muc = muconate dicarboxylate)[148] by a dip-coating method. Uniform nanocrystals with a diameter close to 20-40 nm were obtained by applying the coordination modulation method with acetate as modulator. The same group also deposited nanocrystals of MIL-101(Cr)[149] and ZIF-8[150] by means of dip-coating process. For the latter systems, the authors tuned the thickness of the thin films and the compactness of the nanocrystals by modulating the withdrawal speed and the colloidal solution concentration. Porous properties of the films were investigated by isopropanol adsorption performed by environmental ellipsometry and the existence of an interparticular mesoporosity was clearly evidenced.

Lotsch and co-workers alternatingly spin-coated ZIF-8 nanocrystals and titania nanoparticles on silicon wafers in order to prepared one-dimensional photonic architectures.[151] Qiu et al. prepared luminescent thin films with controllable thickness by spin-coating of modulated $[Ln(btc)(H_2O)]_n$ (where Ln = Dy(III), Eu(III), or Tb(III)) nanocrystals.[152] Films of mixed $Eu_{1-x}Tb_x$-MOFs possess strong luminescent properties, efficient Tb(III)-to-Eu(III) energy transferability as well as good mechanical properties. Granick et al.[71] and Eddaoudi et al.[36] casted MOF crystals with a highly uniform morphology on a substrate and showed a directional facet-to-facet attraction between crystals through simple capillary or van der Waals attractions. In this work, a spontaneous process associated with solvent evaporation triggered the formation of domains of closely packed monolayers.

The hydrophilic external surface and low density of MOFs made possible the formation of crystal monolayers at the air-water interface using polar alcohols as the suspension media. Furukawa, Kitagawa and co-workers synthesized supported and freestanding monolayers of densely packed MOFs crystals with uniform size and shape by a Langmuir-Blodgett (LB) approach.[153] Uniaxial compression of the crystals floating on the aqueous subphase led to their assembly over large areas. Thin films produced in such ways were then transferred onto various substrates via dip coating. The versatility of the strategy was demonstrated by assembling different types of MOFs, namely $Cu_3(btc)_2$, MIL-96 and $Cu_2(bdc)_2(bpy)$ on glass slices, silicon wafer and gold substrates. Importantly, crystals in the films showed a preferential orientation, which depends on the morphology of the crystals used for the assembly. $Cu_3(btc)_2$ crystals having octahedral morphology were oriented with the {111} lattice planes parallel to the substrates, while the crystals with cubic morphology were oriented with the {100} lattice plane parallel to the substrates

Huo et al. also prepared oriented monolayers of MOF with controlled thickness based on a liquid-air interfacial assembly.[154] Falcaro et al. proposed an easy protocol for the deposition of MOF based on the combination of UV-lithography and hot-pressing techniques, where common epoxy-based photo-resist are thermally treated and used to imprint any type of MOFs.[155]

5.5.2. Crystal delamination. The top-down delamination or "deconstruction" consists in the disintegration of bulk-layered materials into single or multi-layers with large lateral dimensions. This approach, well-established for the synthesis of functional nanosheets from clay minerals,[156] layered double hydroxides (LDH)[157] or graphite,[158] was recently applied for the formation of MOF nanosheets by Xu and co-workers.[159] Delamination of a layered MOF-2 was carried out in acetone by using MOF-2 powder under ultrasonic treatment at room temperature. MOF-2 nanosheets exhibited remarkable amine intercalation property and reversible amine exchangeability.
Wöll and co-workers demonstrated a "lift-off process utilizing poly(methyl methacrylate) (PMMA) as an adhesive to delaminate patterned surface mounted $Cu_3(btc)_2$ grown on COOH-terminated SAMs.[160] Lotsch and co-workers prepared Zn(BeIm)OAc nanosheets (BeIm = benzimidazole and OAc = acetate) by exfoliating BeIm-MIF (MIF = mesostructured imidazolate framework), a mesostructured coordination polymer composed of multilayer stacks of two-dimensional Zn(BeIM)OAc included within the interlayer space of cetyltrimethylammonium bromide (CTAB) mesophases. Interestingly, the authors demonstrated the formation of multiwalled nanotubular structures by rolling up of the lamellar stacks owing to their highly flexible morphology.[161]

6. Applications of MOF two-dimensional structures.

Assembly of MOFs into two-dimensional structures facilitates their implementation into two important application fields: (i) sensing, where the signal transduction schemes requires either the fabrication of thin film optics with tuned refractive indexes

(optical sensors) or the creation of a physical interface between the MOF crystals and a signal transduction device (electromechanical sensors) and (ii) molecular separation, where efficient and large scale separation processes requires highly selective, defect-free and thin porous membranes. Remarkable performances for proton and electric conduction of MOF films were also demonstrated recently. Because MOF two-dimensional structures were already investigated in various application fields, the authors decided to dedicate one entire section to it.

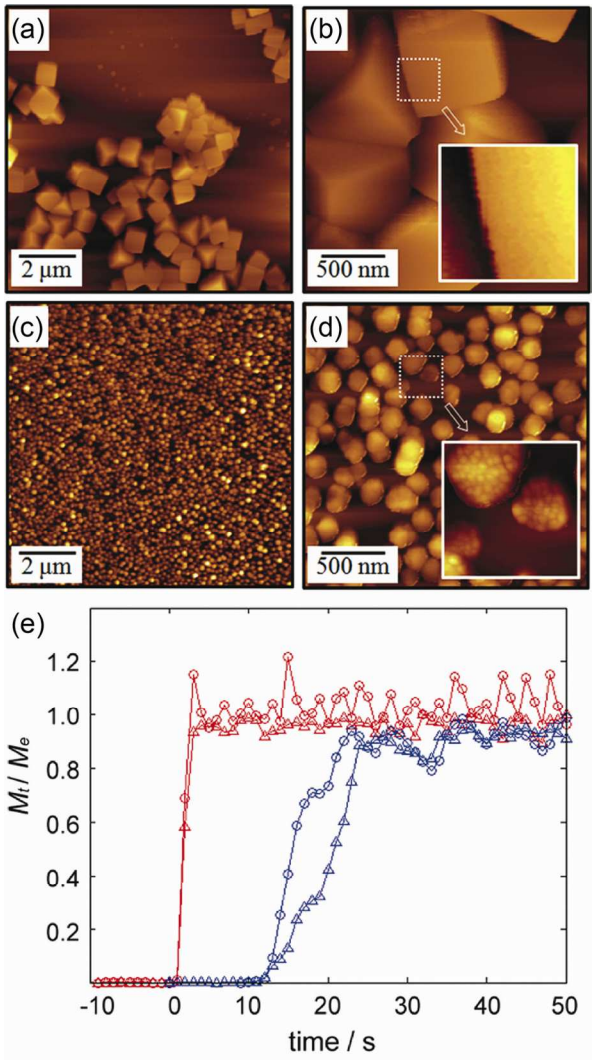

Figure 15. Atomic force microscopy (AFM) images of HKUST-1 nanocrystals deposited on the QCM Au-electrodes: (a, b) film composed of the larger crystals and (c, d) film composed of the smaller crystals. (e) Time-dependent mass uptakes of methanol (O) and hexane (Δ) in small (red) and large (blue) crystals in the low concentration regime (at P/P_0 = 0.002). Reprinted with permission from ref. 167 Copyright© 2011 American Chemical Society.

6.1. Sensing applications.

A direct use of MOFs as chemo-sensory materials is based on luminescent properties derived from the interactions between analytes and lanthanide ions or aromatic fluorophores included in the hybrid frameworks.[162-164] In such case, MOFs are both able to recognize molecules and to produce a signal (an obvious change of color) that can straightforwardly be monitored. However, although a high analyte sensitivity and selectivity can be achieved by the appropriate tuning of their pore structure and chemical functionality, most of MOFs lack in efficient signal transducing ability. Utilization of MOFs as sensors therefore requires their integration with external transduction mechanisms based on the use of microdevices, such as quartz crystal microbalances (QCM) or microcantilever (MCL), or on changes in optical properties.

6.1.1. Quartz crystal microbalance (QCM). Hybridization of MOFs with QCM is a well-suited strategy to develop MOF-based chemical sensors. QCM is a high-resolution mass sensing technique, which detects analytes by sensing small changes in the frequency of a resonant vibration propagating perpendicular to the surface of a quartz crystal coated on both side with gold, copper or silica electrodes.[165] MOF-based sensors using QCM relies on the detection of the loading and depletion with guest molecules of MOFs deposited on the electrodes. Notably, the gravimetric sensing ability of the QCM allows quantitative analysis of molecular adsorption on the nanogram scale and real-time monitoring of sorption processes. The modification of the electrode surface with self-assembled monolayers (SAMs) as a template for MOF nucleation and growth was shown to be directly compatible with QCM functioning. Bein and co-workers first deposited $Cu_3(btc)_2$ thin films on 11-mercaptoundecanol-coated gold electrodes.[166] Modified QCM substrates were exposed to different concentrations of water vapor and complete water sorption isotherms were recorded.

Wöll and co-workers synthesized highly oriented $Cu_3(btc)_2$ layers on SAM-coated gold electrodes by the layer-by-layer deposition.[96] Time-dependent analysis of the QCM uptake curves allowed the authors to determine the diffusion coefficient of pyridine within $Cu_3(btc)_2$. Dense $Cu_3(btc)_2$ films were also grown on top of QCM electrodes by an electrochemical approach.[134] To this end, a layer of metallic copper was deposited on a gold electrode and subsequently transformed into MOF film. The MOF-modified QCM system was then used to monitor changes in relative humidity.

A critical parameter to be considered for the improvement of chemical sensors based on the combination of MOFs with QCM technology is the response time upon introduction of the analytes within the pores of the MOFs. In this context, recent reports investigated the effect of the dimensionality and crystallographic orientation of the crystals deposited on the oscillator. Furukawa, Kitagawa and co-workers investigated the impact of the MOF crystal size on the sorption kinetics in case of methanol and hexane vapors.[167] Size-controlled growth of highly homogeneous HKUST-1 nanocrystals was achieved in the presence of dodecanoic acid as the modulator by controlling the dilution of the crystallization dilution (Fig. 15). The adsorption isotherms of films composed of large crystals (614 ± 11 nm) and small crystals (138 ± 1 nm) at 298 K for methanol and hexane in the range of P/P_0 = 0 to 0.85 were first obtained and presented typical type I sorption profiles. The vapor

adsorption kinetics were then investigated by introducing a vapor flow of methanol and hexane into the QCM chamber at both P/P_0 = 0.002 (low concentration) and 0.85 (high concentration). The time-dependent mass uptakes of small and large crystals in the low concentration regime (Fig. 15) showed a clear dependence of the rate of mass uptake, independent of the analyte species. In contrast, the high concentration dosing at P/P_0 = 0.85 displayed a clear dependence on the analyte. The uptake rates for both small and large crystals were very fast and comparable to one another in the case of methanol, while those for hexane exhibited a marked difference, with a stronger size dependency than at lower concentration. With this study, the authors showed that a small crystal size is appropriate to obtain a faster sensor response, independently of the analyte species.

The same group also demonstrated the control of MOF channel orientation as another mean to improve the response time of hybrid MOF/QCM systems.[168] To this end, a hybrid MOF/QCM system was fabricated based on the zinc-based MOF, Zn(NO_2-ip)(bpy) (Zn-CID-5; NO_2-ip = 5-nitroisophthalate), which exhibits a gate-opening behavior and adsorptive selectivity. Zn-CID-5 crystals with a strong preferred orientation along the [1-1-1] direction were grown on gold electrodes modified with COOH-terminated SAMs, whereas crystal with a [100] orientation were obtained on bare gold surfaces. Zn-CID-5 crystals with a [010] preferred orientation were obtained on the bare gold substrate under microwave irradiation in the presence of 4-phenylpyridine. The vapor adsorption kinetics were investigated by real-time monitoring of the frequency change after the introduction of a vapor flow of methanol at P/P_0 = 0.4 into the QCM chamber containing the differently deposited Zn-CID-5 crystals. Analysis of the time-dependent mass uptakes showed that the pores parallel to methanol vapor flows (the [100] and [010] directions), work to more effectively incorporate the guest molecules, while the pores perpendicular to the substrate (the [1-1-1] direction) are less efficient. The higher gas pressure at the entrance of the pores parallel to the substrate (along the [100] and [010] directions) quickly induces the gate-opening phenomena and therefore quickly adsorbs methanol molecules.

Tuning the response of MOF/QCM systems was also achieved by the synthesis on QCM oscillators of heterostructured MOF materials containing two distinct framework structures by using the hetero-epitaxial growth method. Furukawa, Kitagawa and collaborators combined Cu_2(ndc)$_2$(dabco) (A) with Cu_2(NH_2-bdc)$_2$(dabco) (B) in a sophisticated amphiphilic type heteroporous MOF film (so-called binary Janus MOF coatings) by using the LbL process.[105] The framework B allowing the postsynthetic chemical modification (PSM) with succinic acid anhydride to form Cu_2($HOOC(CH_2)_2OCNH$-bdc)(NH_2-bdc)(dabco) (C), two heteroporous MOF materials with different deposition sequences, Type I(C@A) and Type II(A@C), were deposited on quartz crystal microbalance (QCM) sensors. A third type of material, the homogeneous Type III(AC) made of a statistical distribution of ndc and NH_2-bdc ligands throughout the entire system was also prepared. For this third type of material, the deposition of the homogeneous system was performed in one reaction step, in which the ligands were mixed in the solution, followed by the PSM. The results of single-analyte adsorption experiments performed with methanol and hexane as analytes using Type I(C@A) and Type II(A@C) coatings indicated the possible selective adsorption properties of binary Janus MOF films. Indeed, the adsorption characteristics for methanol as a small and polar VOC did not depend on the sequential arrangement of the frameworks A and C since both MOF systems possessed the suitable pore size and polar environment for methanol accommodation. In contrast, the single-VOC sorption experiment of Type I(C@A) exhibited no uptake for hexane as a large and nonpolar VOC, while 0.5 hexane molecules per copper dimer unit could be adsorbed by Type II(A@C) material. The directional selective adsorption behavior was then examined by changing the spatial arrangement of A and C. The Type I(C@A) coatings could selectively adsorb methanol out of a mixture with hexane, however, the inversed structure of Type II(A@C) showed no selectivity. This result clearly demonstrated that the MOF-on-MOF concept could be applied to precisely tuning the sensing performance MOF/QCM systems.

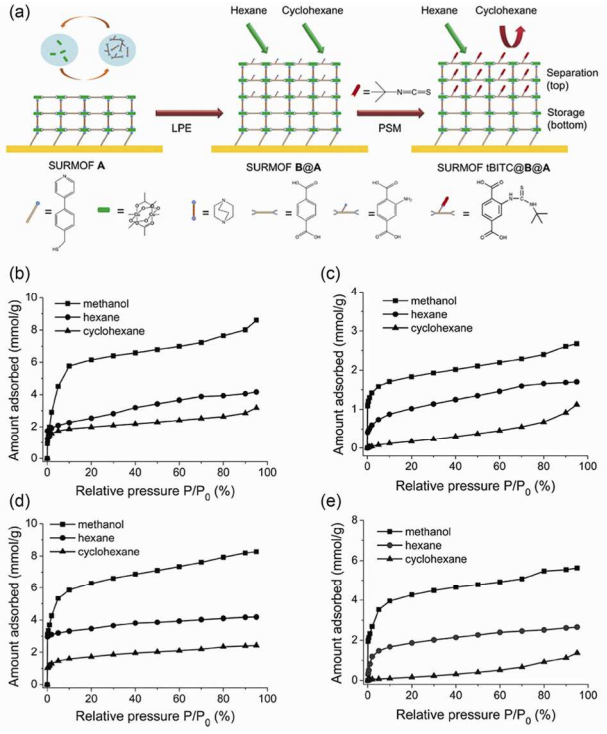

Figure 16. (a) Illustration of the preparation of heterostructured MOF films prepared through liquid phase heteroepitaxial growth and post-synthetic modification. First, Cu_2(bdc)$_2$(dabco) (SURMOF **A,** SURMOF = surface mounted metal–organic frameworks) was grown on pyridyl-terminated SAM on gold covered QCM substrate and then Cu_2(NH_2-bdc)$_2$(dabco) (SURMOF **B**) was grown on the top of the first layer in a second step leading to the heterogeneous SURMOF **B@A**. Finally, the film **B@A** was post-synthetically modified with *tert*-butyl isothiocyanate (*t*BITC) leading to SURMOF tBITC@**B@A**. Adsorption isotherms of methanol, hexane, and cyclohexane at 293K. (b) **B**(40) (40 = prepared with 40 growth cycles); (c) tBITC@**B**(40); (d) **B**(20)@**A**(20) and (e) tBITC@**B**(20)@**A**(20). The saturated vapor pressures P_0 of methanol, hexane and cyclohexane at 293 K are 12.98, 16.18 and 10.33 kPa, respectively. Adapted from Ref. 106 with permission from The Royal Society of Chemistry.

The sorption properties of heterostructured MOF films by using an environmentally controlled QCM instrument was also recently investigated by Fischer and collaborators. $Cu_2(NH_2\text{-}bdc)_2(dabco)$ was grown on the top of $Cu_2(bdc)_2(dabco)$ deposited of a pyridyl-terminated gold QCM substrate by employing the LbL liquid phase epitaxial growth process. The authors selectively reduced the pore size of the top layer by chemically modifying the incorporated non-coordinating group with *tert*-butyl isothiocyanate (*t*BITC) (Fig. 16). The new system hence produced advantageously combined the size selective adsorption of hexane over cyclohexane due to the reduced pores of the top layer with the high storage capacity of the unmodified bottom layer.[106] The same group prepared thin films of the moisture-tolerant $Zn_4O(L)_3$ (L = di-substituted carboxypyrazolate derivatives) on QCM gold substrates by the same LbL liquid phase epitaxial procedure.[169] In situ analysis of the growing films by QCM and grazing incidence X-ray diffraction showed a dependence of the growth regime and crystallinity to the chain functionality at the carboxypyrazolate linkers. Indeed, for some chain functionalities, such as the methyl/isopropyl, the synthesis of highly crystalline homostructured films was not possible. The authors demonstrated that this poor crystallinity could be overcome by achieving the LbL heteroepitaxial growth of the MOF film on the top of an other well-grown and lattice-matched MOF film. In other words, LbL heteroepitaxial process can be seen as an efficient mean to overcome certain nucleation problems. The sorption properties of the heterostructured films were investigated by using the environmentally controlled QCM equipment and their ability to selectively adsorb methanol or isopropanol was demonstrated.

Apart from chemical sensing applications, MOF/QCM hybrid devices are also well suited for the quantitative analysis of dynamic phenomena within MOFs. Furukawa, Kitagawa and collaborators used $Cu_3(btc)_2$/QCM systems to investigate the desorption kinetics of various vapor molecules featuring different degrees of intermolecular (hydrogen bonding) or molecule-framework interactions.[170] The authors showed that the desorption of molecules bearing an -OH functionality such as 1-butanol, methanol or ethanol occurs *via* a metastable state involving the formation of guest molecule clusters within the larger hydrophilic pores of $Cu_3(btc)_2$. Although not directly related to any sensor application, this study demonstrates the efficiency of MOF/QCM hybrid systems to probe the adsorption as well as desorption kinetics of vapor molecules. Recently, Heinke et al. studied the diffusion of large ferrocene compounds into the pillared-layer type MOF $Cu_2(ndc)_2(dabco)$ in a quantitative fashion.[171]

6.1.2. MICROCANTILEVERS (MCL). Allendorf and collaborators proposed a transduction mechanism based on the integration of MOF crystals with a microcantilever surface. In this approach, the distortion of MOF structure upon analyte adsorption induces a measurable stress at the surface of the microcantilever. This stress results in bending that can be detected optically or by means of a built-in piezoresistive sensor. Stress-induced chemical sensors were synthesized by depositing thin films of $Cu_3(btc)_2$ on gold-coated microcantilevers using the LbL method.[172,173] The cantilevers used in this study incorporate a built-in piezoresistive sensor for the stress-based detection. A rapid and reversible response to gas-phase H_2O was observed with $Cu_3(btc)_2$ crystals in their hydrated form (with water molecules coordinated to their exchangeable axial coordination Cu(II) sites). In contrast, no response was obtained with CO_2. However, a fast response was induced when CO_2 was adsorbed in the dehydrated $Cu_3(btc)_2$ film, demonstrating that a detection selectivity of the systems can be achieved by controlling the hydration state of the axial Cu(II) sites of $Cu_3(btc)_2$. Notably, these results indicate that significant stress-based signals can arise under guest adsorption from MOFs with relatively low structural flexibility (such as $Cu_3(btc)_2$). Thus, it is expected that the application of this approach with the MOFs exhibiting exceptionally large changes in unit cell volume reported recently[174,175] would result in the creation of exquisitely sensitive MOF detectors. Recent modeling investigations of the effect of the mechanical properties of MOFs on the sensor response indicated a high tolerance of the sensor sensitivity for parameters such as the uniformity, the thickness and the density of the MOF films.[176]

6.1.3. SENSORS BASED ON OPTICAL PROPERTIES. Several recent reports demonstrated the preparation of films made of luminescent frameworks as potential sensors that use quenching/enhancement of the luminescence, solvatochromic or electrochromic measurements.[177-183] Notably, the transduction scheme of these sensors originates exclusively from the chemical nature of the metal centers and linkers of the MOFs. Their implementation as film is therefore not essential. Alternatively, the deposition/organization of MOF crystals on two-dimensional surfaces makes possible the fabrication of different types of optical sensors for which the signal transduction relies on the change of refractive index (RI) of the MOFs in response to the analyte adsorption. Because the sensing signal originates in the MOF crystal spatial organization and not in the MOF itself, this alternative approach comprises a generalizable sensing scheme applicable to any types of MOF and analyte.

Hupp and co-workers explored the modulation of the refractive index modulation of Fabry-Pérot interference peaks as signal transduction.[184] Fabry-Perot interferences are observed when an incident light experiences multiple reflections off of a filter made of two parallel surfaces. Interferences between the reflected beams will allow only certain angles to be transmitted. At normal incidence, the wavelength of the reflected interference peaks depends on the distance between the two reflecting surfaces as well as on the refractive index of the medium between the two surfaces. The authors prepared transparent films of ZIF-8 on glass or silicon substrates and optically examined the energies of Fabry-Pérot interference peaks as a function of exposure to various analytes. Adsorption of propane induced a reversible shift in the interference fringes within 1 min, proving the viability of the

approach. From the magnitude of the shifts, the authors could determine the volume fraction of analyte in the framework. Interestingly, the ZIF-8 sensor displayed some chemical sensitivity based on size of the analytes.

Integration of MOF into photonic structures also provides a powerful and general signal transduction scheme for the development of MOF as molecular sensors. Potential of photonic crystals as sensor relies on the sensitivity of their photonic band gap to change in their refractive index. Hupp and co-workers prepared MOF-colloidal crystal films by coating colloidal crystal of silica microspheres with $Cu_3(btc)_2$ crystals.[185] Photonic band gap of the MOF-colloidal crystal film red shifted upon exposure to carbon disulfide, ethanol and water and the magnitude of the shifts was dependent on the analyte concentration. Calculation and normalization of the volume fractions of the analytes adsorbed in the MOFs at various concentrations made possible the construction of the adsorption curves. Interestingly, the shapes of these adsorption curves fit perfectly the adsorption curves measured by QCM for thin films of $Cu_3(btc)_2$.

Figure 17. (a) Schematic representation of a multilayered photonic crystal

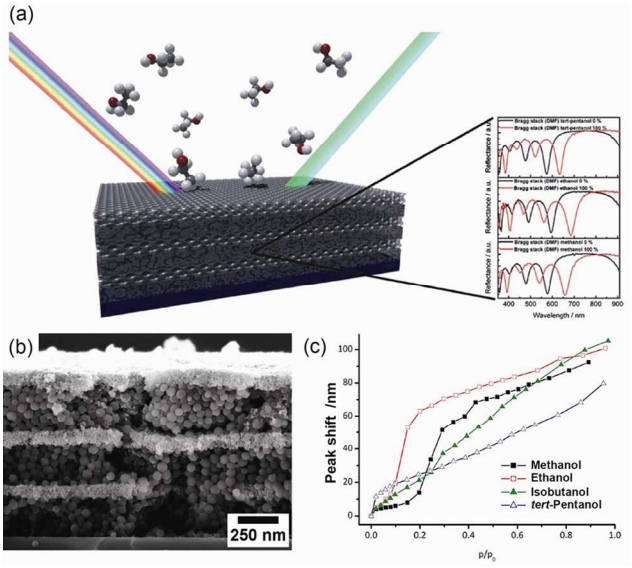

architecture illustrating the structure- and angle-dependent reflection of incident light as well as the optical response upon exposure to external stimuli. (b) Scanning electron microscopy (SEM) image of a 3-bilayer Bragg stack. (c) Adsorption isotherms recorded by using a Bragg-stack during exposure to a series of alcohol vapors. Adapted from Ref. 151 with permission from The Royal Society of Chemistry.

Lotsch and co-workers synthesized one-dimensional photonic crystals (Bragg stacks) based on ZIF-8 and mesoporous titanium dioxide (Fig. 17).[151] The optical response of these photonic crystals to guest adsorption was investigated by performing sorption experiments of methanol, ethanol, isobuthanol and tert-pentanol. Tert-pentanol (2-methyl-1-propanol), for which the kinetic diameter is much larger than the pore entrance of the ZIF-8 could not be detected, evidencing the analyte size selectivity of the sensor response. Optical vapor sorption isotherms were obtained for each of the four alcohols.

MOFs were recently integrated with a signal transduction mechanism based on localized surface plasmon resonance spectroscopy (LSPR). LSPR corresponds to charge density oscillations confined to metallic nanoparticles and metallic nanostructures. Light excitation of LSPR at an incident wavelength where resonance occurs results in a characteristic and intense surface plasmon absorption bands whose frequency and intensity depend on the chemical nature, size and shape of the metallic structure as well as the RI of its environment. Shifts in the extinction spectrum can therefore be used to detect subtle changes in the dielectric environment near metallic nanoparticles. LSPR was shown to be a powerful mean to detect large biological molecules. Its use to sense small molecules is however limited by the difficulty to detect tiny changes in RI. Hupp and co-workers demonstrated the signal amplification for CO_2 sensing by concentrating gas molecules in $Cu_3(btc)_2$ thin films grown directly on patterned silver island films by the LbL procedure.[186] Compared to a bare silver sensor ($\Delta\lambda_{max}$ = 0.13 nm), the sensor coated with 37 cycles of $Cu_3(btc)_2$ exhibited a 14-fold larger signal ($\Delta\lambda_{max}$ = 0.13 nm). In addition to its concentrator effect, $Cu_3(btc)_2$ coating also greatly enhanced the selectivity of the response. Indeed, $Cu_3(btc)_2$ adsorbed almost 10 times more CO_2 than N_2, in accordance with the reported isotherms. The effect of the MOF layer thickness upon the signal amplification was also demonstrated. Last, Férey and co-workers monitored *in situ* the RI of optical MOF films composed of MIL-89[147] and ZIF-8[149] nanocrystals by environmental ellipsometry.

6.1.4. Capacitive sensors. Sensors for detecting vapors commonly convert analyte concentrations into electrical signals through a capacitive transduction scheme. Sensors based on capacitive effect consist of a dielectric material with high uptake ability processed as a film and sandwiched between a pair of electrodes, hence forming a small capacitor. Adsorption of vapors or gas within the dielectric film results in a change of its relative permittivity and therefore of the capacitance measured between the electrodes. Qiu and co-workers proposed continuous $Cu_3(btc)_2$ films as an alternative to the polymers and ceramics currently employed. The authors implemented the MOF film into a capacitive sensing setup by growing the $Cu_3(btc)_2$ crystals directly from the surface of one of the two sensor's electrodes.[187] After depositing circular aluminum electrodes on top of the film by evaporation under vacuum with a mask, the capacitance was monitored under various relative humidity. A linear response with a negligible hysteresis was demonstrated. The authors also proved the good stability of the sensors of days as well as the reproducibility of the measurements.

6.2. Gas separation.

Crystalline MOF membranes for gas separation possess a number of advantages over currently employed membranes. The appropriate selection of metal centers and organic linkers results in MOFs that possess better thermal and chemical stability as well as better selectivities than polymer membranes.

In contrast to zeolites, their high chemical tailorability make their range of available pore size almost unlimited. Last, crystalline MOF membranes do not face the problem of the non-selective void spaces around the filler particles commonly encountered in the case of mixed matrix membranes.

However, the synthesis of efficient MOF membranes is challenging and the optimization of the separation performances requires considering several important parameters. First, the crystal adhesion on the porous support must be optimized. As shown in the section 5, several strategies based on the use of surface modification with organic binders (SAMs, polymers, graphites, the organic linkers), deposition of MOF seeds coupled with a secondary growth or the use of reactive surface were developed to strengthen the attachment of the MOF crystals to the support. Second, the thermal and chemical (water) stability of the MOF must be considered. MOFs based on aluminum or copper-carboxylate coordination bonds as well as the zinc-imidazolate framework (ZIF) series are relatively stable and therefore are good candidates. Note that the stability of frameworks made of water unstable coordination bonds (such as the Zn-O bonds) can be improved by judiciously modifying the organic linker.[188] Moisture stability of MOF membranes was also enhanced by the deposition of amphiphilic surfactants on their surface.[189] Third, the selectivity is commonly affected by the presence of cracks within the membrane, which are mechanically brittle. The formation of cracks is usually avoided by performing slow cooling and drying processes after the synthesis in order to decrease the risk of capillary stresses in the membranes.[114] Fourth, the reduction of the membrane thickness and of the crystal boundary facilitates the gas to flow across the membranes and hence enhance the gas permeation.[190] This issue is crucial in view of an intensification of the separation processes.

As membranes, ZIFs were shown to be interesting materials for the separation of hydrogen[86,92,191] and of CO_2.[192] Metal-carboxylate-based MOF membranes were also reported. $Cu_3(btc)_2$ exhibited good performances for the separation of hydrogen.[89,114,127,128] Membranes made of MIL-53[129] and NH_2-MIL-53,[193] also displayed good gas separation abilities. Membranes made of pillared layer systems of general formula $M_2(L)_2(P)$, such as $Cu_2(1,4\text{-ndc})_2(dabco)$[101] and $Zn_2(cam)_2dabco$[194] (cam = (1R,3S)-(+)-camphorate) were also shown to be promising.

6.3. Proton and electric conduction.

Two recent articles demonstrated the potential of oriented MOF films as proton and electrical conductive materials. Kitagawa and co-workers assembled Cu-TCPP nanosheets (TCPP =5,10,15,20-tetrakis(4-carboxylphenyl)-21H,23H-porphyrin) with a thickness around 15 nm and a diameter of approximately 400 nm as highly oriented thin films by a layer by layer method.[195] The thin film was deposited onto a SiO_2/Si wafer between two electrodes and its proton conductivity was evaluated under various relative humidity (RH) conditions at 25°C. Notably, the conductivity increased from 3.2×10^{-8} S cm^{-1} at 40% RH to 3.9×10^{-3} S cm^{-1} at 98% RH thus reaching the highest value yet recorded for a hydrated MOF sample. The authors assumed that a hydrogen-bonding network created by the adsorbed water, the water coordinated on open metal sites and the dangling carboxyl groups on the external surface of the nanosheets acts as an efficient pathway for proton transport. The oriented packing of the nanosheets is then most likely at the origin of the remarkable proton conductivity of the nanofilm (Fig. 18).

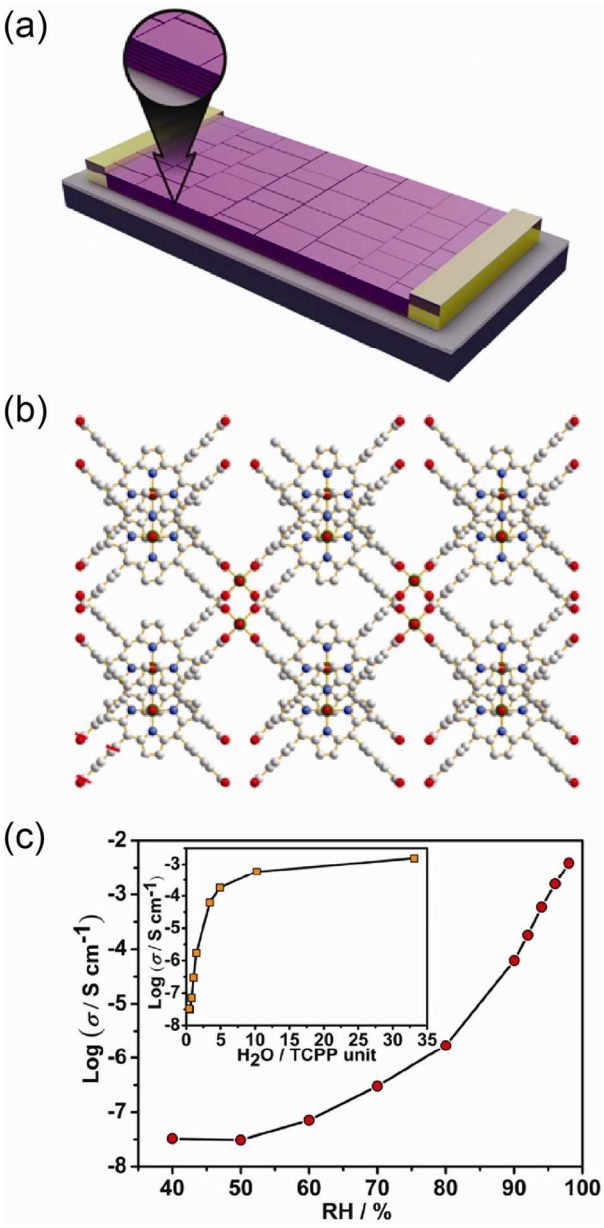

Figure 18. (a) Schematic illustration of the nanosheet -based oriented film (violet) implemented for the electrical measurement and (b) of the model crystal structure of the MOF nanosheet. (c) Proton conductivity of the MOF nanofilm under various RH conditions. Inset: proton conductivity versus adsorbed water. Reprinted with permission from ref. 195 Copyright© 2013 American Chemical Society.

Allendorf and co-workers synthesized electrically conducting $Cu_3(btc)_2$ films by infiltrating the pores of the

MOFs with the redox-active 7,7,8,8-tetracyanoquinododimethane (TCNQ).[196] This approach resulted in the increase of the electrical conductivity of

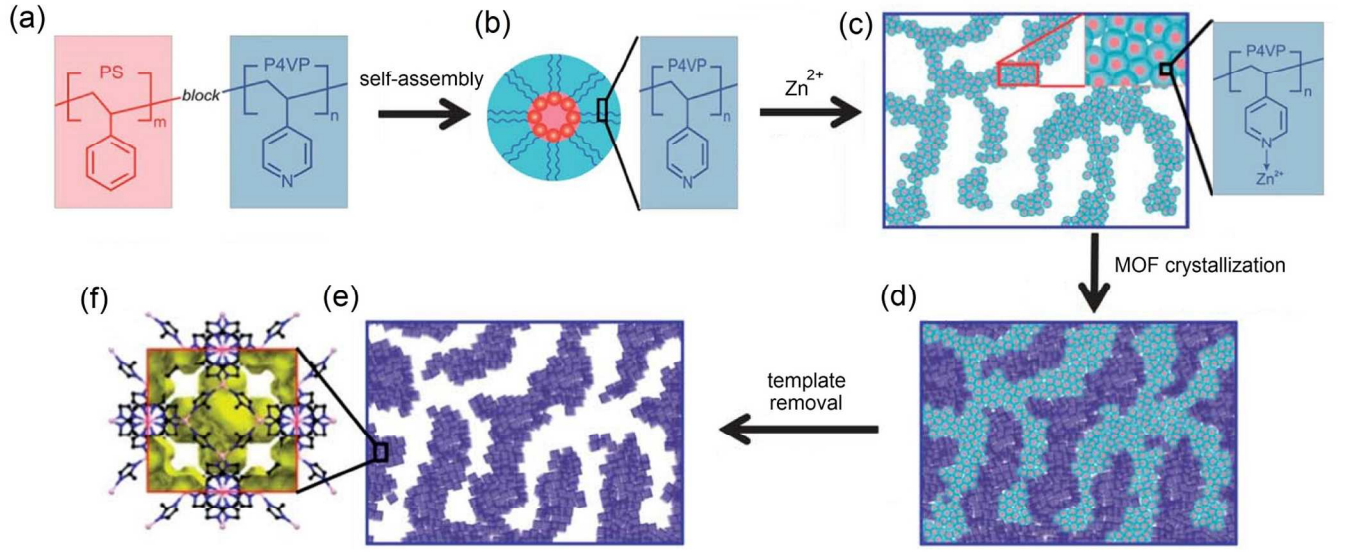

Figure 19. A schematic showing the synthesis of a hierarchical ZIF-8 architecture from a block co-oligomer micelle template. (a) A block co-polymer consisting of poly(styrene)-block-poly(4-vinylpyridine) (PSty-b-P4VP); (b) assembly of micelles with the more hydrophilic P4VP moieties located on the exterior; (c) assembly of the micelle template, and impregnation with Zn^{2+}; (d) synthesis of ZIF-8 in the presence of the template resulting in filling of its voids with a continuous structure; and (e) a hierarchical architecture of pure ZIF-8 (structure shown in panel (f)) obtained following removal of the template. Adapted from ref. 208 with permission Copyright © 2013 The Royal Society of Chemistry.

$Cu_3(btc)_2$ by over six orders of magnitudes. Interestingly, the conductivity of the device could be tuned by changing the TCNQ exposure time. After probing the interactions between the framework and TCNQ by a range of spectroscopic techniques and performing *ab initio* calculations, the authors explained the good performances of the MOF films by proposing that TCNQ guest molecules bridge the binuclear copper paddlewheels in the $Cu_3(btc)_2$ framework leading to strong electronic coupling between the dimeric Cu subunits.

7. Three-dimensional superstructures

The precise immobilization of metal-organic framework crystals in an ordered manner in three-dimensional space is a particularly challenging aspect with regard to the fabrication of precisely designed architectures due to the limited spatial control over the crystallization in a conventional solvothermal reaction. The fabrication of structurally optimized superstructures could allow the underlying properties of the framework to be enhanced with regard to specific applications. For example, the preparation of a macro- or mesoporous three-dimensional architecture of interconnected metal-organic framework crystals would aid in the more rapid diffusion of guest molecules into the micropores (and active sites) of the framework compared to a packed bed system,[197] which could be of benefit for applications in gas adsorption, molecular separations, chemical sensing, and heterogeneous catalysis. In this section, introduce reports that provide a pathway for the generation of both pure metal-organic framework superstructures and composite materials that require the presence of a secondary phase, such as polymers, silicas, or other types of fillers, for structural support in order to maintain the architecture. Note that these composite systems, which have recently been extensively reviewed elsewhere,[5,7,198,199] can carry an advantage in that the form of the architectures can be controlled directly through shaping or morphological control of the support. Importantly, in these cases, this secondary phase must be selected with care in order to provide the overall system with the right properties for a given application.

7.1. Macrostructural template.

The construction of three-dimensional superstructures of metal-organic frameworks with the use of a macrostructured template represents a pathway for gaining a high level of control over the porosity and crystal immobilization within the architecture, provided that suitable templates can be fabricated and subsequently removed following the arrangement of the crystals. This latter point remains as a key challenge in the area, and reports to date have focused on the generation of composite materials in which the template acts as a support of the architecture. A number of different types of templates have been used to date, including activated carbons,[200,201] silicas,[202,203] graphite oxide,[204,205] porous organic polymers,[206] and other macrostructured metal oxides and minerals.[207]

The use of porous silicas as a support is attractive due to its high stability, well-defined pore sizes, and ability to be prepared in a variety of macroscopic forms, including monolithic structures. In one example, $Cu_3(btc)_2$ nanocrystals were grown *in-situ* within a macro- and mesoporous silica monolith by submerging the structure within the reaction medium at the time of formation of the metal-organic framework.[203] Interestingly, crystals of just 7-12 nm in size

were localized within the mesopores of the structure, preserving the macroporous network throughout the solid. The mechanical strength of the support allowed the composite monolith to be studied in liquid phase flow applications. In particular, the material was tested for catalytic activity in a Friedländer reaction between 2-aminobenzophenone and acetylacetonate. Here, a productivity (defined as the amount of product obtained per unit of time per gram of the metal-organic framework) approximately 2.5 times higher compared to a bulk $Cu_3(btc)_2$ sample was observed with a low pressure drop. The results serve to demonstrate the advantage of immobilizing small nano-sized crystals within such a porous support, wherein the diffusion throughout the solid and to the active centers within the metal-organic framework can be enhanced compared to a simple dense packing of crystallites.

Using a similar approach, Eu- and Tb-succinate frameworks were grown *in-situ* within the pores of activated carbon.[201] Here, the quantity of activated carbon could be varied between 1-50 wt %, and a uniform dispersion of the framework throughout the pores of the charcoal phase could be confirmed by scanning electron microscopy, energy-dispersive X-ray scattering, and X-ray diffraction. The composite systems were shown to have a higher efficiency than pure activated carbon in its adsorption of aldicarb, a particularly toxic pesticide, under biological conditions. Under acidic conditions relevant for removal of aldicarb from within the stomach, a sample of the Tb-based framework incorporated within a 40 wt % loading of activated carbon exhibited a 78% removal after 10 min, while the bare charcoal sample and pure framework displayed a 46% and 41% efficiency, respectively. However, the activated carbon alone is a better absorber at alkaline pH, suggesting chemical or physical changes that provide a better binding environment for aldicarb to bind within the composite system under acidic conditions. In this case, and in the broader context of composite materials, a more comprehensive understanding of the interactions between the support and the metal-organic framework could provide greater opportunities for more sophisticated functions targeted for specific applications.

7.2. Molecular templates.

In this strategy, a three-dimensional aggregated structure consisting of a molecular species is assembled, usually prior to the formation of the metal-organic framework. Upon initiation of the crystallization of the framework, the presence of the template directs the spatial positioning of the formed crystals to within the voids or surface of the template. One advantage of the molecular template strategy is the potential for its removal following the formation of the framework, resulting in a three-dimensional superstructure.

In a successful implementation of this approach, a template-assisted method starting with a functionalized block co-oligomer micelle template has been utilized for the fabrication of hierarchically porous ZIF-8 and $Cu_3(btc)_2$ architectures.[208] As shown schematically in Fig. 19, micelles of poly(styrene)-*block*-poly(4-vinylpyridine) (PSty-*b*-P4VP) and poly(styrene)-*block*-poly(acrylic acid) (PSty-*b*-PAA) are initially constructed under conditions in which a core-shell configuration, with the pyridine or carboxylate groups outwardly projected and the styrene groups are located in the center, is formed. Then, Zn(II) and Cu(II) ions that are precursor metal ions for the formation of ZIF-8 and HKUST-1, respectively, are introduced, leading to bridging of the individual micelles and the formation of a three-dimensional assembly. The excess metal ions are then removed by washing, and following introduction of the organic ligand, crystallites of the metal-organic framework are formed along the surface of the architecture. The micelle template is removed by etching with tetrahydrofuran and DMF, leaving intergrown mesoporous network of the framework.

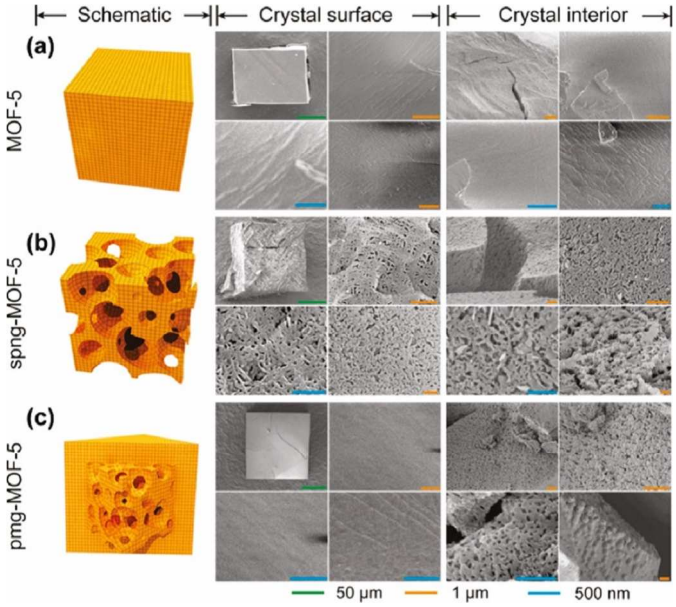

Figure 20. Schematics and SEM images showing the surface and internal pore structures of (a) MOF-5, (b) 'sponge-like' MOF-5 synthesized using a 1:1 H_2bdc:DBA ratio, and (c) 'pomegranate-like' MOF-5 synthesized using a 7:3 H_2bdc:DBA ratio. (scale bars, green 50 µm, red 1 µm, blue 500 nm) Reprinted with permission from ref. 209 Copyright © 2011 American Chemical Society.

More recently, a direct method for the preparation of macro- and mesoporous architectures based on the MOF-5 structure type was reported by Kang, Yaghi and co-workers.[209] In contrast to the previous case where high-dilution was used, here, a 4-(dodecycloxy)benzoic acid (DBA) component was added to the reaction mixture in addition to the H_2bdc linker. Interestingly, in contrast to conventional syntheses of MOF-5 that result in crystals that display only microporosity stemming from its crystalline structure (Fig. 20a), the addition of a 1:1 molar ratio of H_2bdc:DBA resulted in block-shaped crystals possessing a 'sponge-like' morphology in which continuous meso- and macropores between 10-100 nm in diameter were present throughout the architecture (spng-MOF-5; Fig. 20b). When the DBA content within the reaction mixture was lowered to a 7:3 molar ratio of H_2bdc:DBA, the larger pores were only observed at the center of the crystals, resulting in a so-called 'pomegranate-like' structure (pmg-MOF-5; Fig. 20c). The formation of pores in the macro- and mesoporous region is ascribed to the ability of the carboxylate functionality of DBA

to disrupt conventional crystal growth in a manner similar to the coordination modulation method,[44] and for the long alkyl chains to template the formation of large channels during crystal growth. Importantly, from a practical perspective, the DBA could be completely removed from the pores of the material by conventional washing procedures, providing a hierarchically porous architecture available for guest adsorption. The porosity is demonstrated via the preferential adsorption of large dye molecules within the hierarchically porous systems (with little uptake observed for conventional MOF-5 crystals), as well as an enhanced CO_2 adsorption capacity at 195 K that arises as a result of the filling of the macro- and mesopores within the structure.

A number of so-called 'template-free' methods for the synthesis of three-dimensional superstructures, in which the only constituents of the reaction are the metal source, organic ligand, and the solvent, have also been reported in recent years. However, in these cases, it is likely that the solvent acts as the template, providing a stable environment for the formation of permanent intercrystalline voids. In one example, a direct synthetic method for the preparation of mesoporous nanocrystals of MOF-5 was reported by Bai and co-workers.[210] The preparation utilises a reactant concentration that is approximately 400 times more dilute than conventional syntheses, which remarkably results in small cubic structures approximately 400 nm in size with continuous mesopores that are readily visible using scanning electron microscopy. Although the BET surface area for the mesoporous cubes is slightly lower than conventionally-synthesized samples, the uptake of H_2, CO_2 and CH_4 are enhanced as a result of a higher isosteric heat of adsorption of the gases. A more complete examination of the mechanism via which the mesoporosity is obtained, as well as the origins of the higher gas uptakes would be of interest, particularly in the context of developing a convenient method of hierarchically porous superstructures.

Furthermore, a direct, synthetic method for the preparation of microporous- mesoporous structures of Zn_2(dobdc) (Zn-MOF-74, CPO-27-Zn) was recently reported.[211] In this work, solutions of zinc acetate and H_4dobdc were stirred at room temperature for different periods, ranging from 15 min to 10 days to afford samples of Zn_2(dobdc) in a powder form. Interestingly, for each of the samples, scanning electron microscopy revealed a network of interconnected crystallite aggregates with the concomitant formation of continuous mesopores throughout the structure. Although larger aggregates are observed after longer reaction times, the crystallinity of the material and the amount of adsorption in the microporous region of the N_2 isotherm at 77 K is reduced, suggesting the formation of smaller crystallites after an extended period. Nevertheless, the larger aggregates lead to the presence of a greater proportion of mesoporosity, which is investigated *via* adsorption of the dye Brilliant Blue R-250, which possesses a molecular diameter (ca. 2 nm) that is too large to be enclosed within the micropores of Zn_2(dobdc). Indeed, a 6.6-fold increase in the uptake is observed in the case of the microporous-mesoporous structure compared to a bulk powder of Zn_2(dobdc) owing to the accommodation of the molecules within the mesopores of the aggregated structure. While an exact mechanism for the direct formation of such a hierarchical structure from a template-free solvothermal preparation is not established, the authors hypothesise that a ligand exchange mechanism involving the initial displacement of the acetate anions from the dinuclear paddlewheel units leads to a greater degree of particle aggregation from an early stage in the crystal growth process. Further investigations that closely monitor the crystal growth in this system, as well as studies targeted toward expanding this approach to other systems would be of interest in the context of formulating a general strategy for the preparation of hierarchical structures in a convenient one-step synthetic procedure.

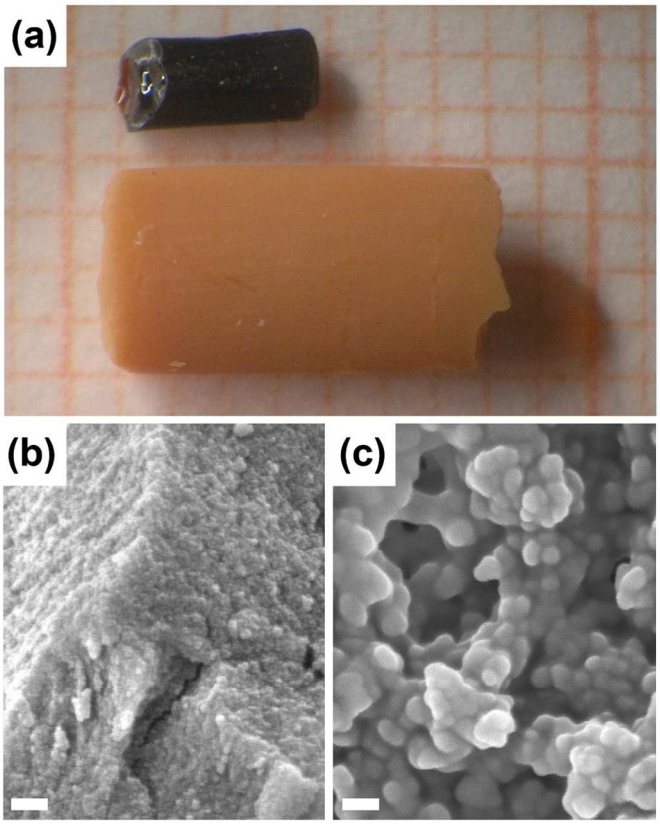

Figure 21. (a) A photograph of an aerogel with an air-dried xerogel of a similar original size and scanning electron micrographs (SEM) of (b) a xerogel and (c) an aerogel sample. Scale bars represent a distance of 100 nm. Adapted from ref. 212 with permission Copyright © 2009 The Royal Society of Chemistry.

7.3. Reaction confinement by gelation.

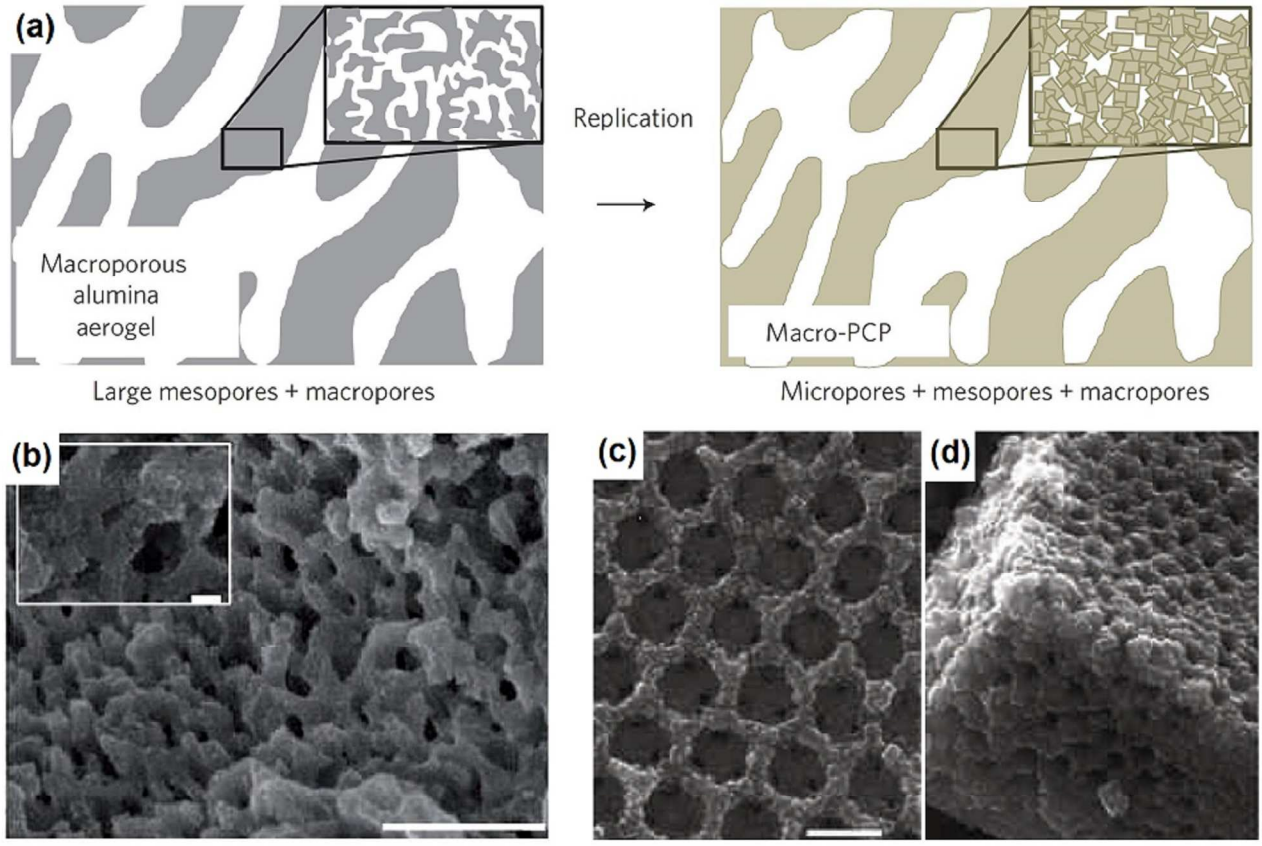

Figure 22. (a) A schematic drawing showing the direct conversion of a macroporous alumina aerogel template in the presence of an organic linker to a three-dimensional metal-organic framework architecture; (b) field-emission scanning electron microscopy (FE-SEM) image of a macroscopic Al(OH)(ndc) aerogel; and an alumina inverse opal structure after coordination replication via microwave treatment as viewed from (c) a top view; and (d) a side view (scale bars represent 10 μm in the main image, 1 μm in the inset). Adapted from ref. 57 with permission Copyright © 2012 Nature Publishing Group.

The preparation of three-dimensional superstructures via sol-gel techniques represents an attractive method in the context of gaining a high degree of control over the shaping of the macroscopic structure of the system. In these syntheses, aggregation of nanoscopic crystallites occurs early in the crystal growth process, with a concomitant swelling of the structure due to the presence of the reaction solvent. Once gelation occurs, the system adopts the shape of the reaction vessel, with a high degree of internal macro- and/or mesoporosity that is supported by the bulk solvent within the pores. Note that conventional drying techniques, such as the application of heat or a vacuum, is often detrimental to this porosity, resulting in powders or xerogel materials with significantly reduced porosity. Thus, supercritical drying techniques are often used, providing full retention of the intercrystalline porosity (aerogels).

In an early example, Kaskel and co-workers reported the direct preparation of a metal-organic framework-based gel from the combination of ethanolic solutions of iron(III) nitrate and H_3btc.[212] Here, gelation is observed within several seconds, and the macroscopic form of the gel adopts the shape of the reaction vessel, suggesting that gels of the desired external dimensions may be readily prepared by selecting a reactor with a suitable internal capacity. Although direct evaporation of the solvent within the pores resulted in significant shrinkage of the structure due to a reduction in its macroporosity (giving xerogels materials), supercritical CO_2 drying afforded an aerogel with minimal change in the size of the solid (see Fig. 21). Indeed, an analysis of the aerogels *via* scanning electron microscopy provided direct evidence of the retention of pores several hundred nm in diameter in the case of the aerogel, while the xerogel possessed a dense network of aggregated particles. This was further probed by N_2 adsorption measurements, which revealed a significantly higher surface area and micropore volume for the aerogel (1618 m^2/g and 0.72 cm^3/g) compared to the xerogel (1183 m^2/g and 0.52 cm^3/g), as well as a broad distribution of meso- and macropores in the former case. Although the precise composition of the gels could not be determined from powder X-ray diffraction due to the amorphous nature of the product, infrared spectroscopy showed a close match of the gel samples with that of bulk MIL-100(Fe), which is consistent with the relatively high surface area and micropore volumes of the materials.

More recently, low-density aerogels consisting of Al-based frameworks were directly prepared using a number of common multitopic carboxylate organic linkers.[63] The formation of the

gels is rationalized by a two-step process involving the initial assembly of small clusters of the framework that aggregate to form crystal nuclei, followed by a gelation step in which the subsequent crystal growth is perturbed, inducing a cross-linking of the crystallites. Furthermore, moderate heating is found to assist gelation by providing a sufficient driving force for framework formation (coordination bonding) to occur while also bringing a variety of other types of interactions (such as intermolecular, or cross-linking interactions) into competition with the crystal growth. Indeed, while the reaction mixtures were found to be indefinitely stable at room temperature, elevation of the temperature to those typically encountered for solvothermal syntheses resulted in crystalline powders. The gels formed from H_2bdc and H_3btc with variation of the metal-ligand ratio and the reactant concentration were further evaluated following drying by supercritical CO_2 activation. In the case of H_2bdc, powder X-ray diffraction and ^{27}Al NMR spectra were indicative of the formation of crystalline components consisting of Al(OH)(bdc) (MIL-53(Al)) as the predominant constituent of the aerogels, while no conclusive evidence could be obtained in the case of the H_3btc-based materials. Adsorption analyses and scanning electron microscopy confirmed the presence of a significant mesoporosity within all of the gels, which was found to vary based on the concentration of the starting reagents. The presence of large mesopores was further probed by the demonstration of adsorption of congo red and brilliant blue R-250 dyes, which are not adsorbed within the micropores of the frameworks.

7.4. Separated biphasic reaction system–coordination replication.

The preparation of three-dimensional superstructures using a structure-directing template is of importance in achieving a high level of control over the structure of the system, such that the pore architecture and mass transport kinetics of the system can be finely tuned. An elegant strategy that employs direct conversion of a structuralized metal oxide parent material into a metal-organic framework superstructure with retention of the pore structure, termed coordination replication, has been recently successfully demonstrated.[57] Here, amorphous Al_2O_3 templates were firstly prepared using a sol-gel preparative procedure, and then subjected to microwave treatment in an aqueous solution containing the ditopic linker H_2(1,4-ndc), inducing conversion to the framework Al(OH)(ndc) with retention of the pore structure (shown schematically in Fig. 22a for an oxide architecture containing both macropores and mesopores). This is attributed to the rapid rate of crystallization of the metal-organic framework compared to the rate of dissolution of alumina, which leads to localization of the crystallization of the framework at the surface of the parent material. A variety of different forms of amorphous alumina could be converted, including macroporous and mesoporous aerogels (Fig. 22b) and inverse opal substrates (Fig. 22c-d), demonstrating the versatility of the technique. In the case of the aerogel materials, the replicated structures were tested against bulk Al(OH)(ndc) for their utility in separating an equimolar binary mixture of ethanol and water via a breakthrough-type experiment, and while the separation efficiency of the bulk material was largely retained following structuralization of the framework, the mass transfer kinetics were significantly enhanced for the macroporous and mesoporous structures. Interestingly, a significant difference in performance was also observed between the hierarchical structures. While a lower inlet pressure and faster separation time were observed for the macroporous metal-organic framework aerogel, the higher surface area attributable to the micropores of Al(OH)(ndc) in the mesoporous structure afforded a longer ethanol retention time and greater separation selectivity. Further optimizations in the composition of such superstructures (e.g. the identity of the metal-organic framework) as well as in the size and connectivity of the pores is expected to allow such systems to be utilized in a variety of gas- and liquid-phase separation applications.

7.5. Separated biphasic reaction system–Liquid-liquid interface.

The use of liquid-liquid interface reactions for the creation of three-dimensional superstructures of metal-organic frameworks depends on the ability to create three-dimensional interfaces between two or more liquid phases. Since liquid-liquid interfaces, either between two immiscible liquids or two miscible reactant solutions that are mutually layered on one another, form two-dimensional interfaces, the application of more sophisticated techniques, such as microfluidics, injection or emulsion methods, would be needed in order to harness this method for the formation of three-dimensional superstructures using this approach.

7.6. Top-down approaches.

Significant recent progress has been made in controlling the positioning of individual metal-organic framework crystals,[88,198] and in generating architectures based on the colloidal assembly of crystals.[213] In principle, these techniques could be extended for the generation of three-dimensional superstructures, although demonstrations of this type have not yet been reported to date. In the case of composite materials, typical techniques for the shaping and composition control of the structure are available for optimization of the properties required for specific applications. For example, the Zr-based metal-organic framework $Zr_6O_4(OH)_4(BDC)_6$ (UiO-66) was incorporated within a polymethylarylic acid-*co*-ethylene dimetharylate (poly(MAA-*co*-EDMA)) copolymer to afford a stationary phase for chromatographic separations by Yan and co-workers.[206] Here, nanoparticles of UiO-66 of approximately 210 nm in diameter are firstly synthesized and activated, and then dispersed at the time of the formation of the polymer monolith. The presence of the metal-organic framework enhances the HPLC separation of aromatic hydrocarbons, anilines, phenols, and substituted naphthalenes owing to the differences in the interaction strength of the various analytes with the metal organic-framework surface. This is further corroborated with the increase in separation of the elution times

with an increasing framework loading for each of the separations. It is expected such a preparative strategy is applicable to a large library of supports and metal-organic frameworks (as described for membrane synthesis in Section 5), which is of tremendous promise for generating three-dimensional structures with the right properties for real-world applications.

8. Conclusion and future outlook

As described in the foregoing sections, the structuring of MOFs at the mesoscopic and macroscopic scales is certainly a promising way to enhance material performance beyond that observed for bulk crystalline powders. This review article has highlighted recent developments of MOF architectures and their functions in the context of the six unique synthetic methodologies (Section 2, Fig. 2) that enable the localization of MOF crystallization. The first three strategies, namely the (1) macrostructural template, (2) molecular template, and (3) reaction confinement methods are straightforward approaches that use mixed solutions of precursors to generate the structures. Since almost all of the syntheses for bulk MOFs are carried out in mixed solutions, these methods are expected to be adapted to generate structuralized variants of a large library of MOFs. In particular, macrostructural template requires little tuning of the reaction conditions, and could be readily employed with little optimization of the reaction conditions.

On the other hand, the interfacial reaction systems, which were categorized into (4) liquid-solid interfacial reactions and (5) liquid-liquid interfacial reactions, take advantage of the modular nature of MOF synthesis. Here, the two major components of MOFs (metal ions and organic ligands) are separated to different phases and are reacted only at the interface in which these phases make contact. These approaches, together with the final strategy of (6) top-down approaches, in which preformed MOF nanocrystals are assembled by microfabrication technologies or large crystals are shaped into the desired dimensions by etching or delamination, have only very recently emerged, and successful demonstrations of these methods are still limited to a small number of prototypical frameworks. However, these methods are such that they could be generalized to any MOF system, provided that the reaction or fabrication conditions can be suitably optimized. Furthermore, it can be anticipated that the application of MOF superstructures at the industrial scale will inevitably be conditioned by economical and ecological considerations regarding their synthesis procedures. From this standpoint, (4) liquid-solid interfacial and (5) liquid-liquid interfacial routes are advantageous, because these strategies do not resort to any costly organic templates and solid supports, this latter acting, in the strategy of (4), as the metal cation source through its dissolution.

Thanks to the development of these synthetic strategies, researchers may readily access superstructures of four different dimensionalities. To date, research in this area has primarily been directed towards 2D architectures, although the focus within these systems has recently begun to shift from the development of synthetic methods (Section 5) to the detailed investigation of their properties (Section 6), particularly for applications in molecular sensing and separation. In other applications, one of the important emerging applications of 2D architectures is in cell biology owing to the potential for MOFs that exhibit suitable molecular storage and release properties to allow the stimulation of living cells that are positioned on these superstructures.[69, 214] Here, the spatial control of the molecular release (and consequently the chemically-induced cellular stimulation) could be achieved by creating a desired patterned MOF superstructure.

Compared to the more established 2D systems, superstructures with 0D, 1D, and 3D dimensionalities have only just begun to emerge, and a greater number of applications featuring these architectures are expected to be targeted in the future. For example, a promising application of 0D architectures with hollow structures would be their use as nanostructured catalysts by integrating catalytic nanoparticles in the interior void space. The MOF shell would provide stabilization of the catalysts, as well as a selectivity toward certain target substrates based on size- or functionality-based discrimination of the incoming molecules.[26,215] The 1D architectures of MOFs are also very new systems, and in most cases are synthesized as composite materials. One of the potential applications of 1D MOF-organic polymer composites would their application as flexible MOF membranes.[62] While the crystalline nature of MOFs usually leads to a mechanical rigidity and fragility such that macroscopic softness is not readily obtained with the framework alone. However, the integration of organic polymers with MOFs and their assembly into 1D architectures (with the possibility of further assembly into MOF textiles) would certainly provide flexible MOF separation membranes that precisely fit according to a required configuration. Lastly, the 3D extended architectures inherently possess larger scale porosities (mesoporosity or macroporosity) in addition to the microporosity stemming from the MOF structures. These hierarchically porous systems certainly afford important advantages for separation and catalytic applications via enhancement of the mass transfer efficiency.[57]

From a more fundamental perspective, it is expected that in addition to the above-mentioned applications, the structuring of MOFs will provide an increasingly vibrant area for novel scientific discoveries to be made. For example, although the superstructured systems described above have been derived predominantly from rigid framework systems, one of the most appealing features of MOFs that distinguish them from conventional porous materials is the possibility for a framework flexibility, in which the framework changes its structure in response to the incorporation of guest molecules in the pores.[216,217] This molecular scale structural transformation seems to be strongly influenced by the physical form of the material.[12] Therefore, the introduction of flexibility into MOF superstructures may introduce new phenomena that appear as macroscopic structural transformations.[218] In such a case, the cooperative change of the structures spanning the various

length scales could allow these MOF superstructures to be used in actuator applications. Overall, investigations directed toward establishing a better understanding of the connection between structural changes in molecular scale and those observed in the macroscopic scale is expected to be a rich scientific endeavor.[219] As such, MOF systems represent ideal platforms for research of this type owing to their highly crystalline nature (which allows direct structural elucidation by X-ray crystallography), as well as their responsive properties that can be readily triggered by guest molecule accommodation (which are often precisely controlled by changes in the vapor pressure of the molecule of interest).

Acknowledgements

iCeMS is supported by supported by World Premier International Research Initiative (WPI), MEXT, Japan. S.F. acknowledge a Grand-in-Aid for Scientific Research (No. 25708010 for Wakate A) from MEXT, Japan. K.S. is grateful to JSPS Postdoctoral Fellowship for Foreign Researchers.

Notes and references

[a] Institute for Integrated Cell-Material Sciences (WPI-iCeMS), Kyoto University, Yoshida, Sakyo-ku, Kyoto 606-8501, Japan. E-mail: shuhei.furukawa@icems.kyoto-u.ac.jp (S.F.) or kitagawa@icems.kyoto-u.ac.jp (S.K.)

Reference list

1 O. M. Yaghi, M. O'Keeffe, N. W. Ockwing, H. K. Chae, M. Eddaoudi and J. Kim, *Nature*, 2003, **423**, 705-714.
2 S. Kitagawa, R. Kitaura and S. Noro, *Angew. Chem., Int. Ed*., 2004, **43**, 2334-2375.
3 Metal Organic Frameworks Themed Issue, *Chem. Soc. Rev*., 2009, **38**, 1201-1508.
4 2012 Metal Organic Frameworks Issue, *Chem. Rev*., 2009, **112**, 673-1268.
5 E. A. Flügel, A. Ranft, F. Haase, B. V. Lotsch, *J. Mater. Chem.*, 2012, **22**, 10119-10133.
6 D. Bradshaw, A. Garai, J. Huo, *Chem. Soc. Rev*., 2012,**41**, 2344-2381.
7 N. Stock, S. Biswas, *Chem. Rev*., 2012, **112**, 933-969.
8 A. Carné, C. Carbonell, I. Imaz, D. Maspoch, *Chem. Soc. Rev*., 2011, **40**, 291-305.
9 P. Horcajada, R. Gref, T. Baati, P. K. Allan, G. Maurin, P. Couvreur, G. Férey, R. E. Morris, C. Serre, *Chem. Rev*., 2012, **112**, 1232–1268.
10 M. D. Allendorf, A. Schwartzberg, V. Stavila, A. A. Talin, *Chem. Eur. J,* 2011, **17**, 11372 – 11388.
11 L. E. Kreno, K. Leong, O. K. Farha, M. Allendorf, R. P. Van Duyne, .J. T. Hupp, *Chem. Rev*., 2012, **112**, 1105–1125
12 Y. Sakata, S. Furukawa, M. Kondo, K. Hirai, N. Horike, Y. Takashima, H. Uehara, N. Louvain, M. Meilikhov, T. Tsuruoka, S. Isoda, W. Kosaka, O. Sakata, S. Kitagawa, *Science,* 2013, **339**, 193-196.
13 M. Kondo, S. Furukawa, K. Hirai, S. Kitagawa, *Angew. Chem. Int. Ed*., 2010, **49**, 5327-5330.
14 X.W. Lou, L. A. Archer, Z. Yang, *Adv. Mater*., 2008, **20**, 3987–4019.
15 X.W. Lou, Y. Wang, C. Yuan, J. Y. Lee, L. A. Archer, *Adv. Mater.,* 2006, **18**, 2325–2329.
16 J. Yu, H. Yu, H. Guo, M. Li, S. Mann, *Small*, 2008, **4**, 87–91.
17 S. E. Skrabalak, J. Chen, Y. Sun, X. Lu, L. Au, C. M. Cobley, Y. Xia, *Acc. Chem. Res*., 2008, **41**, 1587 – 1595
18 A. J. Dzieciol and S. Mann, *Chem. Soc. Rev*., 2012, **41**, 79–85.
19 Y. Piao, J. Kim, H. B. Na, D. Kim, J. S. Baek, M. K. Ko, J. H. Lee, M. Shokouhimehr, T. Hyeon, *Nat. Mater*., 2008, **7**, 242 – 247.
20 T. He, D. Chen, X. Jiao, Y. Xu, Y. Gu, *Langmuir*, 2004, **20**, 8404–8408.
21 M. Hu, S. Furukawa, R. Ohtani, H. Sukegawa, Y. Nemoto, J. Reboul, S. Kitagawa, Y. Yamauchi, *Angew. Chem. Int. Ed*., 2012, **51**, 984 – 988
22 N. Navascues, C. Téllez, J. Coronas, *Micropor. Mesopor. Mater.,* 2008, **112**, 561-572.
23 S. Aguado, J. Canivet, D. Farrusseng, *Chem. Commun*., 2010, **46**, 7999-8001.
24 S. Aguado, J. Canivet, D. Farrusseng, *J. Mater. Chem.,* 2011, **21**, 7582-7588.
25 S. Sorribas, B. Zornoza, C. Téllez, J. Coronas, *Chem. Commun*., 2012, **48**, 9388-9390.
26 C. H. Kuo, Y. Tang, L. Y. Chou, B. T. Sneed, C. N. Brodsky, Z. Zhao, C. K. Tsung, *J. Am. Chem. Soc*., 2012, **134**, 14345-14348.
27 S. Furukawa, K. Hirai, K. Nakagawa, Y. Takashima, R. Matsuda, T. Tsuruoka, M. Kondo, R. Haruki, D.Tanaka, H. Sakamoto, S. Shimomura, O. Sakata, S. Kitagawa, *Angew. Chem. Int. Ed*., 2009, **48**, 1766-1770.
28 S. Furukawa, K. Hirai, Y. Takashima, K. Nakagawa, M. Kondo, T. Tsuruoka, O. Sakata, S. Kitagawa, *Chem. Commun*.**,** 2009*,* 5097-5099.
29 K. Koh, A. G. Wong-Foy, A. J. Matzger, *Chem. Commun*., 2009, 6162-6164.
30 K. Hirai, S. Furukawa, M. Kondo, H. Uehara, O. Sakata, S. Kitagawa, *Angew. Chem. Int. Ed.,* 2011, **50**, 8057-8061.
31 K. Hirai, S. Furukawa, M. Kondo, M. Meilikhov, Y. Sakata, O. Sakata, S. Kitagawa, *Chem. Commun.,* 2012, **48**, 6472-6474.
32 H. J. Lee, W. Cho, M. Oh, *Chem. Commun*., 2012, **48**, 221-223.
33 A. L. Li, F. Ke, L. G. Qiu, X. Jiang, Y. M. Wang, X. Y. Tian, *CrystEngComm,* 2013, **15**, 3554-3559.
34 J. Huo, M. Marcello, A. Garai, D. Bradshaw, *Adv. Mater*., 2013, **25**, 2717-2722.
35 M. Pang, A. J. Cairns, Y. Liu, Y. Belmabkhout, H. C. Zeng, M. Eddaoudi, *J. Am. Chem. Soc*., 2013, **135**, 10234-10237.
36 M. Pang, A. J. Cairns, Y. Liu, Y. Belmabkhout, H. C. Zeng, M. Eddaoudi, *J. Am. Chem. Soc*., 2012, **134**, 13176-13179.
37 L. Peng, J. Zhang, J. Li, B. Han, Z. Xue, B. Zhang, J. Shi, *J Colloid Interface Sci.,* 2014, **416**, 198-204.
38 A. Carné-Sánchez, I. Imaz, M. Cano-Sarabia, D. Maspoch, *Nat. Chem*., 2013, **5**, 203-211.
39 R. Ameloot, F. Vermoortele, W. Vanhove, M. B. J. Roeffaers, B. F. Sels, D. E. De Vos, *Nat. Chem*., 2011, **3**, 382-387.
40 K. Jayaramulu, K. S. Krishna, S. J. George, M. Eswaramoorthy, T. K. Maji, *CrystEngComm*,, 2013, **49**, 3937-3939.
41 H. Kitching, M. J. Shiers, A. J. Kenyon, I. P. Parkin, *J. Mater. Chem. A*, 2013, **1**, 6985–6999.

42 N. Liu, Y. Yao, J. J. Cha, M. T. McDowell, Y. Han, Y. Cui, *Nano Res.*, 2012, **5**, 109–116.
43 O. Shekhah, H. Wang, D. Zacher, R. A. Fischer, C. Wöll, *Angew. Chem. Int. Ed.*, 2009, **48**, 5038–5041.
44 S. Diring, S. Furukawa, Y. Takashima, T. Tsuruoka, S. Kitagawa, *Chem. Mater.*, 2010, **22**, 4531–4538.
45 P. Pachfule, B. K. Balan, S. Kurungot, R. Banerjee, *Chem. Commun.*, 2012, **48**, 2009–2011.
46 M. Maksoud, N. Roques, S. Brandès, L. Arurault, J.-P. Sutter, *J. Mater. Chem. A*, 2013, **1**, 3688–3693.
47 Y. Yoo, H.-K. Jeong, *Chem. Commun.*, 2008, 2441–2443.
48 Y. Mao, W. Cao, J. Li, L. Sun, X. Peng, *Chem. Eur. J.*, 2013, **19**, 11883–11886.
49 L. V. Meyer, J. Vogt, F. A. Brede, H. Schäfer, M. Steinhart, K. Müller-Buschbaum, *CrystEngComm*, 2013, **15**, 9382–9386.
50 M. He, J. Yao, Z.-X. Low, D. Yu, Y. Feng, H. Wang, *RSC Adv.*, 2014, **4**, 7634–7639.
51 C. Petit, T. J. Bandosz, *Adv. Mater.* 2009, **21**, 4753–4757.
52 M. Jahan, Q. Bao, J.-X. Yang, K. P. Loh, *J. Am. Chem. Soc.*, 2010, **132**, 14487–14495.
53 A. Umemura, S. Diring, S. Furukawa, H. Uehara, T. Tsuruoka, S. Kitagawa, *J. Am. Chem. Soc.,* 2011, **133**, 15506-15513.
54 T. Tsuruoka, S. Furukawa, Y. Takashima, K. Yoshida, S. Isoda, S. Kitagawa, *Angew. Chem. Int. Ed.*, 2009, **48**, 4739–4743.
55 M.-H. Pham, G.-T. Vuong, F.-G. Fontaine, T.-O. Do, *Cryst. Growth Des.*, 2012, **12**, 3091–3095.
56 W. Zhan, Q. Kuang, J. Zhou, X. Kong, Z. Xie, L. Zheng, *J. Am. Chem. Soc.*, 2013, **135**, 1926–1933.
57 J. Reboul, S. Furukawa, N. Horike, M. Tsotsalas, K. Hirai, H. Uehara, M. Kondo, N. Louvain, O. Sakata, S. Kitagawa, *Nat Mater*, 2012, **11**, 717–723.
58 J. Puigmartí-Luis, D. Schaffhauser, B. R. Burg, P. S. Dittrich, *Advanced Materials*, 2010, **22**, 2255–2259.
59 J. Wang, Y. L. Bunimovich, G. Sui, S. Savvas, J. Wang, Y. Guo, J. R. Heath, H.-R. Tseng, *Chem. Commun.*, 2006, 3075–3077.
60 J. Puigmartí-Luis, M. Rubio-Martínez, U. Hartfelder, I. Imaz, D. Maspoch, P. S. Dittrich, *J. Am. Chem. Soc.*, 2011, **133**, 4216–4219.
61 M. Faustini, J. Kim, G.-Y. Jeong, J. Y. Kim, H. R. Moon, W.-S. Ahn, D.-P. Kim, *J. Am. Chem. Soc.*, 2013, **135**, 14619–14626.
62 R. Ostermann, J. Cravillon, C. Weidmann, M. Wiebcke, B. M. Smarsly, *Chem. Commun.*, 2010, **47**, 442–444.
63 M. Rose, B. Böhringer, M. Jolly, R. Fischer, S. Kaskel, *Adv. Eng. Mater.*, 2011, **13**, 356–360.
64 Y. Wu, F. Li, H. Liu, W. Zhu, M. Teng, Y. Jiang, W. Li, D. Xu, D. He, P. Hannam, G. Li, *J. Mater. Chem.*, 2012, **22**, 16971–16978.
65 L. Fan, M. Xue, Z. Kang, H. Li, S. Qiu, *J. Mater. Chem.*, 2012, **22**, 25272–25276.
66 M. da S. Pinto, C. A. Sierra-Avila, J. P. Hinestroza, *Cellulose*, 2012, **19**, 1771–1779.
67 E. F. de Melo, N. da C. Santana, K. G. B. Alves, G. F. de Sá, C. P. de Melo, M. O. Rodrigues, S. A. Júnior, *J. Mater. Chem. C*, 2013, **1**, 7574–7581.
68 K. Khaletskaya, J. Reboul, M. Meilikhov, M. Nakahama, S. Diring, M. Tsujimoto, S. Isoda, F. Kim, K. Kamei, R. A. Fischer, S. Kitagawa, S. Furukawa, *J. Am. Chem. Soc.*, 2013, **135**, 10998–11005.
69 S. Diring, D. O. Wang, C. Kim, M. Kondo, Y. Chen, S. Kitagawa, K. Kamei, S. Furukawa, *Nat Commun*, 2013, **4**, 2684.
70 N. Yanai, M. Sindoro, J. Yan, S. Granick, *J. Am. Chem. Soc.*, 2013, **135**, 34–37.
71 N. Yanai, S. Granick, *Angew. Chem. Int. Ed.*, 2012, **51**, 5638–5641.
72 S. Hermes, F. Schröder, R. Chelmowski, C. Wöll, R. A. Fischer, *J. Am. Chem. Soc.*, 2005, **127**, 13744–13745.
73 D. Zacher, O. Shekhah, C. Wöll, R. A. Fischer, *Chem. Soc. Rev.*, 2009, **38**, 1418–1429.
74 D. Zacher, R. Schmid, C. Wöll, R. A. Fischer, *Angew. Chem. Int. Ed.*, 2011, **50**, 176–199.
75 A. Bétard, R. A. Fischer, *Chem. Rev*., 2009, **112**, 1055–1083.
76 D. Zacher, A. Baunemann, S. Hermes, R. A. Fischer, *J. Mater. Chem.*, 2007, **17**, 2785–2792.
77 O. Kozachuk, K. Yusenko, H. Noei, Y. Wang, S. Walleck, T. Glaser, R. A. Fischer, *Chem. Commun.*, 2011, 8509–8511.
78 Y. Liu, Z. Ng, E. A. Khan, H.-K. Jeong, C.-B. Ching, Z. Lai, *Microporous Mesoporous Mater.*, 2009, **118**, 296–301.
79 E. Biemmi, C. Scherb, T. Bein, *J. Am. Chem. Soc.*, 2007, **129**, 8054–8055.
80 G. Lu , O. K. Farha , W. Zhang, F. Huo, J. T. Hupp, *Adv. Mater.*, 2012, **24**, 3970–3974.
81 A. Schödel, C. Scherb, T. Bein, *Angew. Chem., Int. Ed.*, 2010, **49**, 7225–7228.
82 C. Scherb, A. Schödel, T. Bein, *Angew. Chem., Int. Ed.*, 2008, **47**, 5777–5779.
83 A. Huang, H. Bux, F. Steinbach, J. Caro, *Angew. Chem. Int. Ed.*, 2010, **49**, 4958–4961.
84 A. Huang, W. Dou, J. Caro, *J. Am. Chem. Soc.*, 2010, **132**, 15562–15564.
85 A. Huang, J. Caro, *Angew. Chem. Int. Ed.*, 2011, **50**, 4979–4982.
86 A. Huang, N. Wang, C. Kong, J. Caro, *Angew. Chem. Int. Ed.*, 2012, **51**, 10551–10555.
87 P. A. Szilágyi, R. J. Westerwaal, R. van de Krol, H. Geerlings, B. Dam, *J. Mater. Chem. C*, 2013, **1**, 8146–8155.
88 P. Falcaro, A. J. Hill, K. M. Nairn, J. Jasieniak, J. I. Mardel, T. J. Bastow, S. C. Mayo, M. Gimona, D. Gomez, H. J. Whitfield, R. Riccò, A. Patelli, B. Marmiroli, H. Amenitsch, T. Colson, L. Villanova, D. Buso, *Nat. Commun.*, 2011 , **2**, 237.
89 T. Ben, C. Lu, C. Pei, S. Xu, S. Qiu, *Chem. Eur. J.*, 2012, **18**, 10250–10253.
90 M. C. McCarthy, V. Varela-Guerrero, G. V. Barnett, H.-K. Jeong, *Langmuir*, 2010, **26**, 14636–14641.
91 O. Shekhah, H. Wang, S. Kowarik, F. Schreiber, M. Paulus, M. Tolan, C. Sternemann, F. Evers, D. Zacher, R. A. Fischer, C. Wöll, *J. Am. Chem. Soc.*, 2007, **129**, 15118–15119.
92 D. Zacher, K. Yusenko, A. Bétard, S. Henke, M. Molon, T. Ladnorg, O. Shekhah, B. Schu□pbach, T. de los Arcos, M. Krasnopolski, M. Meilikhov, J. Winter, A. Terfort, C. Wöll, R. A. Fischer, *Chem. Eur. J.*, 2011, **17**, 1448–1455.
93 C. Shen, I. Cebula, C. Brown, J. Zhao, M. Zharnikov, M. Buck, *Chem. Sci.*, 2012, **3**, 1858-1865.
94 C. Munuera, O. Shekhah, H. Wang, C. Wöll, C. Ocal, *Phys. Chem. Chem. Phys.*, 2008, **10**, 7257–7261.
95 B. Liu, M. Tu, D. Zacher, R. A. Fischer, *Adv. Funct. Mater.*, 2013, **23**, 3790–3798.

96 O. Zybaylo, O. Shekhah, H. Wang, M. Tafipolsky, R. Schmid, D. Johannsmann, C. Wöll, *Phys. Chem. Chem. Phys.*, 2010, **12**, 8092–8097.
97 V. Stavila, J. Volponi, A. M. Katzenmeyer, M. C. Dixon, M. D. Allendorf, *Chem. Sci.*, 2012 , **3**, 1531–1540.
98 H. Gliemann, C. Wöll, *Mater. Today*, 2012, **15**, 113–116.
99 B. Liu, R. A. Fischer, *Sci. China Chem.*, 2011, **54**, 1851–1866.
100 O. Shekhah, H. Wang, M. Paradinas, C. Ocal, B. Schüpbach, A. Terfort, D. Zacher, R. A. Fischer, C. Wöll, *Nat. Mater.*, 2009, **8**, 481–484.
101 A. Bétard, H. Bux, S. Henke, D. Zacher, J. Caro, Roland A. Fischer, *Micropor. Mesopor. Mater.*, 2012, **150**, 76–82.
102 M. C. So, S. Jin, H.-J. Son, G. P. Wiederrecht, O. K. Farha, J. T. Hupp, *J. Am. Chem. Soc.*, 2013, **135**, 15698−15701.
103 K. Otsubo, T. Haraguchi, O. Sakata, A. Fujiwara, H. Kitagawa, *J. Am. Chem. Soc.*, 2012, **134**, 9605–9608.
104 O. Shekhah, K. Hirai, H. Wang, H. Uehara, M. Kondo, S. Diring, D. Zacher, R. A. Fischer, O. Sakata, S. Kitagawa, S. Furukawa, C. Wöll, *Dalton Trans.*, 2011, **40**, 4954–4958.
105 M. Meilikhov, S. Furukawa, K. Hirai, R. A. Fischer, S. Kitagawa, *Angew. Chem. Int. Ed.*, 2013, **52**, 341–345.
106 M. Tu, S. Wannapaiboon, R. A. Fischer, *Dalton Trans.*, 2013, **42**, 16029–16035.
107 R. Makiura, S. Motoyama, Y. Umemura, H. Yamanaka, O. Sakata, H. Kitagawa, *Nat. Mater.*, 2010, **9**, 565-571.
108 S. Motoyama, R. Makiura, O. Sakata, H. Kitagawa, *J. Am. Chem. Soc.*, 2011, **133**, 5640–5643.
109 R. Makiura, H. Kitagawa, *Eur. J. Inorg. Chem.*, 2010, **24**, 3715–3724.
110 M. Arnold, P. Kortunov, D. J. Jones, Y. Nedellec, J. Karger, J. Caro, *Eur. J. Inorg. Chem.*, 2007, 60–64.
111 S. Takamizawa, Y. Takasaki, R. Miyake, *J. Am. Chem. Soc.*, 2010, **132**, 2862–2863.
112 R. Ranjan, M. Tsapatsis, *Chem. Mater.*, 2009, **21**, 4920–4924.
113 J. Nan, X. Dong, W. Wang, W. Jin, *Microporous Mesoporous Mater.*, 2012, **155**, 90–98.
114 V. Varela-Guerrero, Y. Yoo, M. C. McCarthy, H.-K. Jeong, *J. Mater. Chem.*, 2010, **20**, 3938–3943.
115 Y. Yoo, Z. P. Lai, H. K. Jeong, *Microporous Mesoporous Mater.*, 2009, **123**, 100–106.
116 H. Bux, F. Liang, Y. Li, J. Cravillon, M. Wiebcke, J. Caro, *J. Am. Chem. Soc.*, 2009, **131**, 16000–16001.
117 J. Yao, L. Li, W. Hao, B. Wong, C. Tan, D. Dong, H. Wang, *Mater. Chem. Phys.*, 2013, **139**, 1003–1008.
118 L. Li, J. Yao, R. Chen, L. He, K. Wang, H. Wang, *Microporous Mesoporous Mater.*, 2013, **168**, 15–18.
119 J. Gascon, S. Aguado, F. Kapteijn, *Micropor. Mesopor. Mater.*, 2008, **113**, 132–138.
120 L. Fan, M. Xue, Z. Kang, S. Qiu, *Sci. China Chem.*, 2013, **56**, 459–464.
121 R. Ameloot, E. Gobechiya, H. Uji-i, J. A. Martens, J. Hofkens, L. Alaerts, B. F. Sels, D. E. De Vos, *Adv. Mater.*, 2010, **22**, 2685–2688.
122 C. Carbonell, I. Imaz, D. Maspoch, *J. Am. Chem. Soc.*, 2011, **133**, 2144–2147.
123 C. Carbonell, K. C. Stylianou, J. Hernando, E. Evangelio, S. A. Barnett, S. Nettikadan, I. Imaz, D. Maspoch, *Nature Commun.,* 2013, **4**, 2173.
124 J.-L. Zhuang, D. Ar, X.-J. Yu, J.-X. Liu, A. Terfort, *Adv. Mater.*, 2013, **25**, 4631–4635.
125 M. N. Shah, M. A. Gonzalez, M. C. McCarthy, H.-K. Jeong, *Langmuir*, 2013, **29**, 7896–7902.
126 L. D. Salmi, M. J. Heikkilä, E. Puukilainen, T. Sajavaara, D. Grosso, M. Ritala, *Micropor. Mesopor. Mater.*, 2013, **182**, 147–154.
127 H. Guo, G. Zhu, I. J. Hewitt, S. Qiu, *J. Am. Chem. Soc.*, 2009, **131**, 1646–1647.
128 Y. Mao, W. Cao, J. Li, Yu Liu, Y. Ying, L. Sun, X. Peng, *J. Mater. Chem. A*, 2013, **1**, 11711–11716.
129 Y. Hu, X. Dong, J. Nan, W. Jin, X. Ren, N. Xa, Y. M. Lee, *Chem. Commun.*, 2011, **47**, 737–739.
130 W. Wang, X. Dong, J. Nan, W. Jin, Z. Hu, Y. Chen, J. Jiang, *Chem. Commun.*, 2012, **48**, 7022–7024.
131 X. Dong, K. Huang, S. Liu, R. Ren, W. Jin, Y. S. Lin, *J. Mater. Chem*. 2012, **22**, 19222-19227.
132 X. Zou, G. Zhu, I. J. Hewitt, F. Sun, S. Qiu, *Dalton Trans.*, 2009, 3009–3013.
133 Z. Kang, M. Xue, L. Fan, J. Ding, L. Guo, L. Gao, S. Qiu, *Chem. Commun.*, 2013, **49**, 10569-10571.
134 R. Ameloot, L. Stappers, J. Fransaer, L. Alaerts, B. F. Sels, D. E. De Vos, *Chem. Mater.*, 2009, **21**, 2580–2582.
135 B. Van de Voorde, R. Ameloot, I. Stassen, M. Everaert, D. De Vos, J.-C. Tan, *J. Mater. Chem. C*, 2013, **1**, 7716–7724.
136 R. Ameloot, L. Pandey, M. Van der Auweraer, L. Alaerts, B. F. Sels, D. E. De Vos, *Chem. Commun.*, 2010, **46**, 3735–3737.
137 K. Okada, R. Ricco, Y. Tokudome, M. J. Styles, A. J. Hill, M. Takahashi, P. Falcaro, *Adv. Funct. Mater.*, 2014, in press. DOI: 10.1002/adfm.201303303.
138 Y. Mao, L. Shi, H. Huang, W. Cao, J. Li, L. Sun, X. Jin, X. Peng, *Chem. Commun.*, 2013, **49**, 5666–5668.
139 A. Putnis, *Rev. Miner. Geochem.* 2009, **70**, 87–124.
140 I. Stassen, N Campagnol, J. Fransaer, P. Vereecken, D. E. De Vos, R. Ameloot, *CrystEngComm*, 2013, **15**, 9308–9311.
141 J. Yao, D. Dong, D. Li, L. He, G. Xu, H. Wang, *Chem. Commun.*, 2011, **47**, 2559–2561.
142 M. He, J. Yao, L. Li, Z. Zhong, F. Chen, H. Wang, *Microporous Mesoporous Mater.*, 2013, **179**, 10–16.
143 N. Hara, M. Yoshimune, H. Negishi, K. Haraya, S. Hara, T. Yamaguchi, *RSC Adv.*, 2013, **3**, 14233–14236.
144 H. Lu, S. Zhu, *Eur. J. Inorg. Chem.*, 2013, 1294–1300.
145 S. H. Jhung, J.-H. Lee, J. W. Yoon, C. Serre, G. Férey, J.-S. Chang, *Adv. Mater.*, **2007,** 19, 121–124.
146 W. J. Rieter, K. M. L. Taylor, H. An, W. Lin, W. Lin, *J. Am. Chem. Soc.*, 2006, **128**, 9024-9025.
147 C. Sanchez, B. Lebeau, F. Chaput, J.-P. Boilot, *Adv. Mater.*, 2003, **15**, 1969–1995.
148 P. Horcajada, C. Serre, D. Grosso, C. Boissière, S. Perruchas, C. Sanchez, G. Férey, *Adv. Mater.*, 2009, **21**, 1931–1935.
149 A. Demessence, P. Horcajada, C. Serre, C. Boissière, D. Grosso, C. Sanchez, G. Férey, *Chem. Commun.*, 2009, 7149-7151.

150 A. Demessence, C. Boissière, D. Grosso, P. Horcajada, C. Serre, G. Férey, G. J. A. A. Soler-Illiac, C. Sanchez, *J. Mater. Chem.*, 2010, **20**, 7676–7681.
151 F. M. Hinterholzinger, A. Ranft, J. M. Feckl, B. Rühle, T. Bein, B. V. Lotsch, *J. Mater. Chem.*, 2012, **22**, 10356–10362.
152 H. Guo, Y. Zhu, S. Qiu, J. A. Lercher, H. Zhang, *Adv. Mater.*, 2010, **22**, 4190-4192.
153 M. Tsotsalas, A. Umemura, F. Kim, Y. Sakata, J. Reboul, S. Kitagawa, S. Furukawa, *J. Mater. Chem.*, 2012, **22**, 10159-10165.
154 G. Lu, C. Cui, W. Zhang, Y. Liu, F. Huo, *Chem. Asian J.*, 2013, **8**, 69–72.
155 C. M. Doherty, G. Grenci, R. Riccò, J. I. Mardel, J. Reboul, S. Furukawa, S. Kitagawa, A. J. Hill, P. Falcaro, *Adv. Mater.*, 2013, **25**, 4701–4705.
156 T. Sasaki, M. Watanabe, H. Hashizume, H. Yamada, H. Nakazawa, *J. Am. Chem. Soc.*, 1996, **118**, 8329-8335.
157 Z. Liu, R. Ma, M. Osada, N. Iyi, Y. Ebina, K. Takada, T. Sasaki, *J. Am. Chem. Soc.*, 2006, **128**, 4872–4880.
158 K. S. Novoselov, A. K. Geim, S. V. Morozov, D. Jiang, Y. Zhang, S. V. Dubonos, I. V. Grigorieva, A. A. Firsov, *Science*, 2004, **306**, 666-669.
159 P.-Z. Li, Y. Maeda, Q. Xu, *Chem. Commun.*, 2011, **47**, 8436–8438.
160 M. Darbandi, H. K. Arslan, O. Shekhah, A. Bashir, A. Birkner, C. Wöll, *Phys. Status Solidi RRL*, 2010, **4**, 197–199.
161 S. C. Junggeburth, L. Diehl, S. Werner, V. Duppel, W. Sigle, B. V. Lotsch, *J. Am. Chem. Soc.*, 2013, **135**, 6157−6164.
162 M. D. Allendorf, C. A. Bauer, R. K. Bhakta R. J. T. Houk, *Chem. Soc. Rev*. 2009, **38**, 1330-1352.
163 Y. Cui, Y. Yue, G. Qian, B. Chen, Chem. Rev. 2012, **112**, 1126–1162.
164 Y. Takashima, V. M. Martinez, S. Furukawa, M. Kondo, S. Shimomura, H. Uehara, M. Nakahama, K. Sugimoto, S. Kitagawa, *Nat. Commun.* 2011, **2**, 168.
165 J. W. Grate, *Chem. Rev.*, 2000, **100**, 2627–2648.
166 E. Biemmi, A. Darga, N. Stock, T. Bein, *Microporous Mesoporous Mater.*, 2008, **114**, 380–386.
167 H. Uehara, S. Diring, S. Furukawa, Z. Kalay, M. Tsotsalas, M. Nakahama, K. Hirai, M. Kondo, O. Sakata, S. Kitagawa, *J. Am. Chem. Soc.*, 2011, **133**, 11932–11935.
168 K. Hirai, K. Sumida, M. Meilikhov, N. Louvain, M. Nakahama, H. Uehara, S. Kitagawa, S. Furukawa, *J. Mater. Chem. C*, 2013, in press. DOI: 10.1039/C3TC32101K.
169 S. Wannapaiboon, M. Tu, R. A. Fischer, *Adv. Funct. Mater.*, 2014, in press. DOI: 10.1002/adfm.201302854
170 M. Tsotsalas, P. Hejcik, K. Sumida, Z. Kalay, S. Furukawa, S. Kitagawa, *J. Am. Chem. Soc.*, 2013, **135**, 4608−4611.
171 L. Heinke, C. Wöll, *Phys. Chem. Chem. Phys.*, 2013, **15**, 9295–9299.
172 M. D. Allendorf, R. J. T. Houk, L. Andruszkiewicz, A. A. Talin, J. Pikarsky, A. Choudhury, K. A. Gall, P. J. Hesketh, *J. Am. Chem. Soc.*, 2008, **130**, 14404–14405.
173 R. J. T. Houk, J.-H. Lee, M. D. Allendorf, P.J. Hesketh, *ECS Trans.*, 2009, **19**, 267–278.
174 S. Kitagawa, R. Matsuda, *Coord. Chem. Rev.*, 2007, **251**, 2490–2509.
175 K. Uemura, R. Matsuda, S. Kitagawa, *J. Sol. State Chem.*, 2005, **178**, 2420– 2429.
176 A. Venkatasubramanian, J.-H. Lee, V. Stavila, A. Robinson, M. D. Allendorf, P. J. Hesketh, *Sens. Actuators, B*, 2012, **168**, 256–262.
177 Y.-M. Zhu, C.-H. Zeng, T.-S. Chu, H.-M. Wang, Y.-Y. Yang, Y.-X. Tong, C.-Y. Su, W.-T. Wong, *J. Mater. Chem. A*, 2013, **1**, 11312–11319.
178 J. Zhuang, J. Friedel, A. T. Beilstein, *J. Nanotechnol.*, 2012, **3**, 570–578.
179 A. M. Marti, S. D. Perera, L. D. McBeath, K. J. Balkus Jr., *Langmuir*, 2013, **29**, 5927−5936.
180 Z. Dou, J. Yu, H. Xu, Y. Cui, Y. Yang, G. Qian, *Micropor. Mesopor. Mater.*, 2013, **179**, 198–204.
181 H. Guo, S. Zhu, D. Cai, C. Liu, *Inorg. Chem. Commun.*, 2014, **41**, 29–32.
182 W.-J. Li, S.-Y. Gao, T.-F. Liu, L.-W. Han, Z.-J. Lin, R. Cao, *Langmuir*, 2013, **29**, 8657−8664.
183 C.-W. Kung, T. C. Wang, J. E. Mondloch, D. Fairen-Jimenez, D. M. Gardner, W. Bury, J. M. Klingsporn, J. C. Barnes, R. Van Duyne, J. F. Stoddart, M. R. Wasielewski, O. K. Farha, J. T. Hupp, *Chem. Mater.*, 2013, **25**, 5012–5017.
184 G. Lu, J. T. Hupp, *J. Am. Chem. Soc.*, 2010, **132**, 7832–7833.
185 G. Lu, O. K. Farha, L. E. Kreno, P. M. Schoenecker, K. S. Walton, R. P. Van Duyne, J. T. Hupp, *Adv. Mater.*, 2011, **23**, 4449–4452.
186 L. E. Kreno, J. T. Hupp, R. P. Van Duyne, *Anal. Chem.*, 2010, **82**, 8042–8046.
187 J. Liu, F. Sun, F. Zhang, Z. Wang, R. Zhang, C Wang, S. Qiu, *J. Mater. Chem.*, 2011, **21**, 3775–3778.
188 D. Ma, Y. Li, Z. Li, *Chem. Commun.*, 2011, **47**, 7377–7379.
189 Y. Yoo, V. Varela-Guerrero, H.-K. Jeong, *Langmuir*, 2011, **27**, 2652–2657.
190 Y. Pan, Z. Lai, *Chem. Commun.*, 2011, **47**, 10275–10277.
191 Y. Li, F. Liang, H. Bux, W. Yang, J. Caro, *J. Membr. Sci.*, 2010, **354**, 48–54.
192 Y. Liu, E. Hu, E. A. Khan, Z. Lai, *J. Membr. Sci.*, 2010, **353**, 36–40.
193 F. Zhang, X. Zou, X. Gao, S. Fan, F. Sun, H. Ren, G. Zhu, *Adv. Funct. Mater.*, 2012, **22**, 3583–3590.
194 K. Huang, S. Liu, Q. Li, W. Jin, *Sep. Purif. Technol.*, 2013, **119**, 94–101.
195 G. Xu, K. Otsubo, T. Yamada, S. Sakaida, H. Kitagawa, *J. Am. Chem. Soc.*, 2013, **135**, 7438–7441.
196 A. A. Talin, A. Centrone, A. C. Ford, M. E. Foster, V. Stavila, P. Haney, R. A. Kinney, V. Szalai, F. El Gabaly, H. P. Yoon, F. Léonard, M. D. Allendorf *Science*, 2014, **343**, 66–69.
197 R. Krishna and J. R. Long. *J. Phys. Chem. C*, 2011, **115**, 12941-12950.
198 R. Ricco, L. Malfatti, M. Takahashi, A. J. Hill and P. Falcaro, *J. Mater. Chem. A*, 2013, **1**, 13033-13045.
199 C. M. Doherty, D. Buso, A. J. Hill, S. Furukawa, S. Kitagawa and P. Falcaro, *Acc. Chem. Res.*, 2014, **47**, 396-405.
200 D. Qian, C. Lei, G.-P. Hao, W.-C. Li and A.-H. Lu, *ACS Appl. Mater. Interfaces*, 2012, **4**, 6125-6132.
201 C. A. F. de Oliveira, F. F. da Silva, G. C. Jimenez, J. F. da S. Neto, D. M. B. de Souza, I. A. de Souzac and S. A. Júnior, *Chem. Commun.* 2013, **49**, 6486-6488.
202 Y.-K. Seo, J. W. Yoon, U.H. Lee, Y. K. Hwang, C.-H. Jun and J.-S. Chang, *Micropor. Mesopor. Mater*. 2012, **155**, 75-81.

203 A. Sachse, R. Ameloot, B. Coq, F. Fajula, B. Coasne, D. De Vos and A. Galarneau, *Chem. Commun.* 2012, **48**, 4749-4751.
204 C. Petit and T. J. Bandosz, *Adv. Funct. Mater.* 2011, **21**, 2108-2117.
205 S. Bashkova and T. J. Bandosz, *J. Colloid Interface Sci.* 2014, **417**, 109-114.
206 Y.-Y. Fu, C.-X. Yang and X.-P. Yan, *Chem. Commun.*, 2013, **49**, 7162-7164.
207 E. V. Ramos-Fernandez, M. Garcia-Domingos, J. Juan-Alcañiz, J. Gascon and F. Kapteijn, *Appl. Catal. A* 2011, **391**, 261-267.
208 S. Cao, G. Gody, W. Zhao, S. Perrier, X. Peng, C. Ducati, D. Zhao and A. K. Cheetham, *Chem. Sci.* 2013, **4**, 3573-3577.
209 K. M. Choi, H. J. Jeon, J. K. Kang and O. M. Yaghi, *J. Am. Chem. Soc.*, 2011, **133**, 11920-11923.
210 Z. Xin, J. Bai, Y. Pan and M. J. Zaworotko, *Chem. Eur. J.*, 2010, **16**, 13049-13052.
211 Y. Yue, Z.-A. Qiao, P. F. Fulvio, A. J. Binder, C. Tian, J. Chen, K. M. Nelson, X. Zhu and S. Dai, *J. Am. Chem. Soc.*, 2013, **135**, 9572-9575.
212 M. R. Lohe, M. Rose and S. Kaskel, *Chem. Commun.*, 2009, 6056-6058.
213 M. Sindoro, N. Yanai, A.-Y. Jee and S. Granick, *Acc. Chem. Res.* 2014, **47**, 459–469.
214 M. Tsotsalas, J. Liu, B. Tettmann, S. Grosjean, A. Shahnas, Z. Wang, C. Azucena, M. Addicoat, T. Heine, J. Lahann, J. Overhage, S. Bräse, H. Gliemann, C. Wo□ll, *J. Am. Chem. Soc*. 2014, **136**, 8-11.
215 G.H. Wang, J. Hilgert, F. H. Richter, F. Wang, H. J. Bongard, B. Spliethoff, C. Weidenthaler, F. Schüth, *Nat. Mater*., 2014, **13**, 293-300.
216 S. Kitagawa, M. Kondo, *Bull. Chem. Soc. Jpn*. 1998, **71**, 1739-1753.
217 S. Horike, S, Shimomura, S. Kitagawa, *Nat. Chem*. 2009, **1**, 695-704.
218 D. Masopoch, D. Ruiz-Molina, K. Wurst, N. Domingo, M. Cavallini, F. Biscarini, J. Tejada, C. Rovira, J. Veciana, *Nat. Mater*., 2003, **2**, 190-195.
219 S. Kobatake, S. Takami, H. Muto, T. Ishikawa, M. Irie, *Nature*, 2007, **446**, 778-781.

Caption for the group photograph:

From left to right: Shuhei Furukawa, Stéphane Diring, Kenji Sumida (back), Julien Reboul, Susumu Kitagawa (front)

Shuhei Furukawa received his PhD degree in 2005 from Kyoto University. After a postdoctoral research at Katholieke Universiteit Lueven (KUL), he returned to Kyoto University in 2007 as an assistant professor. In 2008, he moved to the JST ERATO Kitagawa Integrated Pores Project as a group leader and since 2010 he has been an associate professor in the Institute for Integrated Cell-Material Sciences (WPI-iCeMS), Kyoto University. His main research interest is in coordination chemistry and particularly synthesis and property of framework materials in the mesoscale and their applications in electronics and cell biology.

Julien Reboul received his PhD degree in chemistry from the University of Montpellier II (France) in 2009. He was then a post-doctoral fellow at the JST ERATO Kitagawa Integrated Pores Project in Kyoto (Japan). Since 2011, he has been working at the Institute for Integrated Cell-Material Sciences (WPI-iCeMS) at Kyoto University (Japan). His research interests are centered on the synthesis of hybrid porous materials, including metal oxides, porous coordination polymers and mesostructured composites, through self-assembly and replacement processes.

Stéphane Diring received his bachelor degree (B.Sc.) in applied chemistry from the Nottingham Trent University in 2004 and his PhD degree in molecular chemistry from the University of Strasbourg (France) in 2009. He then joined the group of Prof. Kitagawa in Kyoto as a postdoctoral fellow and he is currently an assistant professor in the Institute for Integrated Cell-Material Sciences (WPI-iCeMS), Kyoto University. His research interests include hybrid porous materials and supramolecular chemistry.

Kenji Sumida was born in 1982 in New Zealand, and received his B.Sc. (2003) and M.Sc. (2007) degrees at the University of Auckland. He then joined the laboratory of Prof. Jeffrey R. Long at the University of California, Berkeley, where he earned his Ph.D. (2012) in Chemistry. He is currently a JSPS Postdoctoral Fellow in Prof. Susumu Kitagawa's laboratory at Kyoto University, where his main interests are the fabrication of three-dimensional superstructures of metal-organic frameworks, and the integration of porous solids within functional devices.

Susumu Kitagawa received his PhD from Kyoto University in 1979. He was promoted to a full professor at Tokyo Metropolitan University in 1992, and moved to Kyoto University as a professor of Inorganic Chemistry in 1998. Presently, he is also Director of the Institute for Integrated Cell-Material Sciences (WPI-iCeMS) at Kyoto University. His current research interests include the chemical and physical properties of porous coordination polymers / metal organic frameworks.

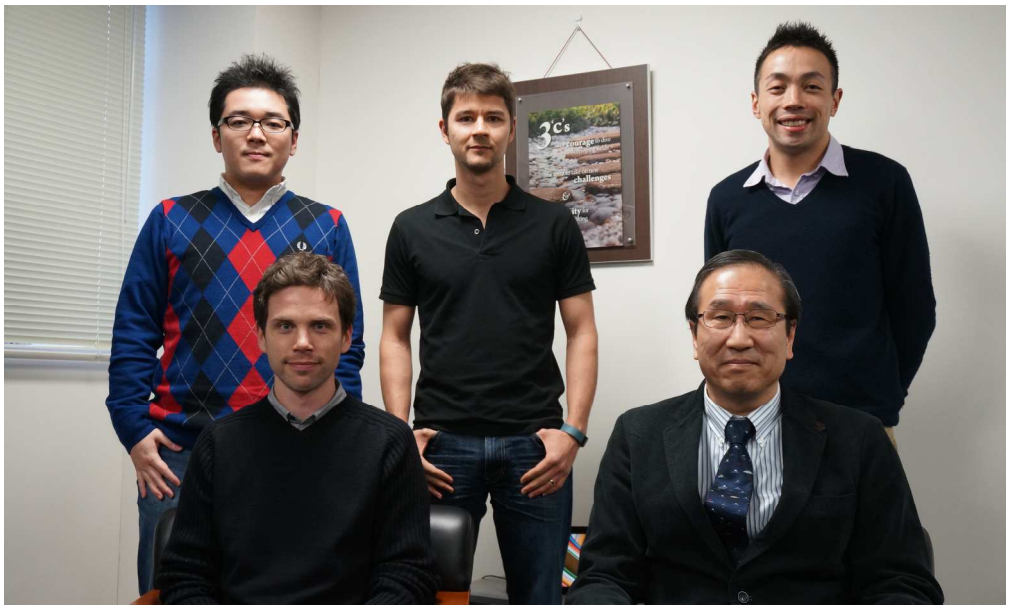

213x127mm (300 x 300 DPI)

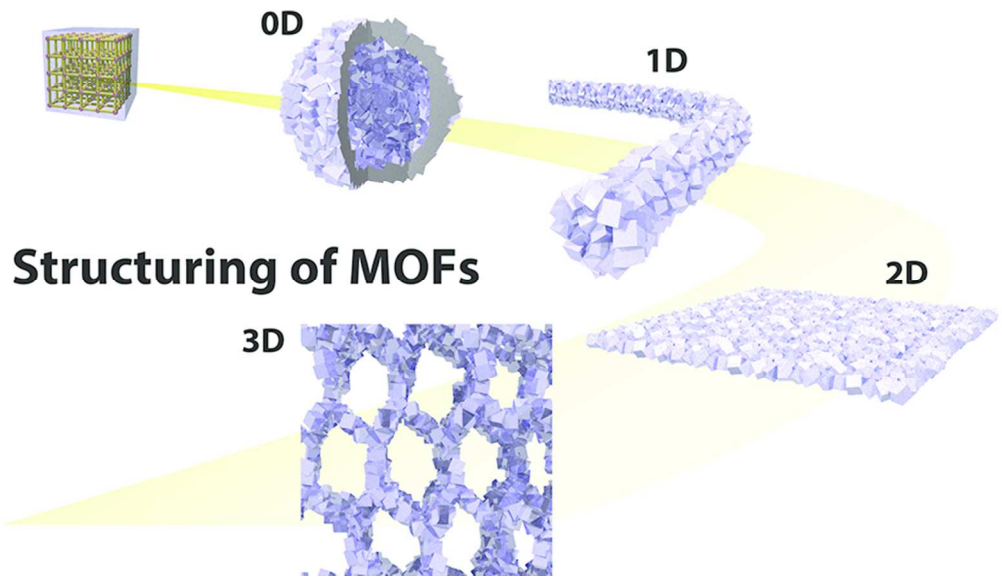

80x47mm (300 x 300 DPI)

This review conceptually categorizes the available synthetic methodologies for structuring of MOFs in the mesoscopic and macroscopic scales